194, 2023, 1, Dowr

om/doi/10.1029/2022TC007541 by Devon Orme - Montana State University Library , Wiley Online Library on [11/01/2023]. See the Terms and Conditions (https://onlinelibrary

Tectonics*

RESEARCH ARTICLE

10.1029/2022TC007541

Key Points:

- Multi-chronometer time-temperature inversions resolve key aspects of the >2.5 Gyr thermal history of the Beartooth Mountains
- 40Ar/³⁹Ar and [U-Th(-Sm)]/He data constrain newly recognized Proterozoic and Paleozoic thermal events
- Models suggest complex, spatially variable cooling associated with basement-involved thrusting initiating >90 Ma

Supporting Information:

Supporting Information may be found in the online version of this article.

Correspondence to:

C. B. Ronemus and D. A. Orme, chanceronemus@email.arizona.edu; devon.orme@montana.edu

Citation:

Ronemus, C. B., Orme, D. A., Guenthner, W. R., Cox, S. E., & Kussmaul, C. A. L. (2023). Orogens of Big Sky Country: Reconstructing the deep-time tectonothermal history of the Beartooth Mountains, Montana, and Wyoming, USA. *Tectonics*, 42, e2022TC007541. https://doi.org/10.1029/2022TC007541

Received 12 AUG 2022 Accepted 19 DEC 2022

Author Contributions:

Conceptualization: Chance B. Ronemus, Devon A. Orme

Data curation: Chance B. Ronemus Formal analysis: Chance B. Ronemus Funding acquisition: Devon A. Orme, William R. Guenthner

Investigation: Chance B. Ronemus, Devon A. Orme, William R. Guenthner, Stephen E. Cox, Christopher A. L. Kussmaul

Methodology: Chance B. Ronemus, Devon A. Orme, William R. Guenthner, Stephen E. Cox

Project Administration: Devon A. Orme **Resources:** Devon A. Orme, William R. Guenthner

Supervision: Devon A. Orme

© 2022. American Geophysical Union. All Rights Reserved.

Orogens of Big Sky Country: Reconstructing the Deep-Time Tectonothermal History of the Beartooth Mountains, Montana and Wyoming, USA

Chance B. Ronemus^{1,2}, Devon A. Orme¹, William R. Guenthner³, Stephen E. Cox⁴, and Christopher A. L. Kussmaul¹

¹Department of Earth Sciences, Montana State University, Bozeman, MT, USA, ²Department of Geosciences, University of Arizona, Tucson, AZ, USA, ³Department of Geology, University of Illinois Urbana-Champaign, Urbana, IL, USA, ⁴Lamont-Doherty Earth Observatory, Columbia University, Palisades, NY, USA

Abstract Archean rocks exposed in the Beartooth Mountains, Montana and Wyoming, have experienced a complex >2.5 Gyr thermal history related to the long-term geodynamic evolution of Laurentia. We constrain this history using "deep-time" thermochronology, reporting zircon U-Pb, biotite ⁴⁰Ar/³⁹Ar, and zircon and apatite [U-Th(-Sm)]/He results from three transects across the basement-core of the range. Our central transect yielded a zircon U-Pb concordia age of $2,805.6 \pm 6.4$ Ma. Biotite 40 Ar/ 39 Ar plateau ages from western samples are $\leq 1,775 \pm 27$ Ma, while those from samples further east are $\geq 2,263 \pm 76$ Ma. Zircon (U-Th)/He dates span 686.4 ± 11.9 to 13.5 ± 0.3 Ma and show a negative relationship with effective uranium—a proxy for radiation damage. Apatite (U-Th)/He dates are 109.2 ± 23.9 to 43.6 ± 1.9 Ma and correlate with sample elevation. Multi-chronometer Bayesian time-temperature inversions suggest: (a) Cooling between ~1.90 and ~1.80 Ga, likely related to Big Sky orogeny thermal effects; (b) Reheating between ~1.80 Ga and ~1.35 Ga consistent with Mesoproterozoic burial; (c) Cooling to ≤100°C between Mesoproterozoic and early Paleozoic time, likely reflecting continental erosion; (d) Variable Paleozoic-Jurassic cooling, possibly related to Paleozoic tectonism and/or low eustatic sea level; (e) Rapid Cretaceous-Paleocene cooling, preceding accepted proxies for flat-slab subduction; (f) Eocene–Miocene reheating consistent with reburial by Cenozoic volcanics and/or sediments; (g) Post-20 Ma cooling consistent with Neogene development of topographic relief. Our results emphasize the utility of multi-chronometer thermochronology in recovering complex, non-monotonic multi-billion-year thermal histories.

Plain Language Summary The Beartooth Mountains in southern Montana and northern Wyoming consist of some of the oldest rocks in North America. These rocks have been exhumed to Earth's surface and reburied numerous times. However, sedimentary rocks recording many of these events have been eroded, erasing much of the primary record of the geologic history of this region. To recover this history, we use minerals within existing rocks that act as heat-sensitive clocks. These "clocks" record a cooling date, reflecting the last time the rock was within a specific temperature range. We measure cooling dates for several different types of minerals and model the history of temperature fluctuations they record, corresponding to burial and erosion events. We interpret the results of these models by comparing them with the geologic history recorded in nearby preserved sedimentary rocks. We find that the Beartooth Mountains were involved in mountain-building events not previously recognized and cooling associated with building of the modern Rocky Mountains began earlier, and is more complex, than is generally recognized. The ability to recover such long histories of temperature fluctuations is important, suggesting we may be able to learn about events far in Earth's past even when the rock record is missing.

1. Introduction

The Beartooth Mountains of southern Montana and northern Wyoming primarily consist of ~3.5–2.8 Ga basement rocks of the Wyoming craton (e.g., Mueller & Frost, 2006; Mueller et al., 2008; Wooden et al., 1988). This region, located ~100 km southeast of the northwest craton margin (Figure 1), has been involved in tectonic events spanning Archean to Cenozoic time (e.g., Chamberlain et al., 2003; Dickinson & Snyder, 1978; Mogk et al., 1992). Precambrian basement in the Beartooth Mountains was exhumed to the surface as an intraforeland uplift associated with the development of the North American Cordillera in late Mesozoic–early Cenozoic time

RONEMUS ET AL. 1 of 34

Validation: Chance B. Ronemus, Devon A. Orme, William R. Guenthner, Stephen E. Cox

Visualization: Chance B. Ronemus, Devon A. Orme, Stephen E. Cox Writing – original draft: Chance B. Ronemus

Writing – review & editing: Chance B. Ronemus, Devon A. Orme, William R. Guenthner, Stephen E. Cox

(e.g., Dickinson & Snyder, 1978). Consequently, the Beartooth Mountains provide not only an opportunity to interrogate the timing and nature of this exhumation event, but also a window into the Archean to recent geodynamic evolution of western Laurentia, where basement rock is commonly inaccessible due to Phanerozoic burial.

Previous application of high- to medium-temperature thermochronometers in the Beartooth Mountains typically yield Archean–early Paleoproterozoic ages (e.g., Gast et al., 1958; Wooden et al., 1988), while conventional low-temperature thermochronology has been used mainly to explore late Mesozoic–early Cenozoic thermal events (e.g., Carrapa et al., 2019; Cerveny, 1990; Omar et al., 1994; Peyton et al., 2012). These disparate data sets comprise snapshots into a vastly more complex thermal history which remains largely unresolved. However, recent work has demonstrated the utility of multi-chronometer thermal history inversions—coupling the broad temperature sensitivity of the zircon (U-Th)/He system with additional information from medium-temperature (i.e., ⁴⁰Ar/³⁹Ar methods) and/or other low-temperature (that is, apatite (U-Th-Sm)/He (AHe) and apatite fission track (AFT)) systems—in constraining nearly continuous thermal histories below ~400°C (see review in McDannell & Flowers, 2020). This approach enables the recovery of ancient thermal events in regions where other evidence of these events is overprinted or eroded (e.g., Baughman & Flowers, 2018, 2020; DeLucia et al., 2018; Krob et al., 2019; McDannell et al., 2018, 2019, 2022). Here, we apply this approach to investigate the deep-time thermal history of the Beartooth Mountains. Key tectonic/geodynamic questions of open debate are testable using an integrated thermal history of this study area. These include:

- 1. What was the extent and nature of Paleoproterozoic thermotectonism in southwest Montana? Paleoproterozoic (~1.8–1.7 Ga) thermal overprinting in the region has long been recognized, with early work suggesting a maximum extent ~100 km west of the Beartooth Mountains (Giletti, 1966). However, subsequent work revealed partial resetting of medium-temperature thermochronometers east of this transitional boundary (e.g., Montgomery & Lytwyn, 1984) and a complex spatiotemporal pattern of tectonism (Condit et al., 2015).
- 2. How did Proterozoic rifting of the western Laurentian margin influence the thermal history of cratonic rocks to the east? The western margin of Laurentia experienced rifting events in early-middle Mesoproterozoic and middle-late Neoproterozoic time (e.g., Lonn et al., 2020; Yonkee et al., 2014). Previous studies have suggested the Neoproterozoic event caused erosional exhumation and cooling of cratonic rocks east of the rifting margin (e.g., Kaempfer et al., 2021; Peak et al., 2021). However, other authors have shown late Neoproterozoic cooling was likely not restricted to regions near the Laurentian margin, instead favoring Cryogenian glaciation as the dominant driver of continental exhumation in this interval (McDannell et al., 2022). Additional data from regions near the margin of Laurentia are essential to increase the spatiotemporal resolution of the thermal history of the craton, potentially helping constrain the thermal effects of rifting and driver(s) of Precambrian exhumation of the Laurentian continent.
- 3. What is the Paleozoic burial and uplift history of the Beartooth Mountains? Sedimentologic and stratigraphic studies in the 1990s suggested the Beartooth Mountains comprised a paleohigh during late Paleozoic time, potentially reflecting uplift associated with the Antler and/or Ancestral Rocky Mountains (ARM) orogenic events (Dorobek et al., 1991; Maughan, 1990, 1993). Despite this sedimentologic support, recent thermochronologic investigation has failed to resolve Paleozoic cooling associated with this hypothesized episode of tectonism (e.g., Carrapa et al., 2019; Peyton et al., 2012).
- 4. What was the timing of late Mesozoic—early Cenozoic intraforeland basement uplift? Interest in the timing of basement deformation in southwest Montana has recently been renewed following the publication of thermochronologic and sedimentologic evidence for exhumation as early as ~100 Ma (Carrapa et al., 2019; Garber et al., 2020; summarized by Orme, 2020). If this is the case, basement exhumation significantly preceded evidence for flat-slab subduction in the region, provoking reconsideration of many existing geodynamic models for intraforeland basement uplift in the North American Cordillera (e.g., Bird, 1984, 1998; Carrapa et al., 2019; Dickinson & Snyder, 1978; Parker & Pearson, 2021). Although the Beartooth Mountains figure centrally in this debate, existing estimates for the timing of cooling initiation vary wildly between studies (that is, ≥110 Ma from Carrapa et al. (2019) versus ≤65 Ma from Omar et al. (1994)) and no study has yet been able to reconcile these disparate results.
- 5. When and why did the Laramide ranges acquire their modern relief? Early thermochronologic work on the Beartooth Mountains suggested the development of significant topographic relief during Miocene–early Pliocene time but was unable to differentiate late-stage erosion of basement versus Oligocene–Miocene reburial and subsequent basin evacuation (Omar et al., 1994). Work in the neighboring Big Horn and Wind River ranges largely support the latter interpretation (e.g., Caylor & Carrapa, 2021; McKenna, 1980; McKenna &

RONEMUS ET AL. 2 of 34

1949194, 2023, 1, Downloaded from https://agupubs.onlinelibrary.wiley.com/doi/10.1029/2022TC007541 by Devon Orme - Montana State University Library , Wiley Online Library on [1101/2023]. See the Terms

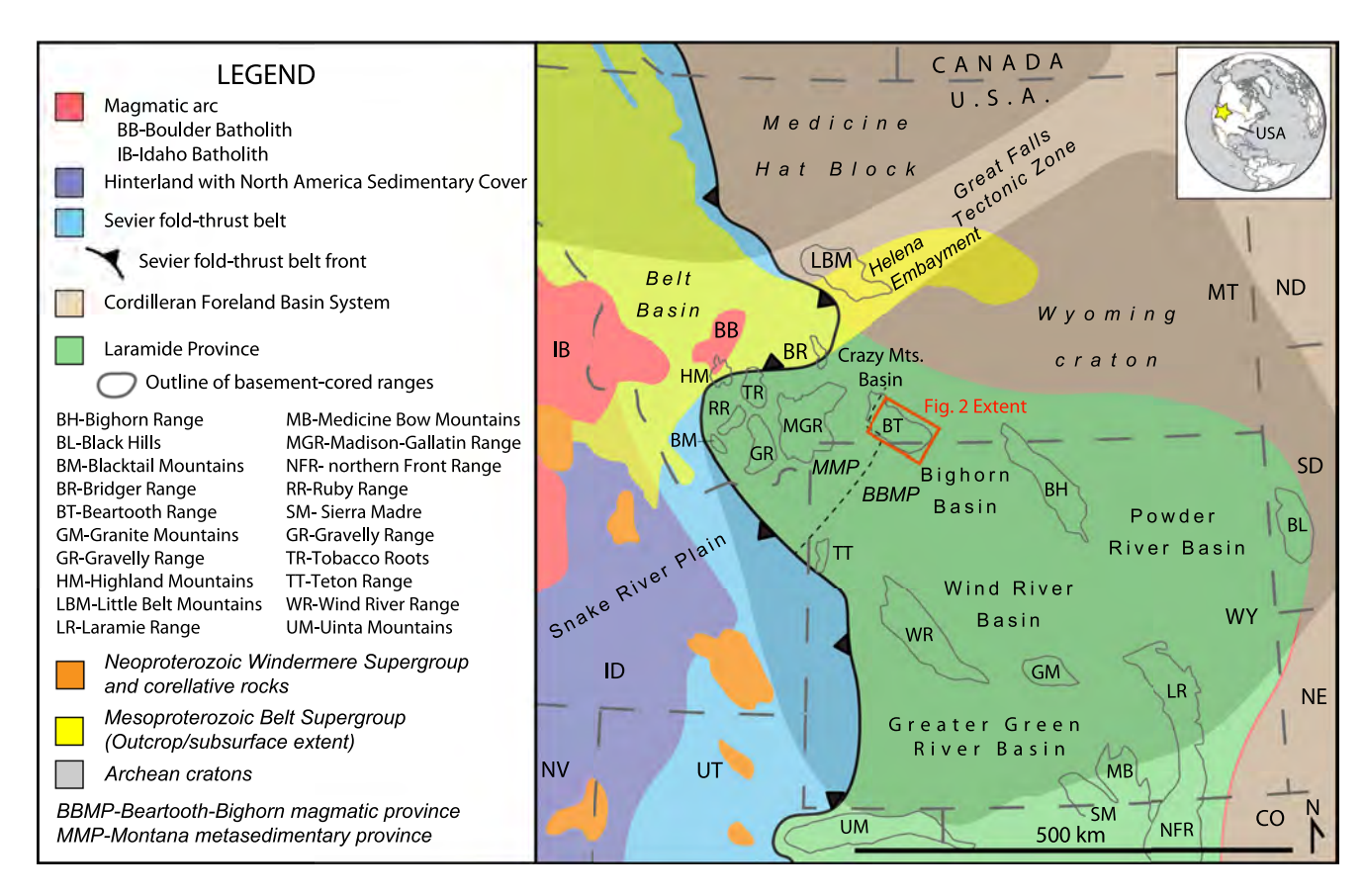


Figure 1. Tectonic map of the Northern Rocky Mountains region, showing the distribution of major tectonic features. The study area (orange extent box) in the Beartooth Mountains lies in the northwestern portion of the Archean Wyoming craton and in the northernmost portion of the Laramide Province, as classically defined (e.g., Dickinson & Snyder, 1978). Dashed line divides provinces of the Wyoming craton (e.g., Mogk et al., 1992). Modified from Ronemus et al. (2020) after Whitmeyer and Karlstrom (2007) and Yonkee and Weil (2015). Other tectonic elements adapted from: Basement-cored ranges—Peyton et al. (2012), Belt Supergroup—Lonn et al. (2020), and Vuke et al. (2007), Windermere Supergroup—Brennan et al. (2020).

Love, 1972; Steidtmann & Middleton, 1991; Steidtmann et al., 1989), but this issue has only been cursorily reexamined in the Beartooth Mountains (Carrapa et al., 2019).

We address these questions using a newly reported data set of zircon U-Pb, biotite 40 Ar/ 39 Ar, ZHe, and AHe geo- and thermochronologic data from samples collected along three transects in the Beartooth Mountains. We input information from these and previously reported data sets in a series of Bayesian QTQt time-temperature (t-T) inversions to explore the thermal evolution of the range. In turn, we integrate results of t-T inversions with structural, sedimentologic, and stratigraphic observations in a kinematic evolution model capable of explaining observed spatiotemporal trends in the Phanerozoic thermal history.

Collectively, our results indicate Paleoproterozoic tectonism affected at least the western Beartooth Mountains, leading to ≤1.8 Ga biotite ⁴⁰Ar/³⁹Ar ages. Models suggest late Paleoproterozoic to early Mesoproterozoic reheating—possibly reflecting burial by unpreserved Mesoproterozoic sediments—followed by cooling to <200°C by the end of Mesoproterozoic time. Model resolution in Neoproterozoic time is generally poor, but our best-resolved models suggest an episode of cooling initiating 800 ± 200 Ma. Models ubiquitously indicate reheating during early Paleozoic time, consistent with burial by passive margin deposits, and suggest at least one previously unresolved later Paleozoic to Mesozoic cooling event. Modeled spatially variable, rapid cooling in middle Cretaceous–Paleogene time reflects the complex evolution of tectonic exhumation likely associated with both foreland basin flexure and compressional stresses linked to retroarc shortening. Several transects suggest Cenozoic reheating coeval with Eocene volcanism and/or Oligocene–early Miocene intermontane basin sedimentation. Final cooling of these samples occurred post-20 Ma, suggesting Neogene basin evacuation and development of intra-foreland topographic relief. This study demonstrates multi-chronometer deep-time thermochronology

RONEMUS ET AL. 3 of 34



can reconstruct broadly continuous Precambrian-to-recent thermal histories, even in regions that have experienced significant Phanerozoic burial and tectonism.

2. Geologic Setting and Tectonic History

2.1. Geographic and Structural Setting

The Beartooth Mountains are a ~8,250 km² northwest-southeast trending mountain range in southern Montana and northernmost Wyoming (Figure 1; e.g., Foose et al., 1961). The range stands with ≥2.5 km of topographical prominence over bordering basins—the Bighorn Basin to the east and southeast, the Crazy Mountain Basin to the north, and the Paradise Valley to the west (Figures 1 and 2). The southern and southwestern regions of the range are buried by the Eocene Absaroka Volcanic Supergroup (Figure 2; Foose et al., 1961). Precambrian rocks in the Beartooth Mountains are divided into four main structural blocks distinguished by differing tectonic histories and lithologies: (a) the main Beartooth block, dominantly orthogneisses comprising the principal structural component of the range, including the study area; (b) the Stillwater mafic layered intrusive complex, exposed along the northeastern margin of the range; and (c) the North Snowy and (d) South Snowy blocks, consisting of rocks of the Montana metasedimentary terrane exposed in northwestern and southwestern portions of the range, respectively (Figure 2; Foose et al., 1961; Mogk et al., 1988, 1992). The eastern Beartooth Mountains form a broad plateau surface (i.e., the Beartooth Plateau)—with an average elevation of >3,000 m (Figure 2).

2.2. Precambrian Tectonic History of the Beartooth Mountains and Surrounding Regions

The Beartooth Mountains are volumetrically dominated by latest Mesoarchean–Neoarchean (~2.9–2.8 Ga) granitoids and gneisses (Figure 2; Wooden et al., 1988). These and similar rocks comprise the Archean Beartooth-Bighorn magmatic province (BBMP), a major sub-province of the Wyoming craton (Figure 1; Mogk et al., 1992; Mueller et al., 2008). Paleo–Mesoarchean (3.5–3.0 Ga) gneissic rocks of dominantly tonalitic to granodioritic to trondhjemitic composition (TTG suite) are preserved throughout the range as meter-scale xeno-liths to km-scale pendants within the 2.9–2.8 Ga suite (Mueller et al., 2008, 2010; Wooden et al., 1988). The Archean metamorphic history experienced by these rocks has been subject to extensive study and is summarized by Wooden et al. (1988) and Mueller et al. (2008).

During Paleoproterozoic time, ~1.86–1.72 Ga thermotectonism associated with the amalgamation of Laurentia impacted basement rocks of the Great Falls tectonic zone and Montana metasedimentary province—north and west of the study area, respectively (Figure 1; e.g., Condit et al., 2015; Gifford et al., 2014, 2020; Giletti, 1966; Harms, Brady, et al., 2004; Mueller et al., 2002). However, existing evidence for this event in the Beartooth Mountains is generally limited to the North and South Snowy blocks on the western margin of the range, where sparse 1.6–1.8 Ga ⁴⁰K/³⁹Ar and Rb-Sr ages have been linked to Paleoproterozoic reheating (Montgomery & Lytwyn, 1984; Reid et al., 1975). Gast et al. (1958) reported older Rb-Sr (2.53–2.8 Ga) and K-Ar (2.29–2.52 Ga) ages from near the Beartooth Highway, interpreting that late Paleoproterozoic thermotectonism did not significantly affect the main Beartooth block.

During Mesoproterozoic time, the Belt Supergroup was deposited in parts of eastern Idaho, western Montana, southeastern British Columbia, and southwestern Alberta (Figure 1; e.g., Winston, 1986). Lower Belt Supergroup rocks deposited within the eastern arm of the Belt Basin, known as the Helena Embayment, are recognized in the subsurface \sim 50 km northwest of the study area (Figure 1; Vuke et al., 2007). Sedimentary thicknesses of \geq 15 km are recognized in western portions of the Belt Basin, where the deposition of middle-upper portions of this succession (Ravalli through Missoula groups) is constrained to ~1.49–1.37 Ga (e.g., Anderson & Davis, 1995; Evans et al., 2000; Hirtz et al., 2022; Lonn et al., 2020; Ross & Villeneuve, 2003; Winston, 1986). By contrast, measured thicknesses total ≤3 km within the Helena Embayment and the depositional timing of these rocks is more poorly constrained, bracketed between ~1.71 and ~1.42 Ga by detrital zircon maximum depositional ages from the LaHood and Helena formations, respectively comprising the lowermost and uppermost units recognized in the Helena Embayment (Hirtz et al., 2022; Mueller et al., 2016). Deposition of the Belt Supergroup slightly preceded the intrusion of a suite of ~1,300 Ma mafic dikes, recognized in the Beartooth Mountains (e.g., Baadsgaard & Mueller, 1973). Both events have been linked to Mesoproterozoic rifting of the western Laurentian margin, possibly related to the breakup of supercontinent Nuna (e.g., Ross & Villeneuve, 2003; Sears & Price, 1978, 2000), also referred to as Columbia (e.g., Rogers & Santosh, 2002). The thermal effects of Mesoproterozoic rifting and sedimentation in the study area are poorly understood.

RONEMUS ET AL. 4 of 34

https://agupubs.onlinelibrary.wiley.com/doi/10.1029/2022TC007541 by Devon Orme

- Montana State University Library , Wiley Online Library on [11/01/2023]. See the Terms and Conditions (https://onlinelibrary

nditions) on Wiley Online Library

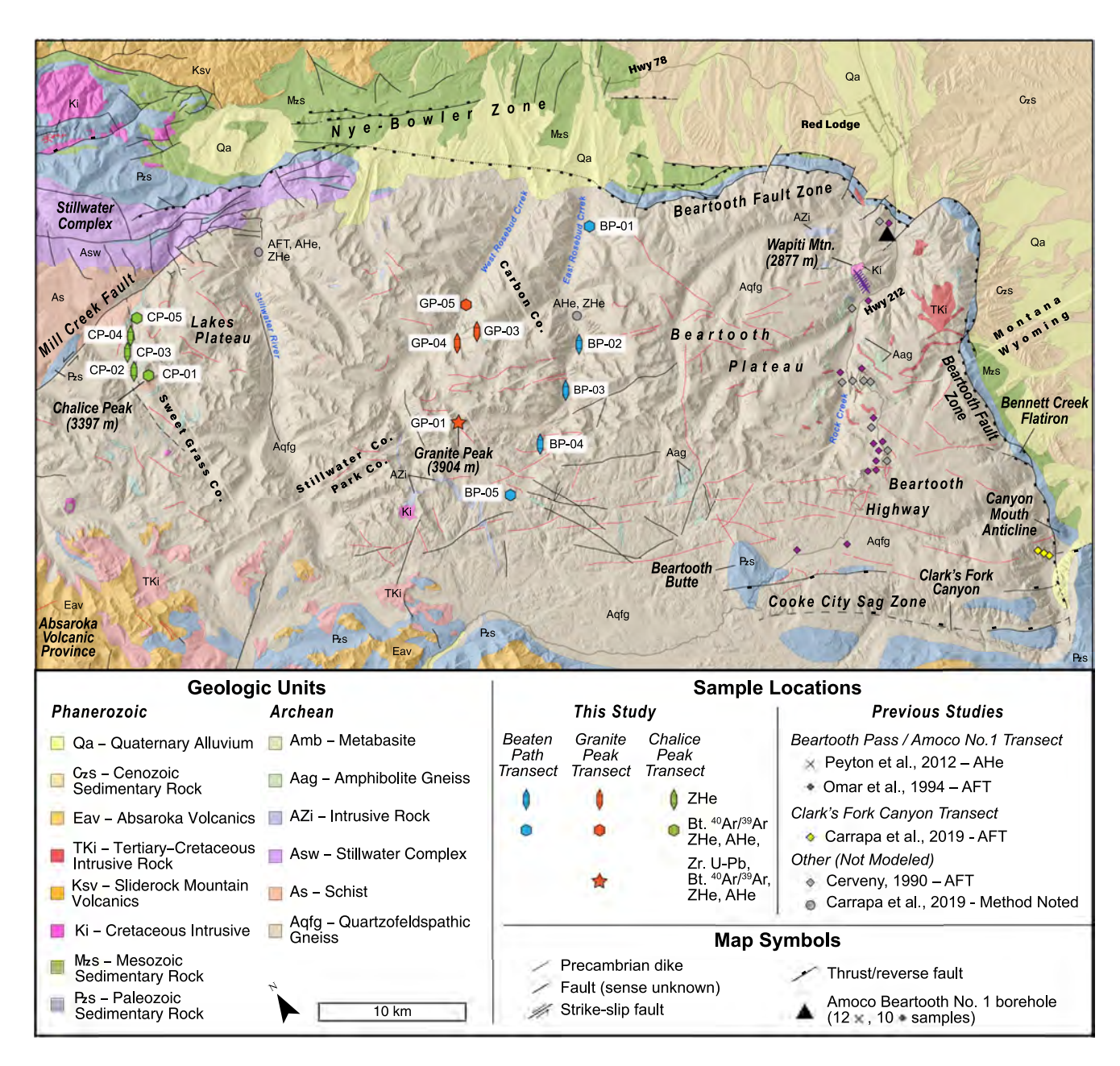


Figure 2. Generalized geology of the southeastern Beartooth Mountains. The range is comprised dominantly of Archean gneiss thrust over Paleozoic-Paleogene sedimentary rocks. Low-temperature thermochronology samples of this study and select previous studies are shown, colored by their corresponding transect used in time-temperature inversions. Geologic units and faults are generalized from Foose et al. (1961), Berg et al. (1999, 2000), Lopez (2001), and Wise (2000), with supplemental original mapping conducted during sample collection. Only Precambrian dikes longer than 2 km are shown. Note that the map is rotated ~30° counterclockwise from north.

During middle—late Neoproterozoic time (\sim 780–600 Ma), the western Montana/Eastern Idaho region was located on the rifting western margin of Laurentia (e.g., Brennan et al., 2020), which developed into the Paleozoic western Laurentian passive margin (Yonkee et al., 2014). Regionally, evidence for the inception of this rifting event includes a suite of \sim 780–708 Ma mafic dikes—preserved in the Beartooth Mountains and elsewhere along the western margin of Laurentia (Figure 2; Baadsgaard & Mueller, 1973; Harlan et al., 2003). Later rifting is recorded by \sim 665–650 Ma alkalic plutonism and \sim 667–601 Ma deposition of syn-rift sedimentary units—likely correlative to the Windermere Supergroup—in east-central Idaho, \sim 300 km SW of the study area (Figure 1; Brennan et al., 2020; Link et al., 2017; Lund et al., 2010). Normal faulting associated with this rifting event has been proposed as a driver of regional erosional exhumation in southwest Montana, based on modeled Neoproterozoic

RONEMUS ET AL. 5 of 34

cooling of basement rock therein (Kaempfer et al., 2021). Notably, Neoproterozoic rifting of western Laurentia temporally overlapped with widespread Cryogenian low-latitude glaciations, including the Sturtian (717–659 Ma) and Marinoan (641–635 Ma) "snowball Earth" events (Hoffman & Schrag, 2002; Hoffman et al., 1998, 2017; Kirschvink, 1992; Prave et al., 2016; Rooney et al., 2015; Walker et al., 1981), and the more enigmatic Gaskiers (~582 Ma; Bowring et al., 2003) and Fauquier (~571 Ma; Hebert et al., 2010) glaciations of the Ediacaran Period. Diamictites associated with Cryogenian glaciation are present in central and eastern Idaho, including within the previously mentioned syn-rift succession, but have not been recognized in Montana (e.g., Brennan et al., 2020; Lund et al., 2003, 2010; Yonkee et al., 2014). Snowball Earth glaciations have similarly been suggested as a driver of km-scale continental erosion based on results of thermochronology (McDannell et al., 2022) and analysis of the global geochemical, sedimentary, and terrestrial bolide impact records (Keller et al., 2019). However, there is no existing geologic or thermochronologic evidence for erosion related to late Neoproterozoic rifting or glaciation in the Beartooth Mountains.

2.3. Phanerozoic Burial and Tectonic History

At Beartooth Butte in the southeastern Beartooth Mountains, Phanerozoic sedimentary rocks nonconformably overlie Archean orthogneiss, representing a ~2.3 Gyr "gap" in the rock record (Figure 2; Thomas, 2008). This nonconformity coincides with similar global observations of a major unconformity at or near the base of the Phanerozoic section (e.g., Peters & Gaines, 2012; Walcott, 1914), frequently comprising a nonconformity developed atop Precambrian basement rocks (e.g., Flowers et al., 2020; Karlstrom & Timmons, 2012). The temporal correlation of these unconformities of late Precambrian age is referred to as the "Great Unconformity" (Definition 3 of McDannell et al., 2022; see discussion of variable usage of this term therein). In the region of the study area, the Flathead Sandstone—overlying the Great Unconformity surface—has been variably dated as upper Ediacaran, lower Cambrian, or middle Cambrian via Rb-Sr geochronology, paleopedology, and biostratigraphy, respectively (Chaudhuri & Brookins, 1969; Deiss, 1938; Norris & Price, 1966; Retallack, 2013; Thomas, 2007). Subsequent Paleozoic passive margin-style sedimentation is recorded by onlapping successions of sandstone, limestone, and shale, with intervening unconformities associated with periods of non-deposition and erosion (Mallory, 1972; Maughan, 1993). Regionally, deposition was punctuated by localized uplift during Devonian to Early Mississippian and Late Mississippian to Permian time, likely associated with the Antler and Ancestral Rockies orogenic events, respectively (Dorobek et al., 1991; Maughan, 1990). Along the northeastern Beartooth front, a maximum thickness of ~1 km of Paleozoic stratigraphy is preserved (Lopez, 2001; Maughan, 1993).

During Middle Triassic to Late Jurassic time, the western margin of North America evolved into a tectonically consolidated margin associated with east-dipping subduction of the Farallon oceanic plate beneath the North American continent (e.g., Colpron et al., 2007; Dickinson, 2004). This evolution culminated in the establishment of the North American Cordillera, a retroarc orogenic system extending more than 6,000 km from southern Mexico to Alaska, USA (DeCelles, 2004; Yonkee & Weil, 2015). A complex and extensive foreland basin system developed eastward of the retroarc fold-thrust belt (Figure 1; DeCelles, 2004; Kauffman & Caldwell, 1992). In areas near the Beartooth Mountains, stratigraphy deposited in this foreland basin constitute Jurassic through Paleogene rocks with a maximum thickness of ~4.5 km (Lopez, 2001; Mallory, 1972; Maughan, 1993).

The Beartooth Mountains comprise one of the northernmost features in an elongate series of intraforeland uplifts cored by Precambrian basement rock spanning from New Mexico to southwestern Montana that partitioned the Cordilleran foreland basin during a mountain building event classically referred to as the Laramide orogeny (Figure 1; e.g., Armstrong, 1968; Coney & Reynolds, 1977; Dickinson & Snyder, 1978). The timing of initiation of this event has been subject to recent debate (see Orme, 2020 for a review). Stratigraphic and sedimentologic evidence has been interpreted to suggest segmentation of the foreland basin by incipient intraforeland highs by late Early Cretaceous time (DeCelles, 1986; Parcell & Williams, 2005; Schwartz & Decelles, 1988), while more recent detrital zircon studies suggest partitioning of the southwest Montana foreland basin may have been delayed until ~88 Ma (Garber et al., 2020; Rosenblume et al., 2021). The synorogenic Beartooth Conglomerate member of the Paleogene Fort Union Formation, deposited on the east-northeast flank of the Beartooth Mountains, preserves thrust-related growth strata and an unroofing sequence recording exhumation of the uplift (Ayers, 1986; DeCelles, Gray, Ridgway, Cole, Srivastava, et al., 1991; Gingerich, 1983). Clasts of metamorphic basement occur high in the section, providing unequivocal evidence that basement rocks of the Beartooth Mountains were actively eroding by the deposition of this unit at ~57–55 Ma (DeCelles, Gray, Ridgway, Cole, Srivastava, et al., 1991; Flueckinger, 1970; Jobling, 1974; Koenig, 2015).

RONEMUS ET AL. 6 of 34



3. Methodology

3.1. Sample Collection and Mineral Separation

Samples were collected from exposed quartzofeldspathic gneiss along three pseudo-vertical transects in the Beartooth Mountains (Figure 2). Reconnaissance mapping was conducted to ensure samples were collected an adequate distance from intrusions (Figure 2). Five samples were collected along the East Rosebud "Beaten Path" trail; 4 samples were collected on the approach to and summit of Granite Peak; and 5 samples were collected on the approach to and summit of Chalice Peak (Figure 2). Sample elevations ranged from 1,742 to 3,909 m. Biotite, zircon, and apatite grains were extracted by crushing, grinding, and sieving with a 100-mesh screen, followed by separation with water, a Frantz magnetic separator, and heavy liquids.

3.2. Zircon U-Pb Geochronology

U-Pb geochronology was conducted on zircons (n=50) from sample GP-01, collected from the summit of Granite Peak (Figure 2). Though extensive U-Pb geochronology has been conducted on basement rocks from the Beartooth Mountains, these data are concentrated in locations near the Beartooth Highway and relatively few data exist for the central portions of the range (Figure 2; e.g., Carrapa et al., 2019; Mueller et al., 2008, 2010; Wooden et al., 1988). The high T_c of the U-Pb system means that zircon U-Pb ages generally reflect crystallization of the phase and provide robust starting constraints for thermal history models (e.g., Gehrels et al., 2008). Zircon grains were hand selected from the heavy fraction of mineral separates, prepared for analysis, and imaged with cathodoluminescence (CL) at the Arizona LaserChron Center (ALC; Tucson, Arizona, USA). CL images were used to select analysis spots targeting unzoned cores and rims of zircon grains. U-Pb geochronology of zircons was conducted by laser ablation multicollector inductively coupled plasma mass spectrometry (LA-MC-ICP-MS) at the ALC. Detailed description of methods is provided in Text S1 in Supporting Information S1 and analytical settings are provided in Data Set S1.

3.3. Biotite ⁴⁰Ar/³⁹Ar Medium-Temperature Thermochronology

⁴⁰Ar/³⁹Ar thermochronology was conducted on biotite from the highest and lowest elevation samples from each transect (N = 6). This thermochronometer provides information about the medium-temperature ($\sim 300^{\circ}$ C) thermal history of our samples (Grove & Harrison, 1996). Existing Ar dating in the Beartooth Mountains predominantly utilizes the K-Ar method and is concentrated on dating of intrusive dikes, which don't provide direct information about the thermal history of the gneissic basement rocks we sampled (e.g., Baadsgaard & Mueller, 1973; Condie et al., 1969). Visually unaltered, inclusion-free flakes of biotite were selected from the light fraction of separates and co-irradiated at the Oregon State TRIGA Reactor. Single-grain aliquots were analyzed using single- and multi-step heating experiments on a VG5400 and an Isotopx NGX mass spectrometer at the Argon Geochronology for the Earth Sciences Laboratory at the Lamont-Doherty Earth Observatory, Columbia University (Palisades, New York, USA). We conducted bulk age analyses (the samples were fused and analyzed in a single step) and two sets of step-heating experiments—the first with 9 heating steps to determine the Ar release characteristic of the samples, and the second with 12 heating steps. We calculated plateau biotite 40Ar/39Ar ages from the results of the second step-heating experiment. A natural plateau was defined following accepted criteria $(2\sigma \text{ overlap of each step}, \geq 50\%^{39}\text{Ar}, \geq \text{three subsequent steps})$. Where natural plateaus were not achieved, we calculated forced plateau ages and then weighed the apparent standard error of the mean (SEM) uncertainties by the square root of the mean square weighted deviation (\sqrt{MSWD}) to account for the additional spread beyond analytical uncertainties in the heating steps forced onto the plateau (Powell et al., 2020). Analytical uncertainties for each heating step are reported as 1σ SEM (see Data Set S2). See Text S2 in Supporting Information S1 for a detailed description of biotite 40Ar/39Ar analytical methods.

3.4. Apatite and Zircon [U-Th(-Sm)]/He Low-Temperature Thermochronology

Apatite and zircon [U-Th(-Sm)/He] thermochronology leverage the time-dependent production and temperature-dependent diffusion of radiogenic ⁴He through the crystal lattice. Trace U, Th, and Sm decay to ⁴He at a rate controlled by the half-life of these radioactive parent isotopes; radiogenic ⁴He escapes from the crystal lattice at higher temperatures, while it is retained at lower temperatures (e.g., Reiners et al., 2004). We use these thermochronometers to provide constraints on the <200°C thermal history of the Beartooth Mountains.

RONEMUS ET AL. 7 of 34

Recent advancements in the understanding of the influence of radiation damage and annealing on helium diffusivity in apatite and zircon show that these factors exert a strong control on the closure temperature of the systems (e.g., Flowers et al., 2009; Ginster et al., 2019; Guenthner, 2021; Guenthner et al., 2013; Johnson et al., 2017). Damage to the crystal lattice accumulates as uranium undergoes alpha decay, while heating of the crystal can anneal accumulated radiation damage; the level of net radiation damage consequently affects He retentivity (Flowers et al., 2009; Guenthner et al., 2013). Owing to these effects, each crystal of a given level of accumulated radiation damage develops a unique "effective" partial retention zone (PRZ) temperature and consequently commonly records a unique cooling date (Flowers et al., 2009; Guenthner et al., 2013). For samples with a t-T history characterized by long duration at temperatures permitting accumulation of radiation damage followed by moderate reheating and/or slow cooling, date dispersion commonly manifests as a relationship (also referred to as correlation or trend; e.g., Guenthner et al., 2013; Orme et al., 2016) between single-grain date and parent isotope concentration (or effective uranium; eU; a proxy for radiation damage, formally derived by Cooperdock et al., 2019; eU = [U] + 0.28[Th] + 0.0012[Sm]). In apatite, radiation damage generally decreases the diffusivity of the crystal, resulting in a positive relationship between date and eU (Flowers et al., 2009). Zircon exhibits similar behavior at low levels of radiation damage, while moderate to high levels increase diffusivity, resulting in a negative relationship between date and eU (Guenthner et al., 2013). The specific t-T history of a sample controls the shape of the resultant date-eU relationship, such that key aspects of the former can be recovered from the latter (Flowers et al., 2009; Guenthner, 2021; Guenthner et al., 2013). For these reasons, thermal modeling efforts incorporating a radiation damage and annealing model are particularly salient in reconstructing complex deeptime thermal histories (e.g., DeLucia et al., 2018; Flowers et al., 2020; McDannell et al., 2019; Orme et al., 2016; Reade et al., 2020).

Between 1 and 7 zircons grains were hand-picked from the heavy fraction of mineral separates from each sample for a total of 84 single zircon grain aliquots (N = 14; n = 84). Grains were selected for maximum intrasample eU variability. We used the visual metamictization of grains as a proxy for accumulated radiation damage (and eU concentration) such that clear grains reflect low levels of radiation damage and opaque grains reflect high levels of radiation damage (Ault et al., 2018). Euhedral grains of similar half-widths ($\sim 60 \, \mu m$) free from fluid or mineral inclusions were preferentially selected, when possible. The presence of broken crystal terminations or internal imperfections was noted when observed (see Data Set S3). Grain photos are available in Data Set S4, https://doi.org/10.5281/zenodo.7443913. Selected grains were photographed, measured to determine surface area to volume ratios for alpha ejection correction (Farley et al., 1996; Hourigan et al., 2005; Ketcham et al., 2011), and packed into Nb foil tubes to ensure even heating of the grain and prevent volatilization of parent nuclides during He extraction. Isotopic analysis was conducted at the Helium Analysis Laboratory (HAL) at the University of Illinois, Urbana—Champaign (Urbana, Illinois, USA). Uncertainties on individual ZHe dates, reflecting the combination of measurement and systematic error, are reported at the 2σ level. Detailed analytical methods for ZHe thermochronology are provided in Text S3 in Supporting Information S1.

AHe thermochronology was conducted on apatites from the highest and lowest elevation samples from each transect. Three apatite grains were hand-picked from the medium-density fraction of mineral separate for each selected sample for a total of 18 single grain aliquots (N = 6, n = 18; see Data Set S5). Grains were photographed, measured, and packed into Nb foil tubes in the same manner as described above for ZHe analyses. He extraction and measurement, as well as isotopic dissolution for U-Th-Sm content, was conducted at the University of Colorado (U-Th)/He thermochronology laboratory (Boulder, CO, USA). Analytical uncertainties reflecting the combination of measurement and systematic error are reported at the 2σ level. Detailed analytical methods for AHe thermochronology are provided in Text S4 in Supporting Information S1.

3.5. Bayesian Time-Temperature Inversions

To explore plausible time-temperature histories of the Beartooth Mountains, we performed Bayesian inverse thermal history modeling of newly reported biotite 40 Ar/ 39 Ar, ZHe, and AHe data and previously published AFT and AHe data from the Beartooth Mountains using the QTQt v. 5.8.0 software package (Gallagher, 2012). This approach facilitates the testing of many (10^6) potential thermal histories using a transdimensional reversible jump Markov chain Monte Carlo (rjMCMC) approach. QTQt infers the complexity of the thermal history solution from the data directly and will generally favor simpler thermal histories unless the model fit is significantly improved by additional complexity (i.e., additional t-T points).

RONEMUS ET AL. 8 of 34

The helium model in QTQt takes parent isotope concentrations, grain radii, measured dates, and date uncertainties as input. The radiation damage and annealing models of Flowers et al. (2009) and Guenthner et al. (2013) were implemented for modeling of AHe and ZHe data, respectively. To expand uncertainty accounting, we implemented Hierarchical Bayesian resampling of [U-Th(-Sm)]/He date uncertainty. Analytical uncertainties were input into QTQt and, during inverse modeling, were randomly rescaled by a value of 1–5 (Gallagher, 2012; Malinverno & Briggs, 2004). Thereby, the variance of the date uncertainties is estimated from their most probable value, given the data. This approach helps account for the discrepancy between typically small calculated analytical uncertainties (typically \leq 5%) and the much larger uncertainty indicated by studies analyzing large numbers of replicate analyses of natural aliquots and continuous ramped heating experiments (\geq 15%; e.g., McDannell et al., 2018, 2022).

To invert biotite 40 Ar/ 39 Ar data, we used the helium model in QTQt modified by inputting diffusion parameters for 40 Ar* diffusion in biotite calculated by Grove and Harrison (1996) for an infinite cylinder geometry. We assumed a 150 µm grain size. Although we did not measure individual biotite grains, this assumption is reasonable because we selected the largest biotite flakes which passed through a 100-mesh screen (\sim 150 µm), and previous studies have suggested a \sim 150 µm effective radius of diffusion (Harrison et al., 1985). Biotite 40 Ar/ 39 Ar plateau ages and corresponding uncertainties, described in Section 3.3, were input into QTQt. This allowed us to screen spurious heating steps, potentially affected by processes not accounted for by the model (e.g., McDougall & Harrison, 1999). Additional details on our approach to modeling biotite 40 Ar/ 39 Ar data in QTQT are available in Text S2 in Supporting Information S1.

The AFT multi-kinetic model of Ketcham et al. (2007) was implemented for modeling of AFT data previously published by Carrapa et al. (2019) and Omar et al. (1994). All relevant AFT count and length data from Carrapa et al. (2019) were input into the AFT model directly. The full data set of Omar et al. (1994) was not available, so the values of ρ d and Nd were resampled using the reported date, date uncertainty, and Ns/Ni for each sample; the Dpar value was resampled from a distribution of 2.0 ± 2.0 , and the QTQt default values of 340 and 5 were accepted for ζ and $\partial \zeta$, respectively. Although portions of these data sets were modeled by their original authors, we remodel them herein using the same software and parameters as our newly reported models to facilitate direct comparison of results. Additionally, our approach allows for the integration of multiple samples in a vertical profile, which was not used in previous studies.

All thermal history inversions employed a general prior of $2.812-0\,\mathrm{Ma}$ and $0-400^\circ\mathrm{C}$. This broad prior allows models to explore time space from the present to the older limit of observed concordant zircon U-Pb ages and temperature space spanning surface temperatures to those above the closure temperature of the highest-temperature thermochronometer modeled. We note that modeled thermal history complexity is generally inversely proportional to the size of the general prior in QTQt because more data are required to resolve the model across a greater range of time and temperature space. We justify our broad general prior because we input a large and diverse suite of thermochronology data recording dates spanning $\sim 2.5\,\mathrm{Gyr}$ and sensitive to a broad range of temperatures. In the Bayesian context of QTQt, our unconstrained models therefore comprise a lower limit on the complexity of the thermal history required to fit the observed data (Gallagher, 2021).

A subset of models included three constraints, using robust geologic and geochronologic information to guide the inversions: (a) 2,812–2,799 Ma and 390°C–400°C—the crystallization age of the main orthogneiss suite in the Beartooth Mountains (e.g., Carrapa et al., 2019; Wooden et al., 1988; Mueller et al., 2008; this study); (b) 550–520 Ma and 0°C–100°C—the timing of deposition of the Cambrian Flathead Sandstone atop the Great Unconformity surface (e.g., Chaudhuri & Brookins, 1969; Retallack, 2013; Thomas, 2008), constraining basement rocks near the unconformity to near-surface temperatures; and (c) 60–50 Ma and 0°C–100°C—the depositional timing of the syn-orogenic Beartooth Conglomerate, which includes clasts of basement rock eroded at the surface (DeCelles, Gray, Ridgway, Cole, Srivastava, et al., 1991). The relatively broad temperature constraints (≤100°C) for (b) and (c) reflect the uncertainty regarding the thickness of basement rock eroded from the Beartooth Mountains (e.g., Omar et al., 1994; Simons & Armbrustmacher, 1976).

To promote thorough exploration of modeled time-temperature space, more complex models were accepted for equivalent likelihood and proposal jumps were resampled if the proposal fell outside of the general prior. Models were run for 1,500,000 total iterations, consisting of 750,000 burn-in iterations that were discarded and an additional 750,000 post-burn-in iterations retained to estimate the posterior probability of the model parameters. The sampling distribution reached stationary—with no structure in the likelihood or posterior chains—by the end of

RONEMUS ET AL. 9 of 34

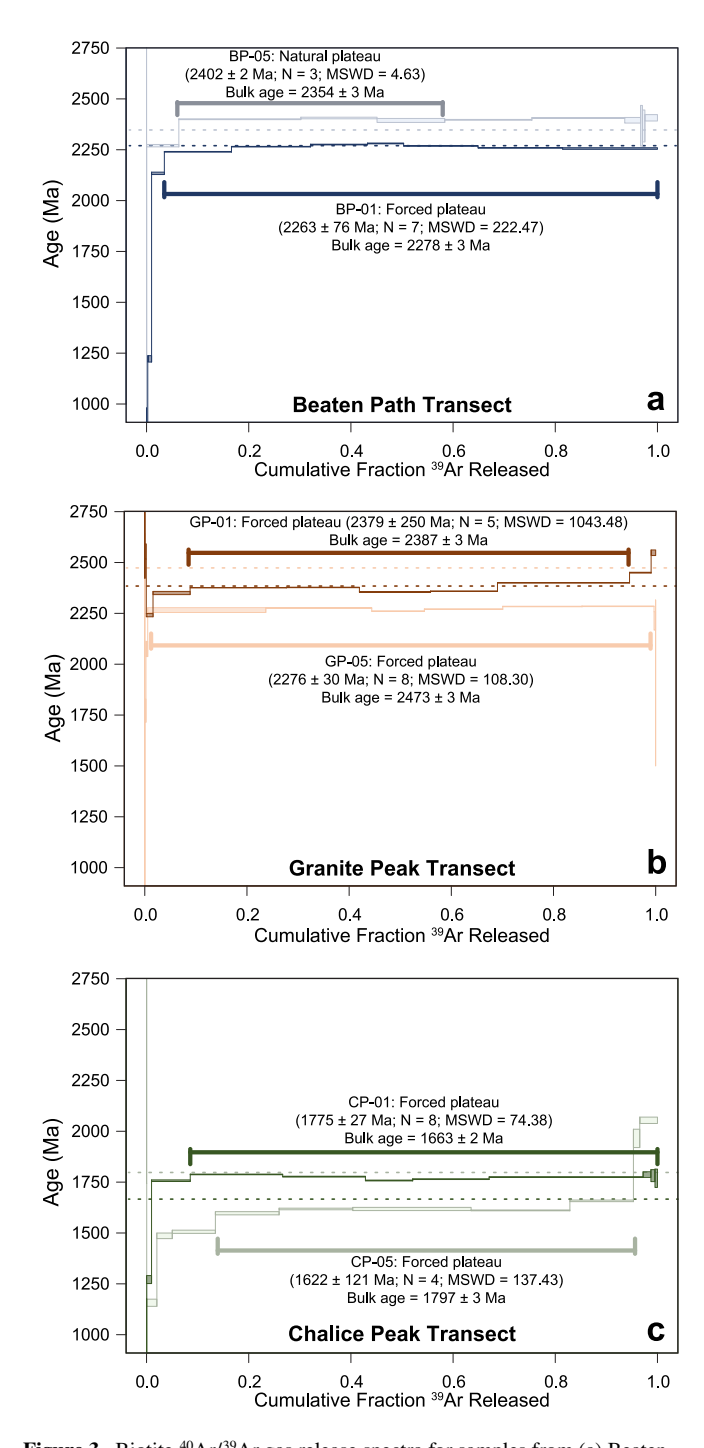


Figure 3. Biotite ⁴⁰Ar/³⁹Ar gas release spectra for samples from (a) Beaten Path, (b) Granite Peak, and (c) Chalice Peak transects in the Beartooth Mountains. Steps used for plateau determination are highlighted by bold brackets. Bulk ages are indicated by dotted lines. For samples not meeting the accepted criteria for a plateau, a plateau calculation using steps comprising a visual plateau was forced, and uncertainty was calculated using the product of the SEM uncertainty and the square root of the mean square weighted deviation (as defined in the text).

the burn-in period, signifying model convergence. Model input and output files, detailed information on model setup, and justification for constraints are available in Data Set S6, https://doi.org/10.5281/zenodo.7443913, Tables S1 and S2 in Supporting Information S1, respectively.

4. Analytical Results

4.1. Zircon U-Pb Results

Eleven zircon U-Pb analyses meeting concordance cutoffs were obtained (<20% discordance, <5% reverse discordance). Ages meeting concordance cutoffs are Neo-Mesoarchean-ranging from 2,689.0 ± 12.9 to $3,124.0 \pm 38.4$ Ma (Figure S1 in Supporting Information S1). Four analyses have error ellipses intersecting concordia, giving a concordia age of 2,805.6 \pm 6.4 Ma (mean square weighted deviation [MSWD] = 0.79; $p(\chi^2) = 0.37$; calculated using IsoplotR; Vermeesch, 2018; see Figures S2a and S2b in Supporting Information S1). The probability distribution of U-Pb ages is defined by a peak at ~2,803.5 Ma with a second, bimodal peak centered at ~2,957 Ma and a tail at lower probability to ~3,200 Ma (Figure S1c in Supporting Information S1). These results are consistent with previous zircon U-Pb geochronology results from the Beartooth Mountains (Mueller et al., 2008; Wooden et al., 1988). Analyses with ages $\geq 2,791.4$ Ma, comprising 10/11 concordant analyses, had Th/U values > 0.2 (see Figure S1d in Supporting Information S1), suggesting these ages record magmatic growth of zircon (e.g., Pystina & Pystin, 2019). A lower Th/U value of 0.04 was obtained for a single analysis with an age of 2,688.97 ± 12.90 Ma, consistent with minor Neoarchean metamorphic growth of zircon. The bulk of ages coincide with the volumetrically dominant ~2.8-2.9 Ga magmatic suite in the range, while older ages may reflect inherited zircons from the Mesoarchean TTG suite (Mueller et al., 2008). Detailed analytical data is available in Data Set S1.

4.2. Biotite 40Ar/39Ar Results

Apart from GP-01, age spectra from biotite ⁴⁰Ar/³⁹Ar step-heating diffusion experiments for all samples rise from younger values to a plateau-like sequence of steps within the first 5%–20% of ³⁹Ar release (Figure 3). Sample GP-01 exhibits a saddle-like spectrum, with older values exhibited during the first and last ~5% of ³⁹Ar release (Figure 3b). Older values within the last several steps are also present in the spectrum of sample CP-05 (Figure 3c). Young step ages during initial increments of ³⁹Ar release may suggest minor episodic ⁴⁰Ar loss, slow cooling through the PRZ, or degassing of (sub) microscopic inclusions within biotites (Onstott & Peacock, 1987; Ross & Sharp, 1988). The saddle-shaped spectrum of sample GP-01 may indicate the presence of minor excess Ar in this sample (Figure 3b; e.g., Lanphere & Brent Dalrymple, 1976). However, all age spectra are generally flat for the central ≥80% of ³⁹Ar release and yield a clear visual sequence of plateau-like steps, suggesting these potential sources of discordance are of relatively minor importance (Figure 3).

A natural plateau was obtained only for sample BP-05. For other samples, we report forced plateau ages and uncertainties using the methods described in Section 3.3. Using this approach, biotite samples yielded ⁴⁰Ar/³⁹Ar plateau

ages ranging from $1,622 \pm 121$ to $2,402 \pm 2$ Ma (Figure 3). We additionally report bulk ages from single-step heating experiments for separate aliquots of each sample (Figure 3). These bulk ages range from $1,663 \pm 2$ to

RONEMUS ET AL. 10 of 34

 $2,472 \pm 3$ Ma and demonstrate general agreement with the plateau ages (Figure 3). Biotite 40 Ar/ 39 Ar plateau ages comprise two distinct groups with internal overlap at 2σ uncertainty: (a) samples from the westernmost transect (CP) yield ages between $1,662 \pm 121.22$ and $1,775 \pm 27.08$ Ma; (b) samples from the eastern two transects (Granite Peak and Beaten Path) yield ages between $2,263 \pm 75$ Ma and $2,402 \pm 2$ Ma (Figure 3). High elevation samples in each transect record older cooling dates than those from low elevation. See Data Set S2 for detailed isotopic results.

4.3. Zircon (U-Th)/He Results

Corrected ZHe dates range from 686.4 ± 11.9 to 13.5 ± 0.3 Ma while eU concentrations span 113–3,565 ppm (Figure 4; detailed isotopic results available in Data Set S3). ZHe dates from the Beartooth Mountains are relatively evenly distributed with few obvious date probability peaks (Figure 5b). Correlation between ZHe date and grain size is poor (Figure S2 in Supporting Information S1). By contrast, ZHe dates exhibit a coherent, negative relationship with eU, a proxy for radiation damage, which is expected given that we purposefully selected for grains with a wide range of observable damage (Figure 4). The trend is strongly negative for eU values less than ~500 ppm, consistent with moderate to high levels of accumulated damage (>1.0 α /g × 10¹⁷; Guenthner et al., 2013). For all transects, grains of >800 ppm eU form a pediment of ages of ~10 Ma to ~110 Ma before reaching dates <50 Ma at >1,200 ppm eU (Figure 4). Eastern transects (Beaten Path and Granite Peak) define a more gradual transition into this pediment, with an initial inflection to a lower-angle date-eU slope at ~400 ppm and a second inflection to a nearly flat slope at ~800 ppm eU (well-defined for only the Beaten Path transect; Figures 4a and 4b). By contrast, the Chalice Peak transect exhibits a steeper date-eU slope at low-eU concentrations and a more abrupt inflection at ~500 ppm eU (Figure 4c). Elevation has a second-order influence on ZHe date (Figure 4 insets). Although intrasample date dispersion is high—likely primarily owing to radiation damage effects—median ZHe dates of each sample (red Xs in Figure 4 insets) generally trend toward older values at higher elevations. Samples BP-05 and CP-03 noticeably deviate from this trend. However, this is likely due these analyses sampling only moderate-high eU grains (384-3,565 ppm). Consequently, radiation damage effects may mask the date-elevation relationship for these samples.

4.4. Apatite (U-Th-Sm)/He Results

AHe dates span from 109.2 ± 23.9 to 43.6 ± 1.9 Ma and eU concentrations range from 3.3 to 35.4 ppm (Figure 5; see Data Set S5 https://doi.org/10.5281/zenodo.7443913 for detailed analytical data). AHe dates exhibit moderate intrasample dispersion (average intrasample $\sigma = 11.87$ Myr). Compared to previously reported AHe dates from the Beartooth Mountains, the present distribution of dates is flatter and lacks tails <40 and >110 Ma, but the dominant Paleocene date probability peak is consistent between new and previously reported data sets (Figure 5b; Bricker, 2016; Carrapa et al., 2019; Mueller et al., 2008; Peyton et al., 2012). Newly reported AHe dates are less dispersed than those of Mueller et al. (2008), Bricker (2016), and Carrapa et al. (2019), who reported dates ranging from ~190 to ~32 Ma from samples collected along the Beartooth Highway, East Rosebud Creek, and Stillwater River drainages (Figures 2 and 5).

Correlation between AHe date and grain size is poor (Figure S3a in Supporting Information S1). Aliquots from most newly reported samples span a relatively restricted array of eU concentrations (\leq 20 ppm), and AHe dates are not strongly correlated with eU (Figure S3b in Supporting Information S1). The Beaten Path and Granite Peak transects display a positive date-elevation relationship, while this trend is less coherent in samples from the Chalice Peak transect (Figure 5a). The lack of a clear inflection point toward older AHe dates with increasing elevation suggests that a fossil AHe PRZ is not preserved in the eastern Beartooth Mountains, contrary to suggestions of Bricker (2016) and Mueller et al. (2008). Rather, previously reported, highly dispersed AHe dates at \sim 1,300–3,200 m ASL may have been affected by other sources of AHe date overdispersion (e.g., Brown et al., 2013; Guo et al., 2021; Murray et al., 2014). For instance, Peyton et al. (2012) observed clear overdispersion in a sample from an intrusive porphyry in the Beartooth Mountains with AHe dates of up to 138 \pm 19 Ma and a zircon U-Pb date of 98.3 + 0.3/–1.0 Ma (gray Xs at 2,868 m ASL in Figure 5a).

4.5. Time-Temperature Inversion Results

Results of Bayesian *t-T* inversions implemented in QTQt show the relative probability of thermal history solutions for transects in the Beartooth Mountains (Figures 6 and 7). We report the results of models without geologic

RONEMUS ET AL. 11 of 34

19449194, 2023, 1, Downloaded from https://agupubs.onlinelibrary.wiley.com/doi/10.1029/2022TC007541 by Devon Orme

- Montana State University Library, Wiley Online Library on [11/01/2023]. See the Terms and Conditions (https://onlinelibrary

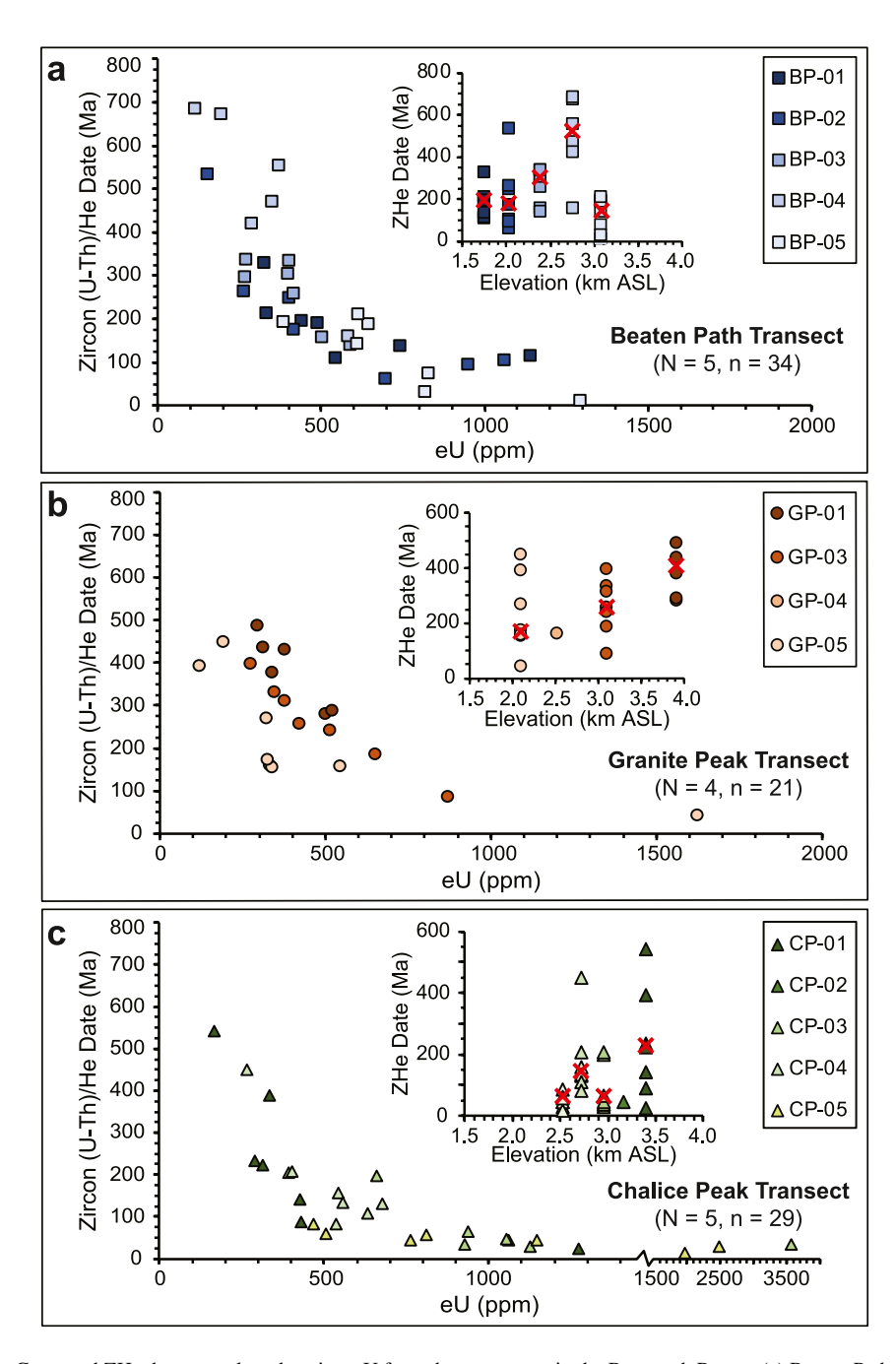


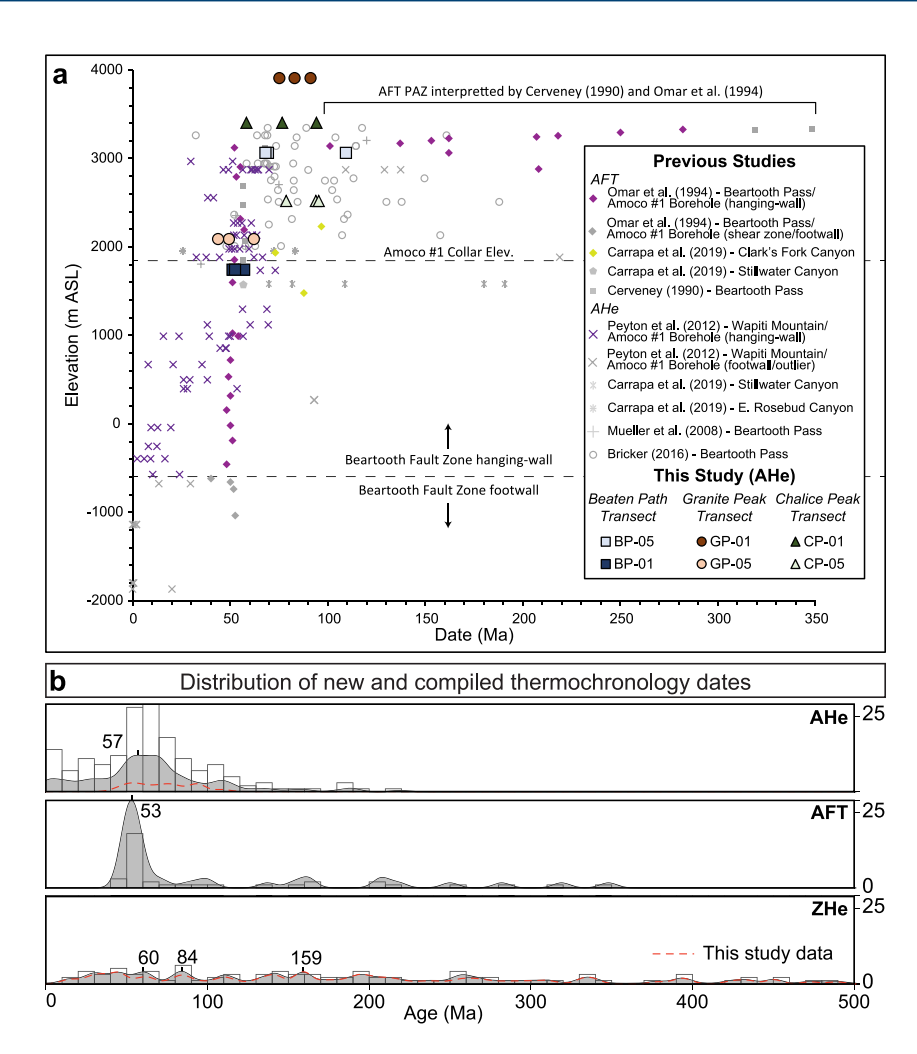
Figure 4. Corrected ZHe dates are plotted against eU from three transects in the Beartooth Range: (a) Beaten Path trail; (b) Granite Peak; and (c) Chalice Peak. A negative relationship between ZHe date and eU concentration exists independently all transects. Note the change in *x*-axis scale at 1,500 ppm eU in panel (c). Insets show corrected ZHe date plotted against sample elevation. Red Xs denote median ZHe date for samples with multiple aliquots.

constraints ("unconstrained models"; Figures 6a, 6c, and 6e) primarily as a sensitivity test, allowing us to better examine the resolution of the thermochronology data themselves and isolate possible artifacts of imposed boundary conditions. These model results represent the simplest thermal history solutions consistent with the observed thermochronology data but do not necessarily honor geologic data. By contrast, models including geologic constraints ("constrained models"; Figures 6b, 6d, and 6f; Figure 7) represent the most probable thermal history solutions considering all available sources of information—both thermochronologic and geologic—and are therefore primarily used for geologic interpretation. The agreement between observed and predicted thermochronometer dates is generally good for all models, with exceptions noted (Figure 8).

RONEMUS ET AL. 12 of 34

19449194, 2023, 1, Downloaded from https://agupubs.onlinelibrary.wiley.com/doi/10.1029/2022TC007541 by Devon Orme

- Montana State University Library , Wiley Online Library on [11/01/2023]. See the Terms and Conditions (https://onlinelibrary



Tectonics

Figure 5. (a) Existing and newly reported AHe and apatite fission track (AFT) dates from the Beartooth Mountains as a function of elevation. Sample locations are shown in Figure 2. Data with colored symbols were used in time-temperature inversions, while gray symbols were not. Note that several outlier aliquots from the data set of Peyton et al. (2012), which the authors identified as being overdispersed, were excluded from our modeling. (b) Kernel density estimation (KDE) and histogram plots summarizing new and previously reported AHe, AFT, and ZHe dates from the Beartooth Mountains between 0 and 500 Ma; note that newly reported ZHe dates >500 Ma plot off the scale. KDE and histogram bin widths are 5 and 10 Myr, respectively, and KDEs are normalized such that each plot contains the same area under the curve. Prominent date-probability peaks are indicated by vertical ticks and labeled. Scales at right correspond to the number of analyses in each histogram bin. Data sources: AHe—Bricker (2016), Carrapa et al. (2019), Mueller et al. (2008), Peyton et al. (2012), and this study; AFT—Carrapa et al. (2019), Cerveny (1990), and Omar et al. (1994), ZHe—Carrapa et al. (2019) and this study.

The Precambrian portion of our thermal history models resolves several first-order thermal events previously unrecognized in the Beartooth Mountains, discussed here in detail (Figure 6). Model results are described for the highest elevation sample in each transect. Modeled thermal histories for lower elevation samples follow the same *t-T* paths, offset according to a geothermal gradient resampled during modeling. We discuss model results in terms of both relative path density, which is proportional to relative probability, and the expected model—a weighted mean model, where the weighing is provided by the posterior probability for each thermal history solution, and the preferred single model output in QTQt (Gallagher, 2012; Figure 6). The results of supplemental models, testing the effects of modifying the resampling parameters, are available in Figure S4 in Supporting Information S1.

4.5.1. Modeled Precambrian Thermal History

Model results for the Beaten Path transect indicate at least three distinct Proterozoic cooling events (Figures 6a and 6b). The most probable solution for the constrained model, reflected by the highest path density, suggests

RONEMUS ET AL. 13 of 34

1949/194, 2023, Dowloaded from http://agupubs. onlineibabray.wiley.com/doi/10.1092/1922TC007541 by DevonOmer - Montana Sate University Library, Wiley Online Library on (1101/1023). See the Terms and Conditions (https://onlineibabray.wiley.com/terms-and-conditions) on Wiley Online Library for rules of use; OA articles are governed by the applicable Centric Commons Licross

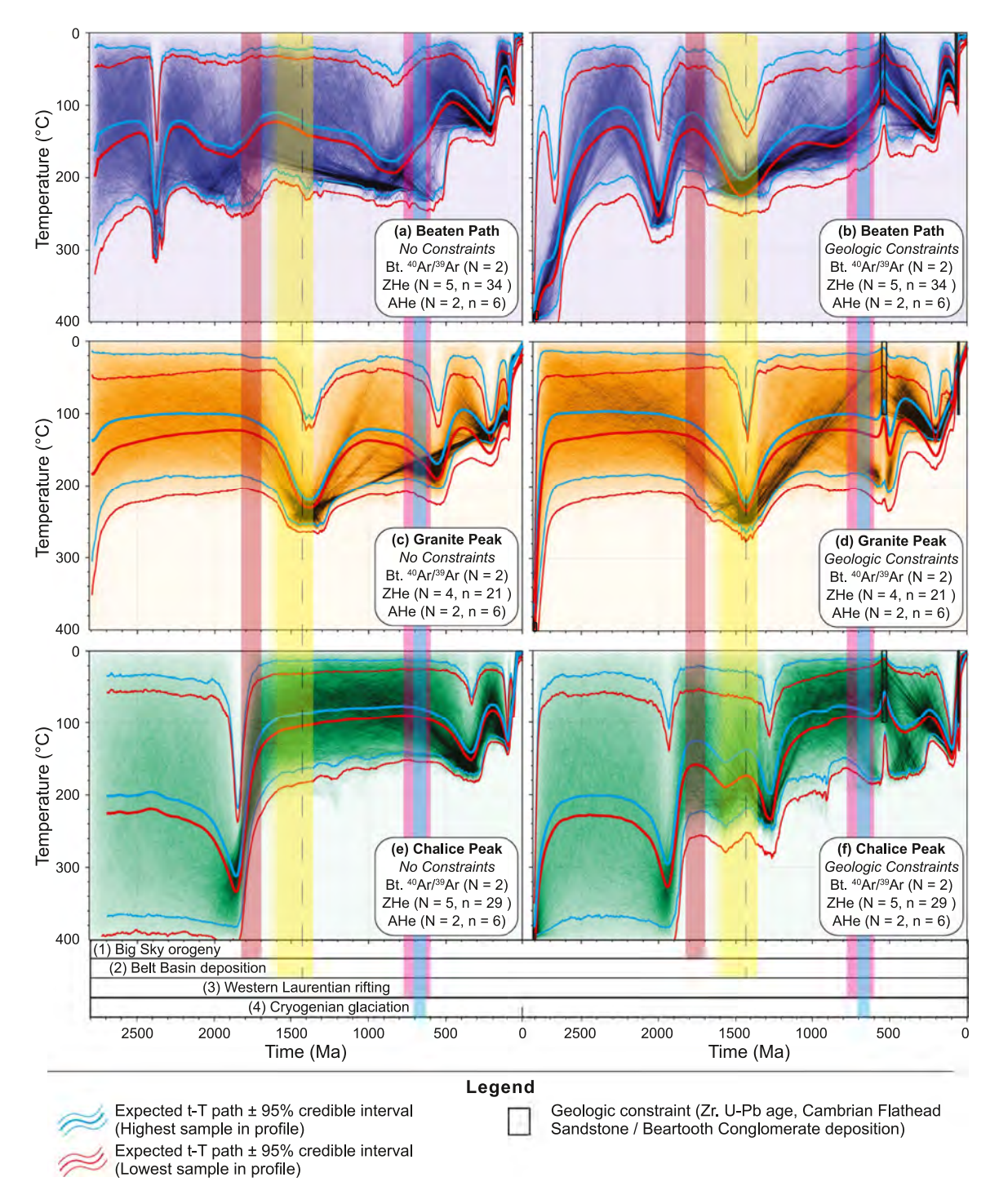


Figure 6. Results of QTQt *t-T* inversions of thermochronology data from (a, b) Beaten Path, (c, d) Granite Peak, and (e, f) Chalice Peak transects. Panels on the left (a, c, and e) show results of unconstrained models while panels on the right (b, d, and f) show results of constrained models. Post-burn-in *t-T* path density is shown for the highest elevation sample in each profile by colored gradient (blue, orange, and green). Path density is proportional to relative probability such that higher saturation indicates higher relative probability in *t-T* space. Expected model results and corresponding 95% credible intervals are shown by cyan (highest elevation sample in each profile) and red (lowest elevation sample in each profile) envelopes. "N" refers to the number of samples in each transect for the respective thermochronometer, while "n" refers to the total number of aliquots. Constraints imposed on thermal history models are shown as black boxes (described in methods section). Vertical bars show the approximate timing of geologic events potentially responsible for major aspects of the modeled *t-T* histories. The dashed line for the Belt Basin deposition event divides poorly-constrained deposition of Lower Belt Supergroup units of the Helena Embayment from better-constrained deposition of the Ravalli through Missoula groups in the main Belt Basin. Geologic event references: (1) Condit et al. (2015) and references therein; (2) Lonn et al. (2020) and references therein; Hirtz et al. (2022); (3) Brennan et al. (2020), Link et al. (2017), Lund et al. (2010), and Yonkee et al. (2014); (4) Hoffman et al. (1998, 2017), Hoffman and Schrag (2002), Kirschvink (1992), Prave et al. (2016), Rooney et al. (2015), and Walker et al. (1981).

RONEMUS ET AL. 14 of 34

1949 1942, 2023, D. Dowloaded from the "lagupubs of ministrary viely com doi/10.1092/022TC007541 by Devon Orme - Montana State University Library Wiley Online Library wiley com fem-s and Conditions (https://onlinelibrary.wiley.com/tem-sand-conditions) on Wiley Online Library for rules of use; OA articles are governed by the applicable Creative Commons Licross

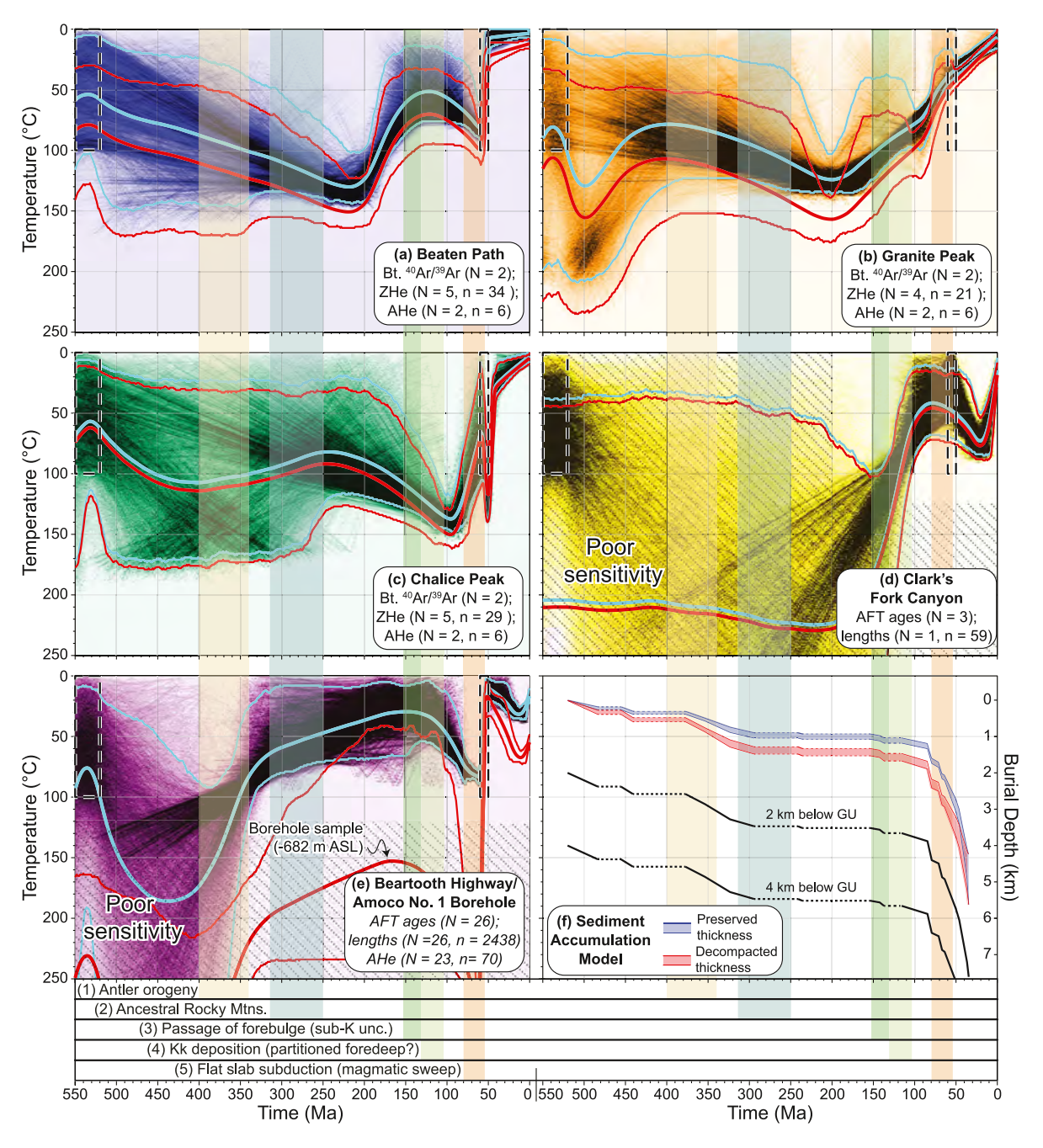


Figure 7. QTQt *t-T* inversions of new and previously reported thermochronology data resolve Phanerozoic cooling and reheating events. The ≤800 Ma and ≤250°C portion of *t-T* inversions are shown for the (a) Beaten Path, (b) Granite Peak, (c) Chalice Peak, (d) Clark's Fork Canyon (Carrapa et al., 2019), and (e) Beartooth Highway/Amoco No. 1 borehole (Omar et al., 1994; Peyton et al., 2012) transects. All models enforced geologic constraints (black boxes). Stippled regions show time-temperature space poorly constrained by AFT/AHe-only models (panels d and e). Path densities and expected model results are symbolized as in Figure 6. (f) Results of decompacted sediment accumulation models: compacted (blue envelopes) and decompacted (red envelopes) sedimentary thicknesses are defined by the minimum (upper envelope bound) and maximum (lower envelope bound) thickness of preserved stratigraphy near the study area. Dashed lines indicate hiatuses in the stratigraphic record. Black lines show modeled reference maximum burial depths for samples originally 2 and 4 km below the sub-Cambrian unconformity surface (i.e., 2 or 4 km of basement overburden). Temperature scale assumes 20°C surface temperature and a 30°C/km geothermal gradient. Shaded vertical bars show the approximate timing of geologic events potentially impacting the thermal history of the region. Geologic event references: (1) Beranek et al. (2016), Blakey and Ranney (2018), and Dorobek et al. (1991); (2) Kluth and Coney (1981) and Maughan (1990); (3) DeCelles (2004), DeCelles and Burden (1992), and Fuentes et al. (2011); (4) DeCelles (1986) and Schwartz and Decelles (1988); (5) Coney and Reynolds (1977) and Copeland et al. (2017). Kk—Cretaceous Kootenai Formation; unc.—unconformity.

RONEMUS ET AL. 15 of 34

1949194, 2023, 1, Downloaded from https://agupubs.onlinelibrary.wiley.com/doi/10.1029/2022TC007541 by Devon Orme - Montana State University Library, Wiley Online Library on [1101/2023]. See the Terms and Conditions (https://onlinelibrary.

nditions) on Wiley Online Library for

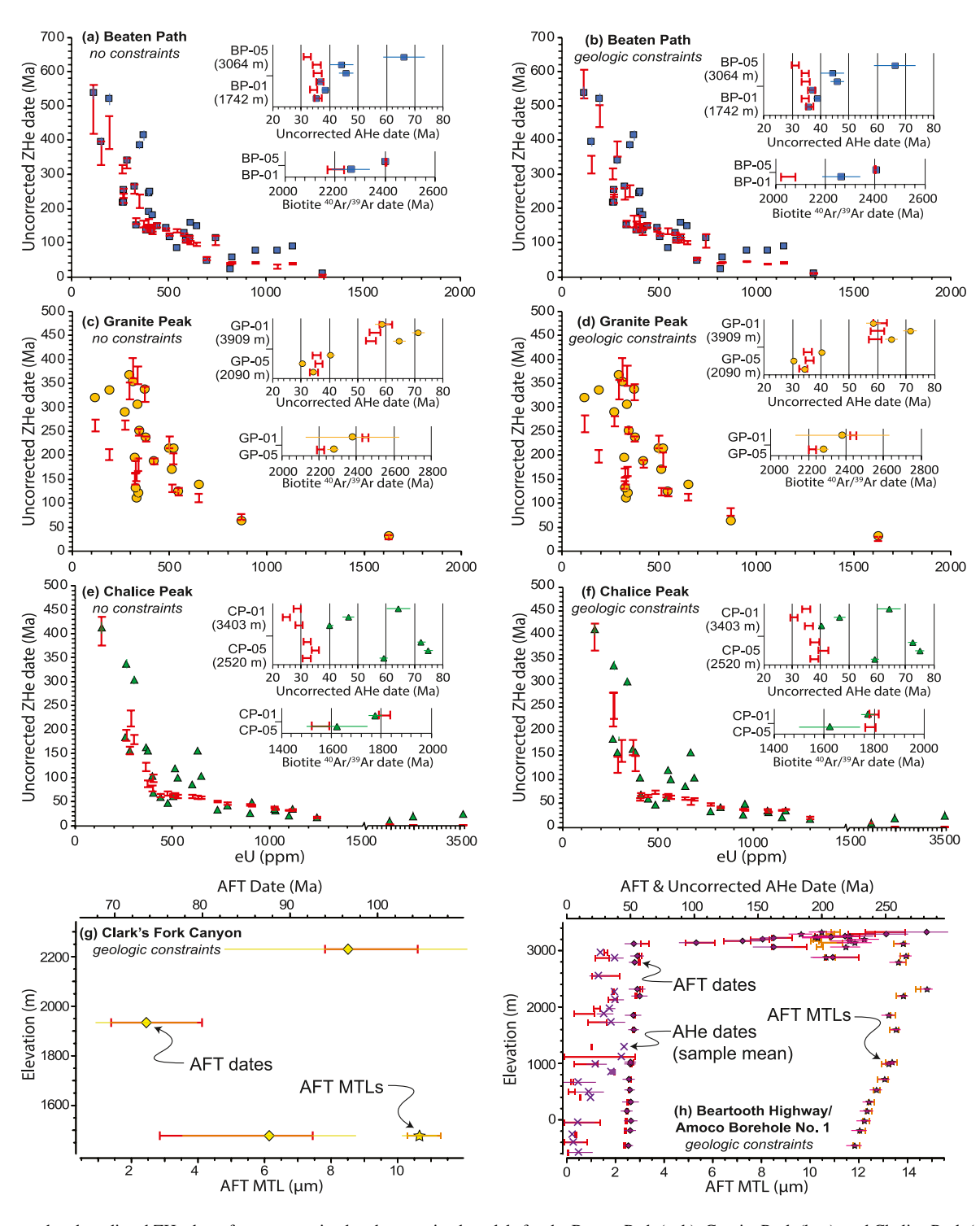


Figure 8. Observed and predicted ZHe dates for unconstrained and constrained models for the Beaten Path (a, b), Granite Peak (b, c), and Chalice Peak (e, f) transects (inversion results in Figures 6 and 7a–7c) are shown with respect to eU. Insets show predicted AHe dates and ⁴⁰Ar/³⁹Ar ages, grouped by sample. Observed and predicted AHe and apatite fission track (AFT) dates and AFT mean track lengths (MTL) for constrained models from the Beartooth Pass/Amoco No. 1 Borehole (g) and Clark's Fork Canyon (h) transects (inversion results in Figures 7d and 7e) are plotted with respect to elevation. Colored bars without ticks show reported uncertainty. Red bars with ticks show 95% credible range of dates sampled by post-burn-in models (i.e., predicted dates of the stationary distribution). For samples with AFT length data (g, h), orange bars with ticks show 95% credible range of AFT MTL sampled by post-burn-in models. For readability, AHe dates in (h) are shown as the mean of all sample aliquots. Observed AHe dates for individual aliquots are shown in Figure 5. Note that plotted [U-Th(-Sm)]/He dates are uncorrected for α-ejection. This is the default input and output of QTQt, which handles corrections during modeling. Observed ZHe and AHe dates corrected for α-ejection are provided in Figures 4 and 5, respectively.

RONEMUS ET AL. 16 of 34

post-crystallization cooling to <150°C by ~2.3 Ga followed by reheating to ~250°C by ~2.0 Ga. Subsequent cooling to <200°C by ~1.8 Ga is followed by reheating to \geq 200°C by ~1.4 Ga (Figure 6b). Model resolution throughout the remainder of the Proterozoic is relatively poor, with subsets of paths indicating either a cooling-reheating-cooling trajectory or monotonic cooling until Cambrian time. The most probable solution suggests relatively slow cooling to ~150°C \pm 25°C between 1.45 \pm 0.5 and 0.8 \pm 0.2 Ga, followed by more rapid cooling to <100°C by Cambrian time (Figure 6b). The unconstrained model for the Beaten Path is less well resolved. In contrast to the constrained model, it indicates a reheating event at ~2.4 Ga and does not resolve a reheating-cooling inflection point at ~1.4 Ga (Figure 6a). However, the unconstrained model similarly resolves Orosirian and Tonian through Cambrian cooling, suggesting these events are directly informed by the thermochronologic data and not an artifact of imposed model boundary conditions.

The fit between observed and predicted thermochronometer dates is similar for unconstrained and constrained models for the Beaten Path transect, matching the observed date-eU relationship of the ZHe data well (Figures 7a and 7b). Both models achieve good fits to the biotite 40 Ar/ 39 Ar age of sample BP-05, but the unconstrained model produces a better fit for sample BP-01. This thermochronometer is partially reset by ~2.0 Ga reheating in the constrained model, resulting in a predicted age ~0.2 Ga younger than that observed (Figures 6b and 7b).

Both unconstrained and constrained models for the Granite Peak transect suggest reheating to >200°C at ~1.3–1.4 Ga (Figures 6c and 6d). This reheating event apparently obscures the earlier Precambrian history. Both models suggest temperatures of ≤200°C post-1.3 Ga with cooling to <150°C by early Paleozoic time. The trajectory of this cooling is relatively poorly resolved, with a subset of paths in the unconstrained model suggesting latest Neoproterozoic–early Paleozoic cooling (Figure 6c). However, these paths are largely inconsistent with geologic evidence suggesting near-surface temperatures during deposition of the Cambrian Flathead Sandstone (e.g., Simons & Armbrustmacher, 1976). Enforcing this constraint results in poor resolution of late Precambrian cooling (Figure 6d). Predicted biotite ⁴⁰Ar/³⁹Ar ages overlap at uncertainty with those observed, and predicted ZHe dates generally reproduce the observed date-eU relationship (Figures 7c and 7d). However, predicted dates for the two lowest-eU grains, both from the lowest elevation sample, are ~50–150 Myr younger than observed.

Temperatures of $\sim 300^{\circ}$ C at $\sim 1.9 \pm 0.1$ Ga are indicated by both unconstrained and constrained models for the Chalice Peak transect (Figures 6e and 6f). These temperatures are required to reproduce observed Statherian biotite 40 Ar/ 39 Ar ages (Figures 7e and 7f). Notably, the unconstrained model better reproduces the 40 Ar/ 39 Ar age of sample CP-05 (Figure 7e). Subsequent cooling to $<250^{\circ}$ C by ~ 1.75 Ga is indicated by both models. The unconstrained model is poorly resolved throughout the remainder of Proterozoic time (Figure 6e), while the constrained model indicates reheating to $>200^{\circ}$ C by 1.25 ± 0.5 Ga and subsequent, poorly constrained cooling (Figure 6f). While ZHe predictions of both models reproduce the observed steeply negative date-eU relationship at <400 ppm eU, predicted dates are significantly younger than observed for a cluster of 5 zircons at $\sim 500-800$ ppm eU. Additionally, zero dates predicted for zircons of >2,000 ppm eU conflict with non-zero observed dates (Figures 7e and 7f).

4.5.2. Modeled Phanerozoic Thermal History

Model results suggest that at least two distinct Phanerozoic reheating-cooling events best reproduce the observed thermochronologic data (Figures 7 and 8). Following early Paleozoic reheating, a subset of paths of the constrained Granite Peak and Chalice Peak models suggest an episode of Paleozoic cooling, initiating between 500 and 300 Ma (Figures 7b and 7c). This cooling event is resolved by both unconstrained and constrained models for the Chalice Peak transect (Figures 6e, 6f, and 7c), indicating it is directly informed by the data. By contrast, the unconstrained model for the Granite Peak transect produces a good fit to the data without requiring Paleozoic initiation of cooling, suggesting rapid early Paleozoic reheating followed by cooling indicated by a subset of paths in the Granite Peak constrained model may be an artifact of imposed constraints (Figure 6c). The Beaten Path and Granite Peak transects indicate cooling during Jurassic time, initiating 200 ± 20 Ma (Figures 6a–6d, Figures 7a and 7b). All transects additionally resolve cooling during Late Cretaceous and/or Paleocene time (Figure 7). Following Late Cretaceous–Paleocene cooling, the Beaten Path and Granite Peak transects indicate slow cooling while the Chalice Peak transect suggests an episode of rapid reheating and cooling between ~60 and ~40 Ma (Figure 7c).

In addition to our newly reported transects, we modeled 3 AFT dates and one set of track lengths from the Clark's Fork Canyon transect of Carrapa et al. (2019; Figure 7d). Model results are similar to those of Carrapa

RONEMUS ET AL. 17 of 34

et al. (2019), who conducted a single-sample HeFTy model of their sample CF4. Their best-fit model solution suggested rapid cooling at \sim 110 Ma followed by reheating to \sim 80°C between 40 and 20 Ma followed by monotonic cooling to surface temperatures at the present. Our results demonstrate this thermal history produces a good fit to observed AFT dates of the entire Clark's Fork transect modeled as a vertical profile (Figure 8g).

Finally, we modeled an extensive set of AFT dates and track lengths (N = 26, n = 2.438) and AHe dates (N = 23, n = 2.438)n = 70) collected from the subsurface in the Amoco No. 1 Beartooth borehole and surface exposures near the Beartooth Highway by Omar et al. (1994) and Peyton et al. (2012; Figure 7e). Omar et al. (1994) modeled the post-80 Ma thermal history of samples from two end-member elevations using the Monte-Carlo approach of Lutz and Omar (1991), which suggested rapid cooling between ~60 and 55 Ma followed by either residence at or reburial to ≥50°C until ~10 Ma, after which samples cooled to the surface. Peyton et al. (2012) inverted three aliquots from one sample in HeFTy, which indicated ≥30°C of cooling between 74 and 41 Ma and didn't require later reheating. Our inversion approach combines samples from both previous studies into a single vertical profile. Our models indicate very rapid cooling between ~62 and ~50 Ma (Figure 7e), generally consistent with previous models (Omar et al., 1994; Peyton et al., 2012). However, our models apparently achieve greater sensitivity to the Cenozoic thermal history, favoring reburial to, rather than residence at, temperatures of $\geq 30^{\circ}$ C by 6 Ma. Most significantly, our inversion resolves a major cooling event initiating in Devonian time, not recognized by previous modeling efforts (Figure 7g). Paleozoic cooling is required to reproduce AFT dates of up to 282 ± 16 Ma and short MTLs in samples above 3 km ASL, which define a nearly flat date-elevation relationship (Figure 8h; we note that Cerveny (1990) documented dates of up to 348 ± 31 Ma at similar elevation, but we were unable to model his data due to insufficient reporting). Although Omar et al. (1994) reported Paleozoic AFT ages, they began their models at 80 Ma and consequently did not resolve the Paleozoic cooling recorded by their samples. The full model results for these transects (i.e., 2.812–0 Ma) are available in Figure S4 in Supporting Information S1; however, Precambrian thermal events therein are unresolved.

To assess the compatibility of the results of *t-T* inversions with the Phanerozoic sedimentary record preserved in nearby areas, we constructed a set of decompacted sediment accumulation models (Figure 7f). Details on the setup of decompacted sediment accumulation models are available in Text S5 and Table S3 in Supporting Information S1. Results show that the total decompacted thickness of all Phanerozoic sedimentary rocks is 4.13–5.47 km. Less than 0.57 km of sediment was deposited prior to Paleozoic cooling resolved by the Chalice Peak and Beartooth Highway/Amoco No. 1 borehole transects, which initiated during an Ordovician–Devonian depositional hiatus (~444–384 Ma) and persisted throughout the regional deposition of 0.78–0.86 km of Devonian–Pennsylvanian sediment (Figure 7). Assuming a typical geothermal gradient, early Paleozoic reheating temperatures indicated by these models cannot be accounted for based on burial reheating consistent with preserved stratigraphy alone, requiring additional overburden of unpreserved sediments or eroded basement. Initiation of cooling of the Beaten Path and Granite Peak transects at ~200 Ma occurred during a Triassic–late Jurassic deposition hiatus. Modeled Cretaceous reheating of the Beaten Path, Chalice Peak, and Beartooth Highway/Amoco No. 1 borehole transects is consistent with reburial by foreland basin deposits, which total 2.83–3.99 km of decompacted thickness. These results inform our interpretations of modeled Phanerozoic thermal events, discussed below.

5. Discussion

5.1. The Extent of Paleoproterozoic Thermotectonism in Southwest Montana

Biotite ⁴⁰Ar/³⁹Ar results from samples CP-01 and CP-05 comprise the easternmost instance of <1.8 Ga medium-temperature thermochronometer ages recognized in southwestern Montana and the first from the BBMP (Figures 1, 3, and 9; references in Figure 9 caption). These ages partially overlap with Paleoproterozoic (~1.78–1.72 Ga) thermotectonism observed within the Montana metasedimentary province, west of the Beartooth Mountains, where peak metamorphic conditions of ~0.8–1.2 Gpa and >700°C have been documented (Figure 9; e.g., Ault et al., 2012; Condit et al., 2015; Harms, Brady, et al., 2004). This episode of thermotectonism, known as the Big Sky orogeny, has been attributed to collision between the Wyoming and Medicine Hat cratons (i.e., part of the wider Great Falls orogeny; Mueller et al., 2002) and/or between the Wyoming craton and an arc terrane to the west (i.e., Selway terrane of Foster et al., 2006).

Previously documented evidence for thermal effects associated with the Big Sky orogeny is dominantly limited to basement exposures northwest of a northeast-trending transitional boundary, commonly referred to as "Giletti's

RONEMUS ET AL. 18 of 34

19449194, 2023, 1, Downloaded from https://agupubs.onlinelibrary.wiley.com/doi/10.1029/2022TC007541 by Devon Orme

- Montana State University Library, Wiley Online Library on [11/01/2023]. See the Terms and Condition

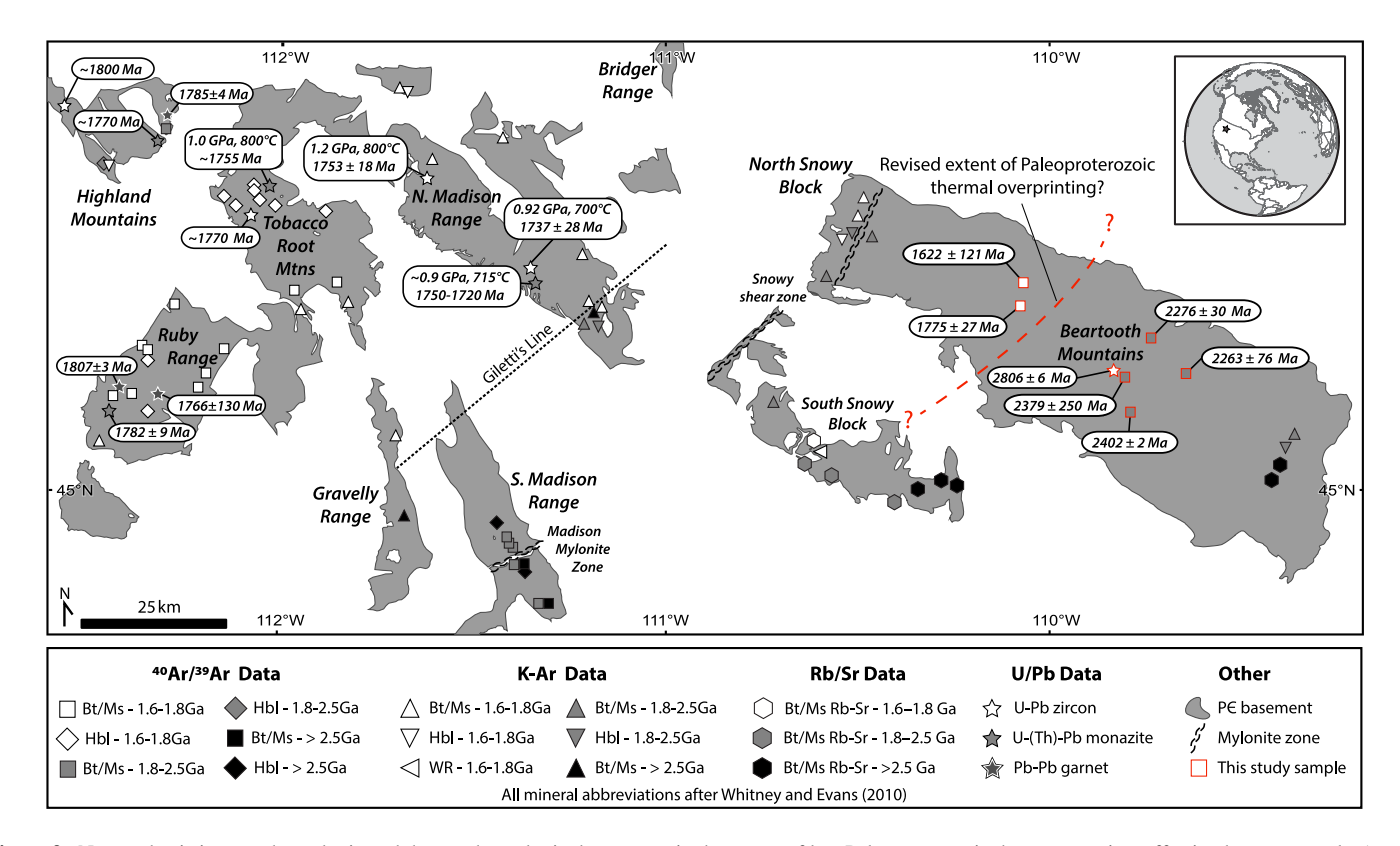


Figure 9. New and existing geochronologic and thermochronologic data constrain the extent of late Paleoproterozoic thermotectonism affecting basement rocks (gray polygons) in southwest Montana. Data from this study are outlined in red. Biotite ⁴⁰Ar/³⁹Ar data from this study are reported as plateau ages and associated uncertainty. Red dashed line denotes a schematic revised extent of Paleoproterozoic thermal overprinting suggested by our data. Data citations: ⁴⁰K/³⁹Ar—Giletti (1966, 1971) and Reid et al. (1975); ⁴⁰Ar/³⁹Ar—Erslev and Sutter (1990), Harlan et al. (1996), Roberts et al. (2002), Brady et al. (2004), Hames and Harms (2013), and this study; zircon U-Pb—Ault et al. (2012), Carrapa et al. (2019), Condit et al. (2015), and this study; monazite U-Th-Pb—Cheney et al. (2004), Alcock et al. (2013), and Condit et al. (2015); garnet Pb-Pb—Roberts et al. (2002), Cheney et al. (2004), Ault et al. (2012), and Condit et al. (2015); Rb-Sr—Reid et al. (1975) and Montgomery and Lytwyn (1984). WR—Whole Rock. Adapted from Condit et al. (2015).

line" (Figure 9; Condit et al., 2015; Giletti, 1966). However, excess Ar was later identified in samples from key localities originally used to define this boundary (Giletti, 1971). Biotite ⁴⁰Ar/³⁹Ar ages of <1.8 Ga observed in samples CP-01 and CP-05 require late Paleoproterozoic residence of these samples at temperatures above the biotite ⁴⁰Ar/³⁹Ar closure temperature (>300°C; Grove & Harrison, 1996; Figures 2 and 9). Constrained time-temperature inversions of the Beaten Path transect resolve an inflection from cooling to reheating approximately temporally coincident with the Big Sky orogeny (Figure 6b), suggesting this event may have also influenced the thermal history of eastern portions of the Beartooth Mountains. These results—in addition to previously documented partially reset K-Ar and Rb-Sr ages in the North and South Snowy blocks (Montgomery & Lytwyn, 1984; Reid et al., 1975)—suggest that reinterpretation of the position and nature of Giletti's line is warranted. Significant uncertainty remains regarding the extent and nature of late Paleoproterozoic tectonism in Montana and associated spatial patterns in medium-temperature thermochronometer ages (e.g., Condit et al., 2015; Harms, Burger, et al., 2004; Mueller et al., 2004). Further detailed thermochronologic work in the region may help resolve this period of uncertainty, contributing to improved understanding of the evolution of ancient orogenic systems.

${\bf 5.2.}\ \ Potential\ Triggers\ of\ Mesoproterozoic-Neoproterozoic\ Thermal\ Events$

Constrained models for all newly reported transects resolve reheating to $\geq 200^{\circ}\text{C}$ by early Ectasian time followed by cooling to $< 100^{\circ}\text{C}$ between late Ectasian and early Paleozoic time (Figures 6b, 6d, and 6f). In the following section, we discuss possible mechanisms driving inflections in this portion of the modeled thermal history. However, we note that unconstrained models do not ubiquitously resolve these inflections, suggesting they are not strictly required by the data. We focus discussion on the best resolved model aspects but emphasize interpretive caution given large model uncertainties.

RONEMUS ET AL. 19 of 34

The Beaten Path and Granite Peak transect suggest peak reheating by ~1.45 Ga, while that for the Chalice Peak transect occurs slightly later. The timing of this modeled reheating overlaps with deposition of Belt Supergroup units within the Helena Embayment (Figure 1), bracketed between 1.71 Ga and 1.42 Ga (e.g., Anderson & Davis, 1995; Hirtz et al., 2022; Mueller et al., 2016; Ross & Villeneuve, 2003). Preserved Mesoproterozoic sedimentary rocks in the Helena Embayment are structurally bound by the Perry line, a system of north-dipping Mesoproterozoic normal faults tracing ~50 km north of the Beartooth Mountains (e.g., Hatcher et al., 1987; McMannis, 1963; Ross & Villeneuve, 2003; Winston, 1986). Despite this, the occurrence of Mesoproterozoic talc deposits ~46-80 km south of the Perry line—defining a WNW-ESE striking "corridor" ~150 km southeast of the Beartooth Mountains-has been interpreted as evidence that the eastern Belt Basin originally extended south of this structural boundary (Anderson et al., 1990; Underwood et al., 2014). The detrital zircon record from the eastern Belt Supergroup is consistent with this interpretation. A paucity of ~2.8 Ga zircons in eastern Belt Supergroup units suggests the BBMP was not an important sediment source to the basin (Fox, 2017; Mueller et al., 2016; Ronemus et al., 2020), consistent with a lack of erosion of BBMP basement during Belt Supergroup deposition. Coupled with these lines of evidence, modeled Mesoproterozoic reheating of rocks in the Beartooth Mountains may support Mesoproterozoic deposition within the study area (Figure 6). In this context, the preserved extent of Belt Supergroup sediments may not reflect the original extent of the basin, but rather that of later erosional truncation. Later faulting along the Perry line may have contributed to erosional beveling of Mesoproterozoic rocks deposited in the hanging-wall of the fault system. We note that the biotite 40Ar/39Ar ages of our samples were not reset in Mesoproterozoic time (Figure 3), and models indicate ≤125°C of Mesoproterozoic reheating (Figure 6). Therefore, any Mesoproterozoic sediments deposited at the location of the study area must have been substantially thinner than the ~15 km of Mesoproterozoic stratigraphy preserved in western portions of the Belt Basin.

Following potential Mesoproterozoic reheating, constrained thermal history models indicate samples cooled from >200° C to <100°C between ~1.45 Ga and early Paleozoic time (Figure 6). Meso–Neoproterozoic cooling events are best resolved by models for the Beaten Path transect, which suggest an initial phase of cooling initiating ~1.45 \pm 0.5 Ga and a later inflection to more rapid cooling beginning ~0.8 \pm 0.2 Ga (Figure 6b). Only the former phase of cooling is well resolved by models for other transects (Figures 6d and 6f). This initial phase approximately coincides with the ~1.4 Ga rifting of western Laurentia associated with breakup of supercontinent Nuna, inferred from a reported disappearance of non-Laurentian detrital zircons in the upper Belt Supergroup (e.g., Ross & Villeneuve, 2003; Stewart et al., 2010; see recent debate in Parker & Hendrix, 2022). Similarly, the modeled inflection to more rapid cooling in Neoproterozoic time overlaps with an additional ~780 to \leq 680 Ma phase of rifting of the western Laurentian margin associated with the breakup of supercontinent Rodina (e.g., Brennan et al., 2020; Li et al., 2013; Link et al., 2017; Lund et al., 2010; Merdith et al., 2019).

Collectively, the observation that both modeled Meso–Neoproterozoic cooling events coincide with the timing of hypothesized rifting of the western Laurentian margin is consistent with a causal relationship between marginal rifting and the exhumation of cratonward basement rock. Resolving ~850–550 Ma cooling for the Madison and Ruby–Gravelly mountain ranges, 75–120 km west of the present study area, Kaempfer et al. (2021) suggested normal faulting associated with the rifting of western Laurentia caused erosional exhumation of horst blocks to the east. They hypothesized southwestern Montana was an eroding topographic high throughout late Neoproterozoic–early Cambrian time. Deep-time thermal history models from the Grand Canyon have similarly been interpreted to suggest a linkage between Rodinia breakup and erosion of the footwall blocks of rift-related normal faults (Peak et al., 2021), although later work showed this phase of cooling may not be required to reproduce observed ZHe dates (Thurston et al., 2022). Similar rifting processes associated with Nuna breakup may have triggered erosional exhumation of southwest Montana basement rock in Mesoproterozoic time as well, although samples apparently experienced reheating during initial phases of Mesoproterozoic normal faulting. We note that inversions of Kaempfer et al. (2021) did not resolve significant Mesoproterozoic reheating or cooling, but this may reflect that their model setup allowed only monotonic cooling during Proterozoic time. Additionally, their data set apparently lacked sensitivity to Mesoproterozoic thermal events, as demonstrated by forward models.

Notably, rifting related to supercontinent breakup is not the only process capable of explaining Neoproterozoic continental exhumation. The modeled cooling timing of basement rock in southwest Montana also temporally overlaps at model resolution with Cryogenian snowball Earth ice-sheet glaciation (~720–635 Ma; Goddéris et al., 2003; Kaempfer et al., 2021; Li et al., 2013). Recent QTQt *t-T* inversions by McDannell et al. (2022; remodeling data from DeLucia et al., 2018, Flowers et al., 2020, and McDannell & Flowers, 2020) highlighted

RONEMUS ET AL. 20 of 34

that late Neoproterozoic cooling was likely not isolated to regions near the western Laurentian margin. Rather, they resolved a similar timing of cooling for basement rock in interior regions of Laurentia, which would have been insulated from the thermal effects of rifting. Therefore, McDannell et al. (2022) argued that erosion associated with snowball Earth ice-sheet glaciation is more consistent with late Neoproterozoic exhumation across both marginal and interior regions of the continent.

In the absence of independent Neoproterozoic geologic constraints in the study area, the resolution of the present models is not sufficient to distinguish between the, notably temporally overlapping, potential cooling mechanisms of Laurentian rifting and snowball Earth glaciations. While continental-scale syntheses may favor ice sheet glaciation as a primary driver in interior portions of Laurentia (i.e., McDannell et al., 2022), rifting and glaciation are not mutually exclusive agents of erosional exhumation. Glaciers most effectively erode regions with preexisting topography, including topography generated by rift-related faulting (e.g., Walsh et al., 2019). Consequently, as most recently noted by McDannell et al. (2022), the "erosional synergy" between rift-related tectonism and ice sheet erosion remains a viable mechanism to explain rapid Neoproterozoic cooling and associated km-scale erosion in regions near the Laurentian margin, such as southwest Montana.

5.3. The Paleozoic Beartooth Mountains

Time-temperature inversions for the Chalice Peak and Beartooth Highway/Amoco No. 1 borehole transects indicate a phase of cooling initiating in early to middle Paleozoic time (Figures 7c and 7e). Modeled cooling temporally overlaps with the Devonian–Early Mississippian Antler orogeny and the Pennsylvanian–Permian ARM orogenic event (e.g., Beranek et al., 2016; Blakey & Ranney, 2018; Dorobek et al., 1991; Kluth & Coney, 1981; Maughan, 1990). Although the ARM event is widely credited as triggering intraforeland basement uplift from Oklahoma through Colorado (e.g., Kluth & Coney, 1981), its effects have been more sparsely documented further north (e.g., Maughan, 1990). Existing evidence includes southward thinning of Mississippian–Pennsylvanian units toward the Montana-Wyoming border, evident in isopach patterns (Maughan, 1993). Additionally, Maughan (1990) documented erosional unconformities and lithologic facies indicative of proximal terrigenous sediment sources in Pennsylvanian rocks near the Beartooth Mountains. This led him to suggest the existence of a subaerially exposed Pennsylvanian high approximately spatially coincident with the present study area, comprising one of the northernmost ARM uplifts. Our thermal history results support this hypothesis, consistent with active erosional exhumation of this high (Figures 7c and 7e).

While a Paleozoic cooling event is clearly required to reproduce AFT data of the Beartooth Highway transect (Figures 7e and 8h), the record thereof has gone unrecognized despite previous modeling by Omar et al. (1994). Our construction of a sufficiently deep-time thermal history model incorporating both AFT and AHe samples in a vertical profile and enforcing geologic constraints facilitated resolution of this newly documented cooling event from these previously reported data (Omar et al., 1994; Peyton et al., 2012). Similar modern inversion techniques applied to data sets from other nearby basement-cored ranges (e.g., Cerveny, 1990; Cerveny & Steidtmann, 1993; Peyton et al., 2012) may help further constrain cryptic Paleozoic cooling in the northern US Rocky Mountains.

5.4. Mesozoic-Cenozoic Growth of an Intraforeland Basement Uplift

Models for the Beaten Path and Granite Peak transects suggest the initiation of a cooling event near the Triassic–Jurassic transition (Figures 7a and 7b). There is little evidence for the influence of active tectonism in the southern Montana region during this time, with documented Early Jurassic shortening dominantly limited to the Luning-Fencemaker fold-and-thrust belt of northern Nevada and southeastern Idaho (e.g., Wyld, 2002). Instead, this cooling may be related to eustacy rather than tectonics; the Triassic–Jurassic transition coincides with the lowest global sea levels of Paleozoic–Mesozoic time (Marcilly et al., 2022). Low sea levels coupled with a lack of tectonic subsidence facilitated sub-aerial erosion of the continental margin, recorded by a widespread Permian or Triassic to Late Jurassic hiatus in the regional sedimentary record (e.g., Maughan, 1993). Alternatively, modeled Jurassic cooling may comprise a model artifact associated with underestimation of [U-Th(-Sm)]/He date uncertainties; models with larger uncertainty rescaling parameters tend to suggest Paleozoic and/or Cretaceous, rather than Jurassic, cooling events for these transects (Figure S4 in Supporting Information S1).

All models resolve rapid cooling ($\sim 1.2-20^{\circ}$ C/Myr) initiating during Early Cretaceous to Paleocene time (Figure 7). The Clark's Fork Canyon transect indicates the earliest cooling, initiating ≥ 110 Ma (Figure 7d;

RONEMUS ET AL. 21 of 34

Carrapa et al., 2019). This cooling significantly precedes that indicated by other transects and consequently may reflect localized exhumation which did not necessarily affect other portions of the range (Figure 10a). Structural analysis and mapping by Wise (1983) and DeCelles, Gray, Ridgway, Cole, Srivastava, et al. (1991) demonstrate that NW-SE striking faults—such as those defining the Cooke City sag zone near the southeastern margin of the range—were truncated by later slip along the main range-bounding fault system. The Clark's Fork canyon transect is located in the proximal hanging-wall of both fault systems. By contrast, the nearby Beartooth Highway/Amoco No. 1 borehole transect—recording cooling initiation ≥50 Myr later—resides in the proximal hanging-wall of only the main range-bounding fault system. Therefore, early cooling recorded by the Clark's Fork Canyon transect may be related to slip on the NW-SE striking system. These faults, oriented sub-parallel to the axis of the Bighorn Basin, may have slipped in response to flexure of the basin during incipient foredeep subsidence and/ or during passage of the flexural forebulge, recorded by a regional time-transgressive unconformity at the base of the Kootenai and Cloverly formations (e.g., DeCelles, 2004; DeCelles & Burden, 1992). Incipient Aptian-Albian intra-foreland uplift is consistent with paleocurrent deflections around the periphery of several southwest Montana basement uplifts-including the Beartooth Mountains-observed in the Lower Cretaceous Kootenai Formation (DeCelles, 1986). However, this interpretation was recently disputed by detrital zircon provenance work >100 km west of the study area, which did not find evidence for basement exhumation or significant partitioning of the foreland basin in southwestern-most Montana during Kootenai Formation deposition (Rosenblume et al., 2021).

Apart from the Clark's Fork Canyon transect, the timing of modeled cooling initiation generally decreases from west to east; the Chalice Peak and Granite Peak transects indicate an inflection to rapid cooling at ~90 Ma, while the Beaten Path and Beartooth Highway transects don't resolve the initiation of this cooling event until ~60 Ma (Figure 8). A decreasing age of cooling in the direction of fault growth and transport is compatible with models conceptualizing the growth of intraforeland basement arches through an overlapping sequence of detachment folding and layer-parallel shortening followed by fault-propagation and fault-bend folding (Figures 10b and 10c; e.g., Erslev et al., 2022; Weil & Yonkee, 2012).

Initial growth of the Beartooth uplift by the former processes may have localized initial uplift and exhumation in eastern portions of the range, consistent with ~95 Ma cooling resolved by models for the Chalice Peak and Granite Peak transects (Figure 10b). Thinning of Coniacian–Early Campanian foreland basin deposits near the incipient Beartooth uplift, evident from isopach patterns, supports the development of positive relief by at least ~90 Ma (Eichler et al., 2020). However, there is no conclusive record of sediment eroding off the Beartooth Mountains until Paleocene time (DeCelles, Gray, Ridgway, Cole, Srivastava, et al., 1991). Earlier uplift of the Beartooth Mountains may have entailed recycling of mainly fine-grained deposits, which were bypassed to distal regions. Proximal accumulation likely did not occur until erosion had exhumed more resistant lithologies and/ or the uplift had reached sufficient size to trigger localized flexural subsidence on its periphery (DeCelles, Gray, Ridgway, Cole, Srivastava, et al., 1991; Dickinson et al., 1988).

During later growth of the main Beartooth Fault, NNE-directed thrusting and associated fault-propagation folding would have focused exhumation on the steep northeastern forelimb (Figure 10c). There, the Beaten Path and Beartooth Highway/Amoco No. 1 borehole transects record rapid cooling between ∼62 and ∼50 Ma, coeval with the timing of growth structure development in the Beartooth Conglomerate (DeCelles, Gray, Ridgway, Cole, Srivastava, et al., 1991; Figure 10c). The lack of major surface-breaking faulting until Paleocene time is further supported by cross-cutting of Turonian–Coniacian (Cody Shale; ≤96.5 Ma; May et al., 2013; Wise, 2000) and likely late Maastrichtian (Lance Formation; ≤67 Ma; Hicks et al., 2002; DeCelles, Gray, Ridgway, Cole, Srivastava, et al., 1991) rocks by the main range-bounding fault. This thrusting folded Phanerozoic strata into a recumbent and tectonically attenuated footwall syncline and generated complex structures at the northeast corner of the uplift (e.g., Wise, 2000), comprising a crescendo in the uplift of the Beartooth Mountains (Figure 10c).

5.5. Implications for Models of Laramide Tectonism

In the previous sections, we suggested that Phanerozoic exhumation and associated cooling in the Beartooth Mountains was a result of protracted tectonism on the margins of Laurentia spanning >300 Myr and culminating in the development of the North American Cordillera. While the previously documented Late Cretaceous—Paleocene phase of rapid cooling was the most significant of these events (e.g., DeCelles, Gray, Ridgway, Cole, Srivastava, et al., 1991; Omar et al., 1994; Peyton et al., 2012), it likely records only an inflection superimposed

RONEMUS ET AL. 22 of 34

19449 194, 2023, 1, Downloaded from https://agupubs.onlinelibrary.wiley.com/doi/10.1029/2022TC007541 by Devon Orme - Montana State University Library, Wiley Online Library on [1101/2023]. See the Terms and Conditions (th

onditions) on Wiley Online Library for rules of use; OA articles are governed by the applicable Creative Commons Licens

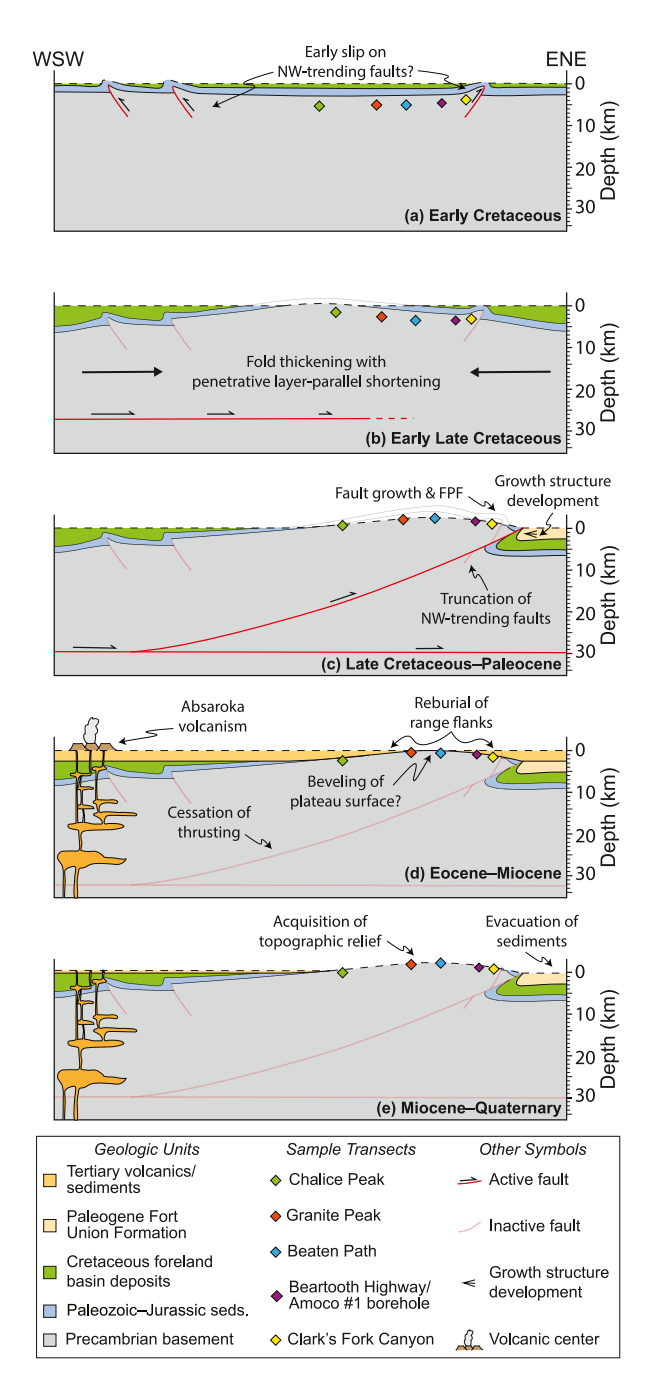


Figure 10. Schematic kinematic evolution of the Beartooth Mountains consistent with results of thermal history inversions. (a) Early Cretaceous deformation involved low-magnitude slip on thrust faults with a dominantly NW−SE trend. Samples in the Clark's Fork Canyon transect, located in the proximal hanging-wall of one such fault, experienced cooling. (b) Early fault-related folding, likely related to detachment folding and layer-parallel slip, uplifted and exhumed rocks in the southwestern portions of the range, recorded by the Chalice Peak and Granite Peak transects as cooling initiating ~95 Ma. Exhumation was poorly preserved in the sedimentary record due to sediment bypassing (e.g., DeCelles, Gray, Ridgway, Cole, Srivastava, et al., 1991; Hoy & Ridgway, 1997). (c) Growth of the main Beartooth fault triggered fault-propagation and fault-bend folding. Transects in the northeastern portion of the range experienced rapid exhumation and cooling. Deformation was recorded by the development of growth structures in the Paleogene Beartooth Conglomerate (DeCelles, Gray, Ridgway, Cole, Srivastava, et al., 1991). Total structural relief of ≥8 km was achieved (Blackstone, 1986). (d) Shortening ceased by early Eocene time. Reburial by Eocene Absaroka volcanics and/or by Oligocene–Miocene sediments caused reheating of transects near the flanks of the range. The Beartooth Plateau paleo-surface may reflect beveling of high topography to the regional basin elevation during this time. (e) Evacuation of Cenozoic sediments from the foreland re-exhumed the range flanks, resulting in the acquisition of significant topographic relief. Scales at right reflect depth below regional basin elevation at each time step. The growth of the Beartooth uplift in (b) and (c) is based after two-stage model of Erslev et al. (2022). Depth to detachment is schematic.

RONEMUS ET AL. 23 of 34

on a longer and more complex Phanerozoic cooling history. Here, we discuss potential implications for the tectonic/geodynamic mechanism(s) of intraforeland basement uplift these results entail.

Original consensus on the timing of the "Laramide" intraforeland basement uplift *sensu* Armstrong (1968) and Dickinson and Snyder (1978) favored mid-Campanian (~75 Ma) initiation. In this interpretation, the initiation of basement deformation was approximately coeval with the hypothesized timing of shallowing of the Farallon slab below North America, as recorded in part by shutdown and eastward migration of the Sierra Nevada arc and localized deep foreland subsidence (e.g., Coney & Reynolds, 1977; Cross & Pilger, 1978; Lipman et al., 1971). At the latitude of the study area, apparent northeastward magmatic migration between 80 and 55 Ma has similarly been interpreted to reflect slab flattening (Constenius et al., 2003; Copeland et al., 2017; Lageson et al., 2001; Lund et al., 2002). Due in part to the ostensible similarity in timing between intraforeland basement uplift and proxies for slab flattening, most leading geodynamic models attribute Laramide basement uplift to some variety of interaction between a shallowly subducting Farallon slab and the overriding North American plate, including basal traction from a flat Farallon slab (e.g., Bird, 1984, 1998; Copeland et al., 2017; Dickinson & Snyder, 1978; Heller & Liu, 2016; Lawton, 2019), oceanic plateau(s) thereon (e.g., Liu et al., 2010; Livaccari et al., 1981), or associated hydration and lithospheric weakening of the North American lithosphere (e.g., Humphreys et al., 2003; Saylor et al., 2020).

However, recent timing constraints from southwest Montana and northern Wyoming demonstrate basement uplift in the region likely initiated significantly prior to the inferred timing of regional insertion of a flat slab. Steidtmann and Middleton (1991) presented evidence for uplift in the Wind River Range as early as 110 Ma, which to them "suggest(ed) either a pre-Laramide event of unknown origin or that Laramide crustal shortening began nearly 35 Myr earlier than commonly assumed." In southwest Montana, sedimentologic and thermochronologic work has produced additional evidence for Aptian–Coniacian exhumation of several basement uplifts—including the Highland, Madison, Blacktail-Snowcrest, and Beartooth mountains (Carrapa et al., 2019; DeCelles, 1986; Garber et al., 2020; Haley, 1985; Ronemus & Orme, 2022; summarized by Orme, 2020). Our results add additional thermochronologic evidence suggesting likely fault-related exhumation of the Beartooth Mountains by at least ~90 Ma. If 80–55 Ma eastward magmatic migration in southwest Montana accurately reflects the timing of regional flat slab subduction, this developing consensus implies initial basement uplift preceded the arrival of a flat slab by ≥10 Myr (e.g., Carrapa et al., 2019; Garber et al., 2020; this study). This observation presents an obstacle for the former theories.

Other models more consistent with ≥90 Ma basement uplift include the propagation of basement deformation ahead of the developing flat slab (e.g., Kulik & Schmidt, 1988), potentially as a result of plate margin end loading driving far-field compression (e.g., Axen et al., 2018; Behr & Smith, 2016; Erslev et al., 2022; Jackson et al., 2019; Livaccari & Perry, 1993; Thacker et al., 2022). Alternatively, early basement deformation in southwest Montana may be largely unrelated to flat-slab subduction. In this case, deformation may be linked to injection of ductile lower crust from the fold-thrust belt (e.g., McQuarrie & Chase, 2000), the transmission of hinterland stresses (e.g., Erslev, 1993; Livaccari, 1991), terrane accretion/translation (e.g., Maxson & Tikoff, 1996; Tikoff et al., 2016), and/or the interaction between the retroarc fold-thrust belt and preexisting stratigraphic (Parker & Pearson, 2021) and/or basement architecture (Tavani et al., 2021). Although these models make less specific and/or more compatible predictions for the timing of basement uplift in southwest Montana and northern Wyoming, they have difficulty accounting for observed eastward migrating magmatism, aspects of basement uplift strain distribution, and foreland subsidence patterns (Bird, 1984, 1998; Coney & Reynolds, 1977; Constenius et al., 2003; Erslev et al., 2022). Given the emerging geologic and thermochronologic evidence contesting the dominant Laramide flat-slab paradigm, future regional syntheses examining the timing of basement uplift in southwest Montana are uniquely poised to test these alternative geodynamic models.

5.6. Evidence for Eocene-Miocene Reburial and Neogene Development of Relief

Model results indicate the termination of rapid cooling likely associated with basement uplift by ~ 50 Ma (Figure 7), approximately coincident with a regional shift from compressional to extensional deformation (e.g., Foster & Mark Fanning, 1997; Foster et al., 2001, 2010; Howlett et al., 2021). This transition in tectonic regime is associated with a widespread phase of volcanism (i.e., ignimbrite flare-up; Best et al., 2016). Ignimbrite volcanism is locally represented by the $\sim 53-43$ Ma Absaroka Volcanic Supergroup, which is preserved in sections up to several kilometers thick overlying the southern portion of the modern Beartooth Mountains and the Absaroka

RONEMUS ET AL. 24 of 34

Mountains to the south (Figures 2 and 10d; e.g., Feeley, 2003; Feeley & Cosca, 2003; Hiza, 1999). Model results from the Chalice Peak, Clark's Fork Canyon, and Beartooth Highway/Amoco No. 1 borehole transects indicate \sim 20°C–45°C of reheating in Eocene to Miocene time (Figures 7c–7e). Although Eocene volcanics are not currently preserved outside the southern flanks of the Beartooth Mountains, this may suggest their original extent was more expansive, burying portions of the Beartooth Mountains further north (Figure 10d), as hypothesized by Carrapa et al. (2019). Reheating coeval with eruption of the Absaroka Volcanic Supergroup is best resolved by the Chalice Peak transect, which indicates temperatures of 110° C \pm 30°C at 50 \pm 5 Ma (Figure 7c) are required to reproduce a pediment of ZHe dates spanning \sim 60–20 Ma at \sim 400–1,200 ppm eU (Figure 8f).

Model results for the Clark's Fork Canyon and Beartooth Highway/Amoco No. 1 borehole transects indicate Cenozoic reheating continued until at least 20 Ma (Figure 7d) and possibly 6 Ma (Figure 7e), suggesting reheating was longer-lived than Eocene volcanism. Later stages of modeled reheating may be instead associated with burial by Oligocene-Miocene sedimentary rocks, as first proposed in the Beartooth Mountains by Omar et al. (1994). Erosional remnants of rocks of this age (South Pass, White River, and Arikaree formations) have been identified at high elevation (≥2.2 km ASL) in the Bighorn and Wind River mountains, WY (McKenna, 1980; McKenna & Love, 1972; Steidtmann & Middleton, 1991; Steidtmann et al., 1989). McKenna and Love (1972) argued that the Bighorn Mountains were buried to the present ~2.7 km elevation by these sediments—an interpretation consistent with recent thermochronologic work in the range (Caylor & Carrapa, 2021). Although similar deposits have not been recognized in the Beartooth Mountains, crude extrapolation of McKenna & Love's (1972) estimate of Tertiary basin elevation in the Bighorn Mountains (~2.7 km ASL) to equivalent modern elevations in the present study area yields total burial of the Clark's Fork Canyon transect (1.48-2.23 km ASL) and near-total burial of the Beartooth Highway/Amoco No. 1 borehole transect (-1.87-3.33 km ASL); other transects not resolving Oligocene-Miocene reheating remain largely or wholly above this hypothetical Tertiary basin elevation. Therefore, it is consistent with regional geologic and thermochronologic evidence that at least the eastern flank of the Beartooth Mountains was reburied by Oligocene-Miocene intermontane sedimentary deposits. In this context, the Beartooth Plateau—with an average modern elevation of ~3 km—may represent an Oligocene–Miocene paleo-surface, analogous to similar Cenozoic erosional surfaces recognized at high elevation in the Colorado Front Range (Epis & Chapin, 1975; McMillan, 2003 and references therein). In this case, the Oligocene–Miocene relief of the Beartooth Mountains was likely on the order of <1 km, with only peaks of >3 km modern elevation exposed above the basin floor.

The most recent phase of cooling recorded by the Clark's Fork Canyon and Beartooth Highway/Amoco No. 1 borehole transects (Figures 7d and 7e) suggests that the erosion of Cenozoic sedimentary rocks initiated between ~20 and 6 Ma. Exhumation likely occurred as these cover rocks were evacuated from the foreland along one or multiple continental-scale paleo-drainage systems (e.g., Corradino et al., 2021; Galloway et al., 2011; Sears, 2013). Considerable debate exists concerning the relative roles of extensional tectonism versus climate change in driving late Cenozoic large-scale drainage reorganization and basin evacuation (e.g., Galloway et al., 2011; McMillan, 2003; McMillan et al., 2006; Sears, 2013). Regardless of the mechanism, our results in addition to other recent thermochronologic data (Caylor & Carrapa, 2021) emphasize that, while the structural relief of ranges in the northern Laramide foreland was likely developed by Paleogene time, their modern topographic relief (≥2.5 km in the Beartooth Mountains) is a more recent, Neogene feature.

6. Conclusions

We demonstrate the utility of a Bayesian approach constrained by multiple thermochronometers in reconstructing complex deep-time thermal histories involving multiple periods of reheating and cooling. An extensive geo/thermochronologic data set of samples from a range of elevations and positions—including dispersed but systematically correlated ZHe dates—facilitates the exploration of complex thermal events that are unresolvable by conventional geochronologic or thermochronologic techniques alone. Our results show evidence of previously unrecognized thermal events affecting rocks of the Beartooth Mountains and constrain the timing and magnitude of documented burial and exhumation episodes, including:

 Western regions of Beartooth Mountains experienced late Paleoproterozoic temperatures above the biotite ⁴⁰Ar/³⁹Ar closure window (>300°C), likely associated with the Big Sky orogeny (e.g., Condit et al., 2015; Harms, Brady, et al., 2004; Harms et al., 2006). These results suggest the thermal effects of this

RONEMUS ET AL. 25 of 34

19449194, 2023, 1, Downl



- Paleoproterozoic tectonism penetrated significantly (~100 km) further east than previously recognized (e.g., Condit et al., 2015; Giletti, 1966).
- 2. Early Mesoproterozoic reheating is indicated for all newly reported constrained models. This is consistent with previous hypotheses for deposition of Belt Supergroup sediments south of their preserved extent (Underwood et al., 2014).

Tectonics

- 3. Model results suggest late Mesoproterozoic and potentially late Neoproterozoic cooling events. The timing of both events overlaps with separate rifting episodes on the western Laurentian margin, consistent with previous hypotheses for rifting-induced exhumation of cratonic basement in the region (Kaempfer et al., 2021). However, model uncertainty is large and Neoproterozoic cooling overlaps with the timing snowball Earth ice-sheet glaciation, another possible driver of continental erosion (e.g., McDannell et al., 2022).
- 4. Models resolve reheating to maximum Phanerozoic temperatures by Devonian time, followed by an episode of later Paleozoic cooling. This cooling is contemporaneous with the Antler and ARM orogenic events, suggesting an episode of tectonic exhumation broadly consistent with sedimentologic and stratigraphic observations (Dorobek et al., 1991; Maughan, 1990). Our data provide the first thermochronologic evidence that the Beartooth Mountains experienced thermal effects associated with Paleozoic tectonism and suggest associated deformation penetrated further into the foreland than formerly appreciated.
- 5. A second phase of Phanerozoic cooling records complex, spatially variable Cretaceous-Paleogene exhumation. We suggest Early Cretaceous cooling reported by Carrapa et al. (2019) was localized, possibly due to minor slip of NW-SE striking faults accommodating flexural stresses in the evolving foreland basin. More widespread exhumation of the range likely initiated in Late Cretaceous time and progressed from west to east. Uplift of the Beartooth Mountains reached a crescendo in Paleocene time, when surface-breaking thrusting triggered very rapid exhumation concentrated near the northeastern range front. Fault-related basement uplift likely initiated ≥90 Ma and preceded the hypothesized arrival of a shallowly subducting slab, adding to a growing number of similar observations requiring reconsideration of canonical flat-slab models for intraforeland basement uplift in the North American Cordillera. Our results help to reconcile previous observations indicating Early Cretaceous uplift of the Beartooth Mountains (e.g., Carrapa et al., 2019; DeCelles, 1986; Schwartz & Decelles, 1988) with those only resolving Late Cretaceous-Paleocene phases of this cooling history (Cerveny, 1990; Omar et al., 1994; Peyton et al., 2012). We suggest the well-documented latter event may reflect only the late stage of a more complex cooling history associated with the development of the orogenic system.
- 6. Data from transects near the margins of the main Beartooth block indicate Cenozoic reheating. This reheating was likely due to reburial by Eocene Absaroka volcanics (e.g., Carrapa et al., 2019) and/or Oligocene—Miocene basin fill (e.g., McKenna & Love, 1972; Omar et al., 1994) and suggests much of the modern topographic relief of the Beartooth Mountains was acquired in Neogene time.

Data Availability Statement

Zircon U-Pb, biotite ⁴⁰Ar/³⁹Ar, ZHe, and AHe data sets, alongside supplementary text and figures referenced in the main text, are available in Supporting Information S1 for this paper. Large files supporting this work, comprising QTQt modeling files (Data Set S6) and grain photographs (Data Set S4), are available on Zenodo (https://doi.org/10.5281/zenodo.7443913). Analytical data sets may also be accessed using this DOI on Zenodo.

References

- Alcock, J., Muller, P. D., & Jercinovic, M. J. (2013). Monazite ages and pressure–temperature–time paths from anatectites in the southern Ruby range, Montana, USA: Evidence for delamination, ultramafic magmatism, and rapid uplift at ca. 1780 Ma. Canadian Journal of Earth Sciences, 50(11), 1069–1084. https://doi.org/10.1139/cjes-2013-0035
- Anderson, D. L., Mogk, D. W., & Childs, J. F. (1990). Petrogenesis and timing of talc formation in the Ruby Range, southwestern Montana. Economic Geology, 85(3), 585–600. https://doi.org/10.2113/gsecongeo.85.3.585
- Anderson, H. E., & Davis, D. W. (1995). U–Pb geochronology of the Moyie sills, Purcell Supergroup, southeastern British Columbia: Implications for the Mesoproterozoic geological history of the Purcell (belt) basin. Canadian Journal of Earth Sciences, 32(8), 1180–1193. https://doi.org/10.1139/e95-097
- Armstrong, E. (1968). Sevier orogenic belt in Nevada and Utah. GSA Bulletin, 79(4), 429–458. https://doi.org/10.1130/0016-7606(1968)79[42 9:SOBINA]2.0.CO;2
- Ault, A. K., Flowers, R. M., & Mahan, K. H. (2012). Quartz shielding of sub-10 µm zircons from radiation damage-enhanced Pb loss: An example from a metamorphosed mafic dike, northwestern Wyoming craton. *Earth and Planetary Science Letters*, 339(340), 57–66. https://doi.org/10.1016/j.epsl.2012.04.025

Acknowledgments

We would like to thank David Mogk for contributing his expertise on the geology of the Beartooth Mountains and Andrew Laskowski for sharing his regional expertise during drafting of this manuscript. This work additionally benefitted from conversations with Caden Howlett, Stuart Parker, Alyssa Abbey, and Kendra Murray. We would also like to thank Sidney Hemming and the staff of the Argon Geochronology for the Earth Sciences Laboratory at Columbia University (New York, NY, USA) for assistance with the generation and interpretation of biotite 40Ar/39Ar data. We thank the Arizona LaserChron Center (Tucson, AZ, USA) for assistance with the generation of zircon U-Pb data, the CU TRaIL laboratory (Boulder, CO, USA) for assistance with generation of apatite (U-Th-Sm)/He data, and Linda Angeloni at the UIUC Helium Analysis Laboratory (Urbana, IL, USA) for assistance with generation of zircon (U-Th)/He data. Funding for this research was provided by Montana State University and the Tobacco Root Geological Society. WRG acknowledges NSF-EAR Grant 1735788 for laboratory support. We would like to thank Emily Finzel Kalin McDannell and an anonvmous reviewer for their reviews of this manuscript, which greatly improved its quality.

RONEMUS ET AL. 26 of 34

19449194, 2023, 1, Downl

Tectonics

- Ault, A. K., Guenthner, W. R., Moser, A. C., Miller, G. H., & Refsnider, K. A. (2018). Zircon grain selection reveals (de)coupled metamictization, radiation damage, and He diffusivity. *Chemical Geology*, 490, 1–12. https://doi.org/10.1016/j.chemgeo.2018.04.023
- Axen, G. J., van Wijk, J. W., & Currie, C. A. (2018). Basal continental mantle lithosphere displaced by flat-slab subduction. *Nature Geoscience*, 11(12), 961–964. https://doi.org/10.1038/s41561-018-0263-9
- Ayers, W. B., Jr. (1986). Lacustrine and fluvial-deltaic depositional systems, Fort Union Formation (Paleocene), Powder River Basin, Wyoming and Montana 1. AAPG Bulletin, 70(11), 1651–1673. https://doi.org/10.1306/94886C90-1704-11D7-8645000102C1865D
- Baadsgaard, H., & Mueller, P. A. (1973). K-Ar and Rb-Sr ages of intrusive Precambrian maric rocks, southern Beartooth Mountains, Montana and Wyoming. GSA Bulletin, 84(11), 3635–3644. https://doi.org/10.1130/0016-7606(1973)84<3635:KARAOI>2.0.CO;2
- Baughman, J. S., & Flowers, R. M. (2018). Deciphering a 2 Gyr-long thermal history from a Multichronometer (U-Th)/He study of the Phalaborwa Carbonatite, Kaapvaal Craton, south Africa. Geochemistry, Geophysics, Geosystems, 19(5), 1581–1594. https://doi.org/10.1029/2017GC007198
- Baughman, J. S., & Flowers, R. M. (2020). Mesoproterozoic burial of the Kaapvaal craton, southern Africa during Rodinia supercontinent assembly from (U-Th)/He thermochronology. Earth and Planetary Science Letters, 531, 115930. https://doi.org/10.1016/j.epsl.2019.115930
- Behr, W. M., & Smith, D. (2016). Deformation in the mantle wedge associated with Laramide flat-slab subduction. Geochemistry, Geophysics, Geosystems, 17(7), 2643–2660. https://doi.org/10.1002/2016GC006361
- Beranek, L. P., Link, P. K., & Fanning, C. M. (2016). Detrital zircon record of mid-Paleozoic convergent margin activity in the northern U.S. Rocky Mountains: Implications for the Antler orogeny and early evolution of the North American Cordillera. *Lithosphere*, 8(5), 533–550. https://doi.org/10.1130/L557.1
- Berg, R. B., Lonn, J. D., & Locke, W. W. (1999). Geologic map of the Gardiner 30' × 60' quadrangle, South-Central Montana (open file report no. 387) (p. 1). Montana Bureau of Mines and Geology.
- Berg, R. B., Lopez, D. A., & Lonn, J. D. (2000). Geologic map of the Livingston 30' × 60' quadrangle, south-central Montana (open file report no. 406) (p. 21). Montana Bureau of Mines and Geology.
- Best, M. G., Christiansen, E. H., de Silva, S., & Lipman, P. W. (2016). Slab-rollback ignimbrite flareups in the southern Great basin and other Cenozoic American arcs: A distinct style of arc volcanism. *Geosphere*, 12(4), 1097–1135. https://doi.org/10.1130/GES01285.1
- Bird, P. (1984). Laramide crustal thickening event in the Rocky Mountain foreland and Great Plains. *Tectonics*, 3(7), 741–758. https://doi.org/10.1029/TC003i007p00741
- Bird, P. (1998). Kinematic history of the Laramide orogeny in latitudes 35°-49°N, western United States. *Tectonics*, 17(5), 780-801. https://doi.org/10.1029/98TC02698
- Blackstone, D., Jr. (1986). Structural geology—Northwest margin, Bighorn basin: Park County, Wyoming and Carbon County, Montana. In P. B. Garrison (Ed.), Geology of the Beartooth uplift and adjacent basins: Montana Geological Society and Yellowstone Bighorn Research Association field conference and symposium (pp. 125–135).
- Blakey, R. C., & Ranney, W. D. (2018). The Antler orogeny and the first suspect terrane: Middle devonian to late Pennsylvanian: Ca. 400–300 Ma. In R. C. Blakey & W. D. Ranney (Eds.), Ancient landscapes of western North America: A geologic history with paleogeographic maps (pp. 73–82). Springer International Publishing, https://doi.org/10.1007/978-3-319-59636-5_5
- Bowring, S., Myrow, P., Landing, E., Ramezani, J., & Grotzinger, J. (2003). Geochronological constraints on terminal Neoproterozoic events and the rise of Metazoan. In EGS-AGU-EUG joint assembly.13219.
- Brady, J. B., Kovaric, D. N., Cheney, J. T., Jacob, L. J., & King, J. T. (2004). 40 Ar/39 Ar ages of metamorphic rocks from the Tobacco Root Mountains region, Montana. In J. B. Brady, H. R. Burger, J. T. Cheney, & T. A. Harms (Eds.), Precambrian geology of the Tobacco Root Mountains, Montana: Geological Society of America special paper 377 (pp. 131–149).
- Brennan, D. T., Pearson, D. M., Link, P. K., & Chamberlain, K. R. (2020). Neoproterozoic Windermere Supergroup near Bayhorse, Idaho: Late-stage Rodinian rifting was deflected west around the Belt Basin. *Tectonics*, 39(8), e2020TC006145. https://doi.org/10.1029/2020TC006145
- Bricker, A. L. (2016). (U-Th)/He thermochronology of the Yellowstone crescent high terrain: Implications for Miocene to recent topographic impacts associated with the Yellowstone hotspot (Masters thesis). University of Florida.
- Brown, R. W., Beucher, R., Roper, S., Persano, C., Stuart, F., & Fitzgerald, P. (2013). Natural age dispersion arising from the analysis of broken crystals. Part I: Theoretical basis and implications for the apatite (U–Th)/He thermochronometer. *Geochimica et Cosmochimica Acta*, 122, 478–497. https://doi.org/10.1016/j.gca.2013.05.041
- Carrapa, B., DeCelles, P. G., & Romero, M. (2019). Early inception of the Laramide orogeny in southwestern Montana and northern Wyoming: Implications for models of flat-slab subduction. *Journal of Geophysical Research: Solid Earth*, 124(2), 2102–2123. https://doi. org/10.1029/2018JB016888
- Caylor, E., & Carrapa, B. (2021). Late Cretaceous-Eocene exhumation history of the Bighorn Mountains, WY: Implications for Laramide tectonics. In *Intersection & integration—Part 3: Oral presentations & discussion: The 18th international conference on thermochronology, Santa Fe, New Mexico.*
- Cerveny, P. F. (1990). Fission-track thermochronology of the Wind River Range and other basement cored uplifts in the Rocky Mountain foreland (Ph.D. Thesis). University of Wyoming.
- Cerveny, P. F., & Steidtmann, J. R. (1993). Fission track thermochronology of the Wind River Range, Wyoming: Evidence for timing and magnitude of Laramide exhumation. *Tectonics*, 12(1), 77–91. https://doi.org/10.1029/92TC01567
- Chamberlain, K. R., Frost, C. D., & Frost, B. R. (2003). Early Archean to Mesoproterozoic evolution of the Wyoming Province: Archean origins to modern lithospheric architecture. Canadian Journal of Earth Sciences, 40(10), 1357–1374. https://doi.org/10.1139/e03-054
- Chaudhuri, S., & Brookins, D. G. (1969). The isotopic age of the Flathead sandstone (Middle Cambrian), Montana. *Journal of Sedimentary Research*, 39(1), 364–366. https://doi.org/10.1306/74D71C76-2B21-11D7-8648000102C1865D
- Cheney, J. T., Webb, A. A. G., Coath, C. D., & McKeegan, K. D. (2004). In situ ion microprobe ²⁰⁷Pb/²⁰⁶Pb dating of monazite from Precambrian metamorphic suites, Tobacco Root Mountains, Montana. In Special paper 377: Precambrian geology of the Tobacco Root Mountains, Montana (Vol. 377, pp. 151–179). Geological Society of America. https://doi.org/10.1130/0-8137-2377-9.151
- Colpron, M., Nelson, J. L., & Murphy, D. C. (2007). Northern Cordilleran terranes and their interactions through time. Geological Society of America Today, 17(4), 4. https://doi.org/10.1130/GSAT01704-5A.1
- Condie, K. C., Leech, A. P., & Baadgaard, H. (1969). Potassium-argon ages of Precambrian mafic dikes in Wyoming. GSA Bulletin, 80(5), 899. https://doi.org/10.1130/0016-7606(1969)80[899:PAOPMD]2.0.CO;2
- Condit, C. B., Mahan, K. H., Ault, A. K., & Flowers, R. M. (2015). Foreland-directed propagation of high-grade tectonism in the deep roots of a Paleoproterozoic collisional orogen, SW Montana, USA. Lithosphere, 7, 625. https://doi.org/10.1130/L460.1
- Coney, P. J., & Reynolds, S. J. (1977). Cordilleran benioff zones. Nature, 270(5636), 403-406. https://doi.org/10.1038/270403a0

RONEMUS ET AL. 27 of 34

Tectonics

- Constenius, K. N., Esser, R. P., & Layer, P. W. (2003). Extensional collapse of the Charleston-Nebo salient and its relationship to space-time variations in Cordilleran orogenic belt tectonism and continental stratigraphy. Rocky Mountain Section (SEPM).
- Cooperdock, E. H. G., Ketcham, R. A., & Stockli, D. F. (2019). Resolving the effects of 2-D versus 3-D grain measurements on apatite (U–Th-Sm)/He age data and reproducibility. *Geochronology*, 1(1), 17–41. https://doi.org/10.5194/gchron-1-17-2019
- Copeland, P., Currie, C. A., Lawton, T. F., & Murphy, M. A. (2017). Location, location, location: The variable lifespan of the Laramide orogeny. Geology, 45(3), 223–226. https://doi.org/10.1130/G38810.1
- Corradino, J. I., Pullen, A., Leier, A. L., Barbeau, D. L., Jr., Scher, H. D., Weislogel, A., et al. (2021). Ancestral trans–North American Bell River system recorded in late Oligocene to early Miocene sediments in the Labrador Sea and Canadian Great Plains. *GSA Bulletin*, 134(1–2), 130–144. https://doi.org/10.1130/B35903.1
- Cross, T. A., & Pilger, R. H. (1978). Tectonic controls of Late Cretaceous sedimentation, western interior, USA. Nature, 274(5672), 653–657. https://doi.org/10.1038/274653a0
- DeCelles, P. G. (1986). Sedimentation in a tectonically partitioned, nonmarine foreland basin: The Lower Cretaceous Kootenai Formation, southwestern Montana. GSA Bulletin, 97(8), 911–931. https://doi.org/10.1130/0016-7606(1986)97<911:SIATPN>2.0.CO;2
- DeCelles, P. G. (2004). Late Jurassic to Eocene evolution of the Cordilleran thrust belt and foreland basin system, western U.S.A. American Journal of Science, 304(2), 105–168. https://doi.org/10.2475/ajs.304.2.105
- DeCelles, P. G., & Burden, E. T. (1992). Non-marine sedimentation in the overfilled part of the Jurassic-Cretaceous Cordilleran foreland basin:

 Morrison and Cloverly Formations, central Wyoming, USA. Basin Research, 4(3–4), 291–314. https://doi.org/10.1111/j.1365-2117.1992.
- DeCelles, P. G., Gray, M. B., Ridgway, K. D., Cole, R. B., Srivastava, P., Pequera, N., & Pivnik, D. A. (1991). Kinematic history of a foreland uplift from Paleocene synorogenic conglomerate, Beartooth Range, Wyoming and Montana. GSA Bulletin, 103(11), 1458–1475. https://doi.org/10.1130/0016-7606(1991)103<1458:KHOAFU>2.3.CO;2
- Deiss, C. (1938). Cambrian formations and sections in part of Cordilleran trough. GSA Bulletin, 49(7), 1067–1168. https://doi.org/10.1130/GSAB-49-1067
- DeLucia, M. S., Guenthner, W. R., Marshak, S., Thomson, S. N., & Ault, A. K. (2018). Thermochronology links denudation of the Great Unconformity surface to the supercontinent cycle and snowball Earth. *Geology*, 46(2), 167–170. https://doi.org/10.1130/G39525.1
- Dickinson, W. R. (2004). Evolution of the North American Cordillera. Annual Review of Earth and Planetary Sciences, 32(1), 13–45. https://doi.org/10.1146/annurey.earth.32.101802.120257
- Dickinson, W. R., Klute, M. A., Hayes, M. J., Janecke, S. U., Lundin, E. R., McKittrick, M. A., & Olivares, M. D. (1988). Paleogeographic and paleotectonic setting of Laramide sedimentary basins in the central Rocky Mountain region. GSA Bulletin, 100(7), 1023–1039. https://doi.org/10.1130/0016-7606(1988)100<1023;PAPSOL>2.3.CO:2
- Dickinson, W. R., & Snyder, W. S. (1978). Plate tectonics of the Laramide orogeny. In V. Matthews (Ed.), Laramide folding associated with basement block faulting in the western United States (Vol. 151, pp. 355–366).
- Dorobek, S. L., Reid, S. K., Elrick, M., Bond, G. C., & Kominz, M. A. (1991). Subsidence across the Antler foreland of Montana and Idaho: Tectonic versus eustatic effects. Kansas Geological Survey Bulletin, 233, 232–251.
- Eichler, C. M., Saylor, J., Julia, W., Rudolph, K., & Davis, E. M. (2020). Along-strike variation in geometry of the late Cretaceous western interior basin tracks multiple geodynamic subsidence mechanisms. GSA 2020 Connects Online, Geological Society of America.
- Epis, R., & Chapin, C. E. (1975). Surface in the Southern Rocky Mountains. In Cenozoic history of the southern Rocky Mountains: Papers deriving from a symposium presented at the Rocky Mountain Section meeting of the Geological Society of America, Boulder, Colorado (Vol. 144). Geological Society of America.
- Erslev, E. A. (1993). Thrusts, back-thrusts, and detachment of Rocky Mountain foreland arches. In *Geological Society of America Special Papers* (Vol. 280, pp. 339–358). Geological Society of America. https://doi.org/10.1130/SPE280-p339
- Erslev, E. A., & Sutter, J. F. (1990). Evidence for Proterozoic mylonitization in the northwestern Wyoming province. GSA Bulletin, 102(12), 1681–1694. https://doi.org/10.1130/0016-7606(1990)102<1681:EFPMIT>2.3.CO;2
- Erslev, E. A., Worthington, L. L., Anderson, M. L., & Miller, K. C. (2022). Laramide crustal detachment in the Rockies: Cordilleran shortening of fluid-weakened foreland crust. *Rocky Mountain Geology*, 57(2), 65–97. https://doi.org/10.24872/rmgjournal.57.2.65
- Evans, K. V., Aleinikoff, J. N., Obradovich, J. D., & Fanning, C. M. (2000). SHRIMP U–Pb geochronology of volcanic rocks, Belt Supergroup, western Montana: Evidence for rapid deposition of sedimentary strata. *Canadian Journal of Earth Sciences*, 37(9), 1287–1300. https://doi.org/10.1139/e00-036
- Farley, K. A., Wolf, R. A., & Silver, L. T. (1996). The effects of long alpha-stopping distances on (U-Th)/He ages. *Geochimica et Cosmochimica Acta*, 60(21), 4223–4229. https://doi.org/10.1016/S0016-7037(96)00193-7
- Feeley, T. C. (2003). Origin and tectonic implications of across-strike geochemical variations in the Eocene Absaroka volcanic province, United States. *The Journal of Geology*, 111(3), 329–346. https://doi.org/10.1086/373972
- Feeley, T. C., & Cosca, M. A. (2003). Time vs. composition trends of magmatism at Sunlight volcano, Absaroka volcanic province, Wyoming. GSA Bulletin, 115(6), 714–728. https://doi.org/10.1130/0016-7606(2003)115<0714:TVCTOM>2.0.CO;2
- Flowers, R. M., Ketcham, R. A., Shuster, D. L., & Farley, K. A. (2009). Apatite (U-Th)/He thermochronometry using a radiation damage accumulation and annealing model. *Geochimica et Cosmochimica Acta*, 73(8), 2347–2365. https://doi.org/10.1016/j.gca.2009.01.015
- mulation and annealing model. *Geochimica et Cosmochimica Acta*, 73(8), 2347–2365. https://doi.org/10.1016/j.gca.2009.01.015 Flowers, R. M., Macdonald, F. A., Siddoway, C. S., & Havranek, R. (2020). Diachronous development of great unconformities before Neopro-
- terozoic snowball Earth. Proceedings of the National Academy of Sciences, 117(19), 10172–10180. https://doi.org/10.1073/pnas.1913131117
 Flueckinger, L. A. (1970). Stratigraphy, petrography, and origin of tertiary sediments off the front of the Beartooth Mountains, Montana-Wyoming (PhD thesis). Pennsylvania State University.
- Foose, R. M., Wise, D. U., & Garbarini, G. S. (1961). Structural geology of the Beartooth Mountains, Montana and Wyoming. GSA Bulletin, 72(8), 1143. https://doi.org/10.1130/0016-7606(1961)72[1143:SGOTBM]2.0.CO;2
- Foster, D. A., Grice, W. C., & Kalakay, T. J. (2010). Extension of the Anaconda metamorphic core complex: ⁴⁰Ar/³⁹Ar thermochronology and implications for Eocene tectonics of the northern Rocky Mountains and the Boulder batholith. *Lithosphere*, 2(4), 232–246. https://doi.org/10.1130/L.94.1
- Foster, D. A., & Mark Fanning, C. (1997). Geochronology of the northern Idaho batholith and the Bitterroot metamorphic core complex: Magmatism preceding and contemporaneous with extension. GSA Bulletin, 109(4), 379–394. https://doi.org/10.1130/0016-7606(1997)109<0379:GOTNIB>2.3.CO;2
- Foster, D. A., Mueller, P. A., Mogk, D. W., Wooden, J. L., & Vogl, J. J. (2006). Proterozoic evolution of the western margin of the Wyoming craton: Implications for the tectonic and magmatic evolution of the northern Rocky Mountains. *Canadian Journal of Earth Sciences*, 43(10), 1601–1619. https://doi.org/10.1139/e06-052

RONEMUS ET AL. 28 of 34

Tectonics

- Foster, D. A., Schafer, C., Fanning, C. M., & Hyndman, D. W. (2001). Relationships between crustal partial melting, plutonism, orogeny, and exhumation: Idaho–Bitterroot batholith. *Tectonophysics*, 342(3), 313–350. https://doi.org/10.1016/S0040-1951(01)00169-X
- Fox, N. R. (2017). Sedimentary tectonics of the mesoproterozoic LaHood formation, southwest Montana, M.Sc. Thesis. Montana State University. Fuentes, F., DeCelles, P. G., Constenius, K. N., & Gehrels, G. E. (2011). Evolution of the Cordilleran foreland basin system in northwestern Montana, U.S.A. GSA Bulletin, 123(3–4), 507–533. https://doi.org/10.1130/B30204.1
- Gallagher, K. (2012). Transdimensional inverse thermal history modeling for quantitative thermochronology: Transdimensional inverse thermal history. *Journal of Geophysical Research*, 117(B2), 1–16. https://doi.org/10.1029/2011JB008825
- Gallagher, K. (2021). Comment on "Discussion: Extracting thermal history from low temperature thermochronology/A comment on the recent exchanges between Vermeesch and Tian and Gallagher and Ketcham", by Paul Green and Ian Duddy. Earth-Science Reviews, 216, 103549. https://doi.org/10.1016/j.earscirev.2021.103549
- Galloway, W. E., Whiteaker, T. L., & Ganey-Curry, P. (2011). History of Cenozoic North American drainage basin evolution, sediment yield, and accumulation in the Gulf of Mexico basin. *Geosphere*, 7(4), 938–973. https://doi.org/10.1130/GES00647.1
- Garber, K. L., Finzel, E. S., & Pearson, D. M. (2020). Provenance of syn-orogenic foreland basin strata in southwestern Montana requires revision of existing models for Laramide tectonism: North American Cordillera. Tectonics, 39(2), e2019TC005944. https://doi.org/10.1029/2019tc005944
- Gast, P. W., Kulp, J. L., & Long, L. E. (1958). Absolute age of early Precambrian rocks in the Bighorn Basin of Wyoming and Montana, and southeastern Manitoba. Eos, Transactions American Geophysical Union, 39(2), 322–334. https://doi.org/10.1029/TR039i002p00322
- Gehrels, G. E., Valencia, V. A., & Ruiz, J. (2008). Enhanced precision, accuracy, efficiency, and spatial resolution of U-Pb ages by laser ablation–multicollector–inductively coupled plasma–mass spectrometry. Geochemistry, Geophysics, Geosystems, 9(3), Q03017. https://doi.org/10.1029/2007GC001805
- Gifford, J. N., Malone, S. J., & Mueller, P. A. (2020). The medicine hat block and the early Paleoproterozoic assembly of western Laurentia. Geosciences, 10(7), 271. https://doi.org/10.3390/geosciences10070271
- Gifford, J. N., Mueller, P. A., Foster, D. A., & Mogk, D. W. (2014). Precambrian crustal evolution in the Great Falls tectonic zone: Insights from xenoliths from the Montana Alkali Province. The Journal of Geology, 122(5), 531–548. https://doi.org/10.1086/677262
- Giletti, B. J. (1966). Isotopic ages from southwestern Montana. *Journal of Geophysical Research*, 71(16), 4029–4036. https://doi.org/10.1029/jz071i016p04029
- Giletti, B. J. (1971). Discordant isotopic ages and excess argon in biotites. Earth and Planetary Science Letters, 10(2), 157–164. https://doi.org/10.1016/0012-821X(71)90001-X
- Gingerich, P. D. (1983). Paleocene-Eocene faunal zones and a preliminary analysis of Laramide structural deformation in the Clark's Fork Basin,
- Wyoming. In Geology of the Bighorn Basin, 34th annual field conference guidebook (pp. 185–195).

 Ginster, U., Reiners, P. W., Nasdala, L., & Chanmuang, N. C. (2019). Annealing kinetics of radiation damage in zircon. Geochimica et Cosmo-
- chimica Acta, 249, 225–246. https://doi.org/10.1016/j.gca.2019.01.033 Goddéris, Y., Donnadieu, Y., Nédélec, A., Dupré, B., Dessert, C., Grard, A., et al. (2003). The Sturtian 'snowball' glaciation: Fire and ice. Earth
- and Planetary Science Letters, 211(1), 1–12. https://doi.org/10.1016/S0012-821X(03)00197-3
 Grove, M., & Harrison, T. M. (1996). 40Ar* diffusion in Fe-rich biotite. American Mineralogist, 81(7–8), 940–951. https://doi.org/10.2138/
- am-1996-7-816

 Guenthner, W. R. (2021). Implementation of an alpha damage annealing model for zircon (U-Th)/He thermochronology with comparison to a
- zircon fission track annealing model. *Geochemistry, Geophysics, Geosystems*, 22(2), e2019GC008757. https://doi.org/10.1029/2019GC008757 Guenthner, W. R., Reiners, P. W., Ketcham, R. A., Nasdala, L., & Giester, G. (2013). Helium diffusion in natural zircon: Radiation damage,
- anisotropy, and the interpretation of zircon (U-Th)/He thermochronology. *American Journal of Science*, 313(3), 145–198. https://doi.org/10.2475/03.2013.01
- Guo, H., Zeitler, P. K., Idleman, B. D., Fayon, A. K., Fitzgerald, P. G., & McDannell, K. T. (2021). Helium diffusion systematics inferred from continuous ramped heating analysis of Transantarctic Mountains apatites showing age overdispersion. *Geochimica et Cosmochimica Acta*, 310, 113–130. https://doi.org/10.1016/j.gca.2021.07.015
- Haley, J. C. (1985). Upper Cretaceous (Beaverhead) synorogenic sediments of the Montana-Idaho thrust belt and adjacent foreland: Relationships between sedimentation and tectonism (Ph.D. Thesis). Johns Hopkins University.
- Hames, W., & Harms, T. (2013). Laser ⁴⁰Arr/³⁹Ar thermochronology of single crystals from Paleoproterozoic to Archean rocks of the northern Wyoming Province, Big Sky orogen, and Great Falls tectonic zone: Giletti's line revisited. In *Geological Society of America abstracts with programs* (Vol. 45).223.
- Harlan, S. S., Geissman, J. W., Snee, L. W., & Reynolds, R. L. (1996). Late Cretaceous remagnetization of Proterozoic mafic dikes, southern Highland Mountains, southwestern Montana: A paleomagnetic and ⁴⁰Ar/³⁹Ar study. GSA Bulletin, 108(6), 653–668. https://doi.org/10.1130/0016-7606(1996)108<0653;LCROPM>2.3.CO;2
- Harlan, S. S., Heaman, L., LeCheminant, A. N., & Premo, W. R. (2003). Gunbarrel mafic magmatic event: A key 780 Ma time marker for Rodinia plate reconstructions. Geology, 31(12), 1053–1056. https://doi.org/10.1130/G19944.1
- Harms, T. A., Brady, J. B., Burger, H. R., & Cheney, J. T. (2004). Advances in the geology of the Tobacco Root Mountains, Montana, and their implications for the history of the northern Wyoming province. In Special paper 377: Precambrian geology of the Tobacco Root Mountains, Montana (Vol. 377, pp. 227–243). Geological Society of America. https://doi.org/10.1130/0-8137-2377-9.227
- Harms, T. A., Brady, J. B., College, S., & Cheney, J. T. (2006). Exploring the Proterozoic Big Sky orogeny in southwest Montana. In 19th annual Keck symposium. 6.
- Harms, T. A., Burger, H. R., Blednick, D. G., Cooper, J. M., King, J. T., Owen, D. R., et al. (2004). Character and origin of Precambrian fabrics and structures in the Tobacco Root Mountains, Montana. In Special paper 377: Precambrian geology of the Tobacco Root Mountains, Montana (Vol. 377, pp. 203–226). Geological Society of America. https://doi.org/10.1130/0-8137-2377-9.203
- Harrison, T. M., Duncan, I., & McDougall, I. (1985). Diffusion of ⁴⁰Ar in biotite: Temperature, pressure and compositional effects. *Geochimica et Cosmochimica Acta*, 49(11), 2461–2468. https://doi.org/10.1016/0016-7037(85)90246-7
- Hatcher, R. D., Jr., Zietz, I., & Litehiser, J. J. (1987). Crystal subdivisions of the eastern and central United States and a seismic boundary hypothesis for eastern seismicity. Geology, 15(6), 528–532. https://doi.org/10.1130/0091-7613(1987)15<528:CSOTEA>2.0.CO;2
- Hebert, C. L., Kaufman, A. J., Penniston-Dorland, S. C., & Martin, A. J. (2010). Radiometric and stratigraphic constraints on terminal Ediacaran (post-Gaskiers) glaciation and metazoan evolution. *Precambrian Research*, 182(4), 402–412. https://doi.org/10.1016/j.precamres.2010.07.008
- Heller, P. L., & Liu, L. (2016). Dynamic topography and vertical motion of the U.S. Rocky Mountain region prior to and during the Laramide orogeny. GSA Bulletin, 128(5-6), 973–988. https://doi.org/10.1130/B31431.1
- Hicks, J. F., Johnson, K. R., Obradovich, J. D., Tauxe, L., & Clark, D. (2002). Magnetostratigraphy and geochronology of the Hell Creek and basal Fort Union Formations of southwestern North Dakota and a recalibration of the age of the Cretaceous-Tertiary boundary. In J. H. Hartman,

RONEMUS ET AL. 29 of 34

Tectonics

- K. R. Johnson, & D. J. Nichols (Eds.), The Hell Creek formation and the Cretaceous-tertiary boundary in the northern Great plains: An integrated continental record of the end of the Cretaceous. Geological Society of America. https://doi.org/10.1130/0-8137-2361-2.35
- Hirtz, J., Constenius, K. N., Valencia, V., Horton, B. K., & Pratt, B. (2022). Provenance of the Belt-Purcell Supergroup of NW Montana, USA and SW Alberta, Canada, Implications for the early Mesoproterozoic paleogeography of Laurentia. In Geological Society of America Connects abstracts with programs, Denver, CO.
- Hiza, M. M. (1999). The geochemistry and geochronology of the Eocene Absaroka volcanic province, northern Wyoming and southwest Montana, United States of America (Ph.D. Thesis). Oregon State University.
- Hoffman, P. F., Abbot, D. S., Ashkenazy, Y., Benn, D. I., Brocks, J. J., Cohen, P. A., et al. (2017). Snowball Earth climate dynamics and Cryogenian geology-geobiology. *Science Advances*, 3(11), e1600983. https://doi.org/10.1126/sciadv.1600983
- Hoffman, P. F., Kaufman, A. J., Halverson, G. P., & Schrag, D. P. (1998). A Neoproterozoic Snowball Earth. Science, 281(5381), 1342–1346. https://doi.org/10.1126/science.281.5381.1342
- Hoffman, P. F., & Schrag, D. P. (2002). The snowball Earth hypothesis: Testing the limits of global change. Terra Nova, 14(3), 129–155. https://doi.org/10.1046/j.1365-3121.2002.00408.x
- Hourigan, J. K., Reiners, P. W., & Brandon, M. T. (2005). U-Th zonation-dependent alpha-ejection in (U-Th)/He chronometry. Geochimica et Cosmochimica Acta, 69(13), 3349–3365. https://doi.org/10.1016/j.gca.2005.01.024
- Howlett, C. J., Reynolds, A. N., & Laskowski, A. K. (2021). Magmatism and extension in the Anaconda metamorphic core complex of western Montana and relation to regional tectonics. *Tectonics*, 40(9), e2020TC006431. https://doi.org/10.1029/2020TC006431
- Hoy, R. G., & Ridgway, K. D. (1997). Structural and sedimentological development of footwall growth synclines along an intraforeland uplift, east-cen-
- tral Bighorn Mountains, Wyoming. GSA Bulletin, 109(8), 915–935. https://doi.org/10.1130/00167606(1997)109<0915:SASDOF>2.3.CO;2
 Humphreys, E., Hessler, E., Dueker, K., Farmer, G. L., Erslev, E., & Atwater, T. (2003). How Laramide-age hydration of North American lithosphere by the Farallon Slab controlled subsequent activity in the western United States. International Geology Review, 45(7), 575–
- 595. https://doi.org/10.2747/0020-6814.45.7.575

 Jackson, W. T., Jr., McKay, M. P., Bartholomew, M. J., Allison, D. T., Spurgeon, D. L., Shaulis, B., et al. (2019). Initial Laramide tectonism recorded by Upper Cretaceous paleoseismites in the northern Bighorn Basin, USA: Field indicators of an applied end load stress. *Geology*,
- 47(11), 1059–1063. https://doi.org/10.1130/G46738.1

 Jobling, J. (1974). Stratigraphy, petrology, and structure of the Laramide (Paleocene) sediments marginal to the Beartooth mountains (Ph.D. Thesis). Pennsylvania State University. University Park.
- Johnson, J. E., Flowers, R. M., Baird, G. B., & Mahan, K. H. (2017). "Inverted" zircon and apatite (U-Th)/He dates from the Front Range, Colorado: High-damage zircon as a low-temperature (<50°C) thermochronometer. Earth and Planetary Science Letters, 466, 80–90. https://doi.org/10.1016/j.epsl.2017.03.002</p>
- Kaempfer, J. M., Guenthner, W. R., & Pearson, D. M. (2021). Proterozoic to phanerozoic tectonism in southwestern Montana basement ranges constrained by low temperature thermochronometric data. *Tectonics*, 40(11), e2021TC006744, https://doi.org/10.1029/2021TC006744
- Karlstrom, K. E., & Timmons, J. M. (2012). Many unconformities make one 'Great Unconformity'. In J. M. Timmons & K. E. Karlstrom (Eds.), Grand canyon geology: Two billion years of Earth's history (Vol. 489). Geological Society of America, https://doi.org/10.1130/2012.2489(04)
- Kauffman, E. G., & Caldwell, W. G. E. (1992). The western interior basin in space and time. In Geologic Association of Canada special paper 39.
 Keller, C. B., Husson, J. M., Mitchell, R. N., Bottke, W. F., Gernon, T. M., Boehnke, P., et al. (2019). Neoproterozoic glacial origin of the Great Unconformity. Proceedings of the National Academy of Sciences, 116(4), 1136–1145. https://doi.org/10.1073/pnas.1804350116
- Ketcham, R. A., Carter, A., Donelick, R. A., Barbarand, J., & Hurford, A. J. (2007). Improved modeling of fission-track annealing in apatite. American Mineralogist. 92(5–6), 799–810. https://doi.org/10.2138/am.2007.2281
- Ketcham, R. A., Gautheron, C., & Tassan-Got, L. (2011). Accounting for long alpha-particle stopping distances in (U-Th-Sm)/He geochronology: Refinement of the baseline case. Geochimica et Cosmochimica Acta, 75(24), 7779–7791. https://doi.org/10.1016/j.gca.2011.10.011
- Kirschvink, J. L. (1992). Late Proterozoic low-latitude global glaciation: The snowball Earth. In J. W. Schopf & C. Klein (Eds.) *The Proterozoic biosphere: A multidisciplinary study* (pp. 51–52). Cambridge University Press.
- Kluth, C. F., & Coney, P. J. (1981). Plate tectonics of the ancestral Rocky Mountains. *Geology*, 9(1), 10–15. https://doi.org/10.1130/0091-7613(1981)9%3C10:PTOTAR%3E2.0.CO;2
- Koenig, D. (2015). Low-temperature thermochronology of the Beartooth Conglomerate (M.S. Thesis). University of Houston.
- Krob, F. C., Glasmacher, U. A., Karl, M., Perner, M., Hackspacher, P. C., & Stockli, D. F. (2019). Multi-chronometer thermochronological modelling of the Late Neoproterozoic to recent t-T-evolution of the SE coastal region of Brazil. *Journal of South American Earth Sciences*, 92, 77–94. https://doi.org/10.1016/j.jsames.2019.02.012
- Kulik, D. M., & Schmidt, C. J. (1988). Region of overlap and styles of interaction of Cordilleran thrust belt and Rocky Mountain foreland. In C. J. Schmidt & W. J. PerryJr. (Eds.), *Interaction of the Rocky mountain foreland and the Cordilleran thrust belt* (Vol. 171). Geological Society of America. https://doi.org/10.1130/MEM171-p75
- Lageson, D. R., Schmitt, J. G., Horton, B. K., Kalakay, T. J., & Burton, B. R. (2001). Influence of Late Cretaceous magmatism on the Sevier orogenic wedge, western Montana. Geology, 29(8), 723–726. https://doi.org/10.1130/0091-7613(2001)029<0723:IOLCMO>2.0.CO;2
- Lanphere, M. A., & Brent Dalrymple, G. (1976). Identification of excess ⁴⁰Ar by the ⁴⁰Ar/³⁹Ar age spectrum technique. *Earth and Planetary Science Letters*, 32(2), 141–148. https://doi.org/10.1016/0012-821X(76)90052-2
- Lawton, T. F. (2019). Chapter 13—Laramide sedimentary basins and sediment-dispersal systems. In A. D. Miall (Ed.), The sedimentary basins of the United States and Canada (2nd ed., pp. 529–557). Elsevier. https://doi.org/10.1016/B978-0-444-63895-3.00013-9
- Li, Z.-X., Evans, D. A. D., & Halverson, G. P. (2013). Neoproterozoic glaciations in a revised global palaeogeography from the breakup of Rodinia to the assembly of Gondwanaland. Sedimentary Geology, 294, 219–232. https://doi.org/10.1016/j.sedgeo.2013.05.016
- Link, P. K., Todt, M. K., Pearson, D. M., & Thomas, R. C. (2017). 500–490 Ma detrital zircons in Upper Cambrian Worm Creek and correlative sandstones, Idaho, Montana, and Wyoming: Magmatism and tectonism within the passive margin. *Lithosphere*, 9(6), 910–926. https://doi. org/10.1130/L671.1
- Lipman, P. W., Prostka, H. J., & Christiansen, R. L. (1971). Evolving subduction zones in the western United States, as interpreted from igneous rocks. Science, 174(4011), 821–825. https://doi.org/10.1126/science.174.4011.821
- Liu, L., Gurnis, M., Seton, M., Saleeby, J., Müller, R. D., & Jackson, J. M. (2010). The role of oceanic plateau subduction in the Laramide orogeny. *Nature Geoscience*, 3(5), 353–357. https://doi.org/10.1038/ngeo829
- Livaccari, R. F. (1991). Role of crustal thickening and extensional collapse in the tectonic evolution of the Sevier-Laramide orogeny, western United States. *Geology*, 19(11), 1104–1107. https://doi.org/10.1130/0091-7613(1991)019<1104:ROCTAE>2.3.CO;2
- Livaccari, R. F., Burke, K., & Şengör, A. M. C. (1981). Was the Laramide orogeny related to subduction of an oceanic plateau? *Nature*, 289(5795), 276–278. https://doi.org/10.1038/289276a0

RONEMUS ET AL. 30 of 34

- Livaccari, R. F., & Perry, F. V. (1993). Isotopic evidence for preservation of Cordilleran lithospheric mantle during the Sevier-Laramide orogeny, western United States. Geology, 21(8), 719-722. https://doi.org/10.1130/0091-7613(1993)021<0719:IEFPOC>2.3.CO;2
- Lonn, J. D., Burmester, R. F., Lewis, R. S., & McFaddan, M. D. (2020). The Mesoproterozoic Belt Supergroup. In Montana Bureau of Mines and geology special publication 122: Geology of Montana (Vol. 1, p. 38).
- Lopez, D. A. (2001). Preliminary geologic map of the red Lodge 30' × 60' quadrangle South-Central Montana (geologic map no. 423) (p. 1). Montana Bureau of Mines and Geology.
- Lund, K., Aleinikoff, J. N., Evans, K. V., du Bray, E. A., Dewitt, E. H., & Unruh, D. M. (2010). SHRIMP U-Pb dating of recurrent Cryogenian and Late Cambrian-Early Ordovician alkalic magmatism in central Idaho: Implications for Rodinian rift tectonics. GSA Bulletin, 122(3-4), 430-453. https://doi.org/10.1130/B26565.1
- Lund, K., Aleinikoff, J. N., Evans, K. V., & Fanning, C. M. (2003). SHRIMP U-Pb geochronology of Neoproterozoic Windermere Supergroup, central Idaho: Implications for rifting of western Laurentia and synchroneity of Sturtian glacial deposits. GSA Bulletin, 115(3), 349–372. https://doi.org/10.1130/0016-7606(2003)115<0349:SUPGON>2.0.CO;2
- Lund, K., Aleinikoff, J. N., Kunk, M. J., Unruh, D. M., Zeihen, G. D., Hodges, W. C., et al. (2002). SHRIMP U-Pb and 40Ar/39Ar age constraints for relating plutonism and mineralization in the Boulder Batholith region, Montana. Economic Geology, 97(2), 241-267. https://doi.org/10. 2113/gsecongeo.97.2.241
- Lutz, T. M., & Omar, G. (1991). An inverse method of modeling thermal histories from apatite fission-track data. Earth and Planetary Science Letters, 104(2), 181-195. https://doi.org/10.1016/0012-821X(91)90203-T
- Malinverno, A., & Briggs, V. A. (2004). Expanded uncertainty quantification in inverse problems: Hierarchical Bayes and empirical Bayes. Geophysics, 69(4), 1005-1016. https://doi.org/10.1190/1.1778243
- Mallory, W. (1972), Geologic Atlas of the Rocky mountain region, Rocky Mountain Association of Geologists,

Tectonics

- Marcilly, C. M., Torsvik, T. H., & Conrad, C. P. (2022). Global Phanerozoic sea levels from paleogeographic flooding maps. Gondwana Research, 110, 128-142. https://doi.org/10.1016/j.gr.2022.05.011
- Maughan, E. (1990). Summary of the Ancestral Rocky mountains Epeirogeny in Wyoming and adjacent areas (open-file report no. of 90-447). U.S. Geologic Survey.
- Maughan, E. K. (1993). Stratigraphic and structural summary for central Montana. In Field conference guidebook: Energy and mineral resources of central Montana (old timers' rendezvous edition) (pp. 3-20). Montana Geologic Society.
- Maxson, J., & Tikoff, B. (1996). Hit-and-run collision model for the Laramide orogeny, western United States. Geology, 24(11), 968. https://doi.org/10.1130/0091-7613(1996)024<0968:HARCMF>2.3.CO;2
- May, S. R., Gray, G. G., Summa, L. L., Stewart, N. R., Gehrels, G. E., & Pecha, M. E. (2013). Detrital zircon geochronology from the Bighorn Basin, Wyoming, USA: Implications for tectonostratigraphic evolution and paleogeography. GSA Bulletin, 125(9-10), 1403-1422. https://doi.org/10.1130/B30824.1
- McDannell, K., Keller, C., Guenthner, W., Zeitler, P., & Shuster, D. (2022). Thermochronologic constraints on the origin of the Great Unconformity. Proceedings of the National Academy of Sciences, 119(5), e2118682119. https://doi.org/10.1073/pnas.2118682119
- McDannell, K. T., & Flowers, R. M. (2020). Vestiges of the ancient: Deep-time noble gas thermochronology. Elements, 16(5), 325-330. https:// doi.org/10.2138/gselements.16.5.325
- McDannell, K. T., Schneider, D. A., Zeitler, P. K., O'Sullivan, P. B., & Issler, D. R. (2019). Reconstructing deep-time histories from integrated thermochronology: An example from southern Baffin Island, Canada. Terra Nova, 31(3), 189–204. https://doi.org/10.1111/ter.12386
- McDannell, K. T., Zeitler, P. K., Janes, D. G., Idleman, B. D., & Fayon, A. K. (2018). Screening apatites for (U-Th)/He thermochronometry via continuous ramped heating: He age components and implications for age dispersion. Geochimica et Cosmochimica Acta, 223, 90-106. https://doi.org/10.1016/j.gca.2017.11.031
- McDougall, I., & Harrison, T. M. (1999). Geochronology and thermochronology by the 40Art/39Ar method (2nd ed.). Oxford University Press on
- McKenna, M. C. (1980). Remaining evidence of Oligocene sedimentary rocks previously present across the Bighorn Basin, Wyoming. In P. Gingerich (Ed.), Early Cenozoic paleontology and stratigraphy of the Bighorn Basin, Wyoming, University of Michigan papers on paleontol-
- McKenna, M. C., & Love, J. D. (1972). High-level strata containing early Miocene mammals on the Bighorn Mountains, Wyoming. American Museum Novitates, 2490.
- McMannis, W. J. (1963). LaHood Formation—A coarse facies of the Belt Series in southwestern Montana. GSA Bulletin, 74(4), 407-436. https:// doi.org/10.1130/0016-7606(1963)74[407:LFCFOT]2.0.CO;2
- McMillan, M. E. (2003). Basin fill, erosion surfaces and tilted markers: Evidence of late Cenozoic tectonic uplift of the Rocky Mountain orogenic plateau (Ph.D. Thesis), University of Wyoming,
- McMillan, M. E., Heller, P. L., & Wing, S. L. (2006). History and causes of post-Laramide relief in the Rocky Mountain orogenic plateau. GSA Bulletin, 118(3-4), 393-405, https://doi.org/10.1130/b25712.1
- McQuarrie, N., & Chase, C. G. (2000). Raising the Colorado plateau. Geology, 28(1), 91–94. https://doi.org/10.1130/0091-7613(2000)028<00 91:RTCP>2.0.CO;2
- Merdith, A. S., Williams, S. E., Brune, S., Collins, A. S., & Müller, R. D. (2019). Rift and plate boundary evolution across two supercontinent cycles. Global and Planetary Change, 173, 1-14. https://doi.org/10.1016/j.gloplacha.2018.11.006
- Mogk, D. W., Mueller, P. A., & Wooden, J. L. (1988). Archean tectonics of the north Snowy block, Beartooth Mountains, Montana. The Journal of Geology, 96(2), 125-141. https://doi.org/10.1086/629205
- Mogk, D. W., Mueller, P. A., & Wooden, J. L. (1992). The nature of Archean terrane boundaries: An example from the northern Wyoming Province. Precambrian Research, 55(1), 155-168. https://doi.org/10.1016/0301-9268(92)90020-O
- Montgomery, C. W., & Lytwyn, J. N. (1984). Rb-Sr systematics and ages of principal Precambrian lithologies in the South Snowy Block, Beartooth Mountains. The Journal of Geology, 92(1), 103-112. https://doi.org/10.1086/628837
- Mueller, P., Mogk, D., Wooden, J., & Spake, D. (2016). U-Pb ages of zircons from the Lower Belt Supergroup and proximal crystalline basement: Implications for the early evolution of the Belt Basin. In Geological Society of America special papers (Vol. 522, pp. 283-303). Geological Society of America. https://doi.org/10.1130/2016.2522(11)
- Mueller, P. A., Burger, H. R., Wooden, J. L., Heatherington, A. L., Mogk, D. W., & D'Arcy, K. (2004). Age and evolution of the Precambrian crust of the Tobacco Root Mountains, Montana. In J. B. Brady, H. R. Burger, J. T. Cheney, & T. A. Harms (Eds.), Precambrian geology of the Tobacco Root Mountains, Montana. Geological Society of America. https://doi.org/10.1130/0-8137-2377-9.181
- Mueller, P. A., & Frost, C. D. (2006). The Wyoming Province: A distinctive Archean craton in Laurentian North America. Canadian Journal of Earth Sciences, 43(10), 1391–1397, https://doi.org/10.1139/e06-075

RONEMUS ET AL. 31 of 34

Tectonics

- Mueller, P. A., Heatherington, A. L., Kelly, D. M., Wooden, J. L., & Mogk, D. W. (2002). Paleoproterozoic crust within the Great Falls tectonic zone: Implications for the assembly of southern Laurentia. Geology, 30(2), 127–130. https://doi.org/10.1130/0091-7613(2002)030
 0127:PCWTGF>2.0.CO;2
- Mueller, P. A., Mogk, D. W., Henry, D. J., Wooden, J. L., & Foster, D. A. (2008). Geologic evolution of the Beartooth Mountains: Insights from petrology and geochemistry. *Northwestern Geology*, 37, 5–20.
- Mueller, P. A., Wooden, J. L., Mogk, D. W., Henry, D. J., & Bowes, D. R. (2010). Rapid growth of an Archean continent by arc magmatism. Precambrian Research, 183(1), 70–88. https://doi.org/10.1016/j.precamres.2010.07.013
- Murray, K. E., Orme, D. A., & Reiners, P. W. (2014). Effects of U–Th-rich grain boundary phases on apatite helium ages. *Chemical Geology*, 390, 135–151. https://doi.org/10.1016/j.chemgeo.2014.09.023
- Norris, D. K., & Price, R. A. (1966). Middle Cambrian lithostratigraphy of southeastern Canadian Cordillera. *Bulletin of Canadian Petroleum Geology*, 14, 20.
- Omar, G. I., Lutz, T. M., & Giegengack, R. (1994). Apatite fission-track evidence for Laramide and post-Laramide uplift and anomalous thermal regime at the Beartooth overthrust, Montana-Wyoming. *Geological Society of America Bulletin*, 106, 74–85.
- Onstott, T. C., & Peacock, M. W. (1987). Argon retentivity of hornblendes: A field experiment in a slowly cooled metamorphic terrane. Geochimica et Cosmochimica Acta, 51(11), 2891–2903. https://doi.org/10.1016/0016-7037(87)90365-6
- Orme, D. A. (2020). New timing constraints for the onset of Laramide deformation in southwest Montana challenge our understanding of the development of a thick-skinned structural style during flat-slab subduction. *Tectonics*, 39(12), e2020TC006193. https://doi.org/10.1029/2020TC006193
- Orme, D. A., Guenthner, W. R., Laskowski, A. K., & Reiners, P. W. (2016). Long-term tectonothermal history of Laramide basement from zircon-He age-eU correlations. Earth and Planetary Science Letters, 453, 119–130. https://doi.org/10.1016/j.epsl.2016.07.046
- Parcell, W. C., & Williams, M. K. (2005). Mixed sediment deposition in a retro-arc foreland basin: Lower Ellis Group (M. Jurassic), Wyoming and Montana, U.S.A. Sedimentary Geology, 177(3), 175–194. https://doi.org/10.1016/j.sedgeo.2005.02.007
- Parker, S. D., & Hendrix, M. S. (2022). Detrital zircon record of the Mesoproterozoic Belt basin and implications for horizontal and vertical tectonic models. In G. R. Foulger, L. C. Hamilton, D. M. Jurdy, C. A. Stein, K. A. Howard, & S. Stein (Eds.), In the footsteps of Warren B. Hamilton: New Ideas in Earth Science (Vol. 553). Geological Society of America. https://doi.org/10.1130/2021.2553(14)
- Parker, S. D., & Pearson, D. M. (2021). Pre-thrusting stratigraphic control on the transition from a thin-skinned to thick-skinned structural style: An example from the double-decker Idaho-Montana fold-thrust belt. *Tectonics*, 40(5), e2020TC006429. https://doi.org/10.1029/2020TC006429
- Peak, B. A., Flowers, R. M., Macdonald, F. A., & Cottle, J. M. (2021). Zirson (U-Th)/He thermochronology reveals pre-Great Unconformity paleotopography in the Grand Canyon region, USA. *Geology*, 49(12), 1462–1466. https://doi.org/10.1130/G49116.1
- Peters, S. E., & Gaines, R. R. (2012). Formation of the 'Great Unconformity' as a trigger for the Cambrian explosion. *Nature*, 484(7394), 363–366. https://doi.org/10.1038/nature10969
- Peyton, S. L., Reiners, P. W., Carrapa, B., & DeCelles, P. G. (2012). Low-temperature thermochronology of the northern Rocky Mountains, western U.S.A. American Journal of Science, 312(2), 145–212. https://doi.org/10.2475/02.2012.04
- Powell, R., Green, E. C. R., Marillo Sialer, E., & Woodhead, J. (2020). Robust isochron calculation. Geochronology, 2(2), 325–342. https://doi.org/10.5194/gchron-2-325-2020
- Prave, A. R., Condon, D. J., Hoffmann, K. H., Tapster, S., & Fallick, A. E. (2016). Duration and nature of the end-Cryogenian (Marinoan) glaciation. *Geology*, 44(8), 631–634. https://doi.org/10.1130/G38089.1
- Pystina, Y., & Pystin, A. (2019). Th/U Relations as an indicator of the genesis of metamorphic zircons (on the example of the North of the Urals). In S. Glagolev (Ed.), 14th international congress for applied mineralogy (ICAM2019) (pp. 129–132). Springer International Publishing. https://doi.org/10.1007/978-3-030-22974-0_30
- Reade, N. Z., Biddle, J. M., Ricketts, J. W., & Amato, J. M. (2020). Zircon (U-Th)/He Thermochronologic Constraints on the Long-Term Thermal Evolution of Southern New Mexico and Western Texas. *Lithosphere*, 2020(1), 8881315. https://doi.org/10.2113/2020/888
- Reid, R. R., McMannis, W. J., & Palmquist, J. C. (1975). Precambrian Geology of North Snowy Block, Beartooth Mountains, Montana. In H. R. Reid, W. J. McMannis, & J. C. Palmquist (Eds.), Precambrian geology of North Snowy Block, Beartooth Mountains, Montana (Vol. 157). Geological Society of America. https://doi.org/10.1130/SPE157-p1
- Reiners, P. W., Spell, T. L., Nicolescu, S., & Zanetti, K. A. (2004). Zircon (U-Th)/He thermochronometry: He diffusion and comparisons with ⁴⁰Ar/³⁹Ar dating. *Geochimica et Cosmochimica Acta*, 68(8), 1857–1887. https://doi.org/10.1016/j.gca.2003.10.021
- Retallack, G. J. (2013). Early Cambrian humid, tropical, coastal paleosols from Montana, USA. In L. C. Nordt & S. G. Driese (Eds.), New frontiers in paleopedology and terrestrial paleoclimatology: Paleosols and Soil surface analog systems (pp. 257–272). Society for Sedimentary Geology, https://doi.org/10.2110/sepmsp.104.09
- Roberts, H., Dahl, P., Kelley, S., & Frei, R. (2002). New ²⁰⁷Pb-²⁰⁶Pb and ⁴⁰Ar-³⁹Ar ages from SW Montana, USA: Constraints on the Proterozoic and Archæan tectonic and depositional history of the Wyoming Province. *Precambrian Research*, 117(1-2), 119-143. https://doi.org/10.1016/s0301-9268(02)00076-1
- Rogers, J. J. W., & Santosh, M. (2002). Configuration of Columbia, a Mesoproterozoic supercontinent. Gondwana Research, 5(1), 5–22. https://doi.org/10.1016/S1342-937X(05)70883-2
- Ronemus, C. B., & Orme, D. A. (2022). Spatial and temporal overlap of structural styles in the Highland Mountains, Montana, USA: An example of collaboration between the Montana Bureau of Mines and Geology and USGS EDMAP program participants. In *Geological Society of America abstracts with programs. Denver, CO*.
- Ronemus, C. B., Orme, D. A., Campbell, S., Black, S. R., & Cook, J. (2020). Mesoproterozoic–Early Cretaceous provenance and paleogeographic evolution of the Northern Rocky Mountains: Insights from the detrital zircon record of the Bridger Range, Montana, USA. *GSA Bulletin*, 133(3–4), 777–801. https://doi.org/10.1130/B35628.1
- Rooney, A. D., Strauss, J. V., Brandon, A. D., & Macdonald, F. A. (2015). A Cryogenian chronology: Two long-lasting synchronous Neoproterozoic glaciations. *Geology*, 43(5), 459–462. https://doi.org/10.1130/G36511.1
- Rosenblume, J. A., Finzel, E. S., & Pearson, D. M. (2021). Early Cretaceous provenance, sediment dispersal, and foreland basin development in Southwestern Montana, North American Cordillera. *Tectonics*, 40(4), e2020TC006561. https://doi.org/10.1029/2020TC006561
- Ross, G. M., & Villeneuve, M. (2003). Provenance of the Mesoproterozoic (1.45 Ga) Belt basin (western North America): Another piece in the pre-Rodinia paleogeographic puzzle. GSA Bulletin, 115(10), 1191–1217. https://doi.org/10.1130/B25209.1
- Ross, J. A., & Sharp, W. D. (1988). The effects of sub-blocking temperature metamorphism on the K/Ar systematics of hornblendes: ⁴⁰Ar/³⁹Ar dating of polymetamorphic garnet amphibolite from the Franciscan Complex, California. *Contributions to Mineralogy and Petrology*, 100(2), 213–221. https://doi.org/10.1007/BF00373587

RONEMUS ET AL. 32 of 34

- Saylor, J. E., Rudolph, K. W., Sundell, K. E., & Wijk, J. (2020). Laramide orogenesis driven by Late Cretaceous weakening of the North American lithosphere. *Journal of Geophysical Research: Solid Earth*, 125(8), e2020JB019570. https://doi.org/10.1029/2020JB019570
- Schwartz, R. K., & Decelles, P. G. (1988). Cordilleran foreland basin evolution in response to interactive Cretaceous thrusting and foreland partitioning, southwestern Montana. *Memoir of the Geological Society of America*, 171(1), 489–513. https://doi.org/10.1130/MEM171-p489
- Sears, J. W. (2013). Late Oligocene-early Miocene Grand Canyon: A Canadian connection. Geological Society of America Today, 23(11), 4–10. https://doi.org/10.1130/gsatg178a.1
- Sears, J. W., & Price, R. A. (1978). The Siberian connection: A case for Precambrian separation of the North American and Siberian cratons. Geology, 6(5), 267–270. https://doi.org/10.1130/0091-7613(1978)6<267:tscacf>2.0.co;2
- Sears, J. W., & Price, R. A. (2000). New look at the Siberian connection: No SWEAT. Geology, 28(5), 423–426. https://doi.org/10.1130/0091-7613(2000)28<423:NLATSC>2.0.CO;2
- Simons, F. S., & Armbrustmacher, T. J. (1976). High-level plateaus of the southeastern Beartooth Mountains, Montana and Wyoming—Remnants of an exhumed sub-Cambrian marine plain. *Journal of Research US Geological Survey*, 4(4), 387–396.
- Steidtmann, J. R., & Middleton, L. T. (1991). Fault chronology and uplift history of the southern Wind River Range, Wyoming: Implications for Laramide and post-Laramide deformation in the Rocky Mountain foreland. GSA Bulletin, 103(4), 472–485. https://doi.org/10.1130/0016-7606(1991)103<0472:FCAUHO>2.3.CO;2
- Steidtmann, J. R., Middleton, L. T., & Shuster, M. W. (1989). Post-Laramide (Oligocene) uplift in the Wind River Range, Wyoming. *Geology*, 17(1), 38. https://doi.org/10.1130/0091-7613(1989)017<0038:PLOUIT>2.3.CO;2
- Stewart, E. D., Link, P. K., Fanning, C. M., Frost, C. D., & McCurry, M. (2010). Paleogeographic implications of non–North American sediment in the Mesoproterozoic upper Belt Supergroup and Lemhi Group, Idaho and Montana, USA. Geology, 38(10), 927–930. https://doi.org/10.1130/G31194.1
- Tavani, S., Granado, P., Corradetti, A., Camanni, G., Vignaroli, G., Manatschal, G., et al. (2021). Rift inheritance controls the switch from thin- to thick-skinned thrusting and basal décollement re-localization at the subduction-to-collision transition. GSA Bulletin, 133(9–10), 2157–2170. https://doi.org/10.1130/B35800.1
- Thacker, J. O., Karlstrom, K. E., Kelley, S. A., Crow, R. S., & Kendall, J. J. (2022). Late Cretaceous time-transgressive onset of Laramide arch exhumation and basin subsidence across northern Arizona—New Mexico, USA, and the role of a dehydrating Farallon flat slab. GSA Bulletin. https://doi.org/10.1130/B36245.1
- Thomas, R. (2007). A field guide to the Cambrian section at Camp Creek, southwest Montana. Northwest Geology, 36, 231-244.
- Thomas, R. C. (2008). A field guide to the Cambrian section at Beartooth Butte, northwestern Wyoming. Northwest Geology, 37, 159–172.
- Thurston, O. G., Guenthner, W. R., Karlstrom, K. E., Ricketts, J. W., Heizler, M. T., & Timmons, J. M. (2022). Zircon (U-Th)/He thermochronology of Grand Canyon resolves 1250 Ma unroofing at the Great Unconformity and <20 Ma canyon carving. *Geology*, 50(2), 222–226. https://doi.org/10.1130/G48699.1
- Tikoff, B., Moores, E., & Hole, J. (2016). The recurring myth of Farallon flat-slab subduction. In *Geological Society of America abstracts with programs* (Vol. 48)
- Underwood, S. J., Childs, J. F., Walby, C. P., Lynn, H. B., Wall, Z. S., Cerino, M. T., & Bartlett, E. (2014). The Yellowstone and Regal talc mines and their geologic setting in southwestern Montana. Field Guides, 37, 161–187. https://doi.org/10.1130/2014.0037(08)
- Vermeesch, P. (2018). IsoplotR: A free and open toolbox for geochronology. Geoscience Frontiers, 9(5), 1479–1493. https://doi.org/10.1016/j.gsf.2018.04.001
- Vuke, S. M., Porter, K. W., Lonn, J. D., & Lopez, D. A. (2007). Geologic map of Montana (geologic map no. 62) (p. 74). Montana Bureau of mines and Geology.
- Walcott, C. (1914). Cambrian geology and paleontology: Smithsonian misc. Collections, 57, 345-412.
- Walker, J. C. G., Hays, P. B., & Kasting, J. F. (1981). A negative feedback mechanism for the long-term stabilization of Earth's surface temperature. *Journal of Geophysical Research*, 86(C10), 9776–9782. https://doi.org/10.1029/JC086iC10p09776
- Walsh, A., Ball, T., & Schultz, D. M. (2019). Extreme sensitivity in Snowball Earth formation to mountains on Paleoproterozoic supercontinents. Scientific Reports, 9(1), 2349. https://doi.org/10.1038/s41598-019-38839-6
- Weil, A. B., & Yonkee, W. A. (2012). Layer-parallel shortening across the Sevier fold-thrust belt and Laramide foreland of Wyoming: Spatial and temporal evolution of a complex geodynamic system. Earth and Planetary Science Letters, 357(358), 405–420. https://doi.org/10.10 16/j.epsl.2012.09.021
- Whitmeyer, S. J., & Karlstrom, K. E. (2007). Tectonic model for the Proterozoic growth of North America. Geosphere, 3(4), 220–259. https://doi.org/10.1130/GES00055.1
- Winston, D. (1986). Sedimentation and tectonics of the Middle Proterozoic Belt Basin and their influence on Phanerozoic compression and extension in Western Montana and northern Idaho. In J. A. Peterson (Ed.), *Paleotectonics and sedimentation in the Rocky mountain region*, *United States* (Vol. 41). American Association of Petroleum Geologists. https://doi.org/10.1306/M41456C5
- Wise, D. U. (1983). Overprinting of Laramide structural grains in the Clarks Fork Canyon area and eastern Beartooth Mountains of Wyoming. In Wyoming geological association 34th annual field conference guidebook (pp. 77–87).
- Wise, D. U. (2000). Laramide structures in basement and cover of the Beartooth uplift near Red Lodge, Montana. AAPG Bulletin, 84(3), 360–375. https://doi.org/10.1306/C9EBCDF1-1735-11D7-8645000102C1865D
- Wooden, J. L., Mueller, P. A., Mogk, D. A., Bowes, D. R., Lewis, S., & Berg, R. (1988). A review of the geochemistry and geochronology of Archean rocks of the Beartooth Mountains, Montana and Wyoming. In S. E. Lewis & R. B. Berg (Eds.), *Precambrian and Mesozoic plate margins: Montana, Idaho and Wyoming* (Vol. 96, pp. 23–42). Montana Bureau of Mines and Geology, Special Publication.
- Wyld, S. J. (2002). Structural evolution of a Mesozoic backarc fold-and-thrust belt in the U.S. Cordillera: New evidence from northern Nevada. GSA Bulletin, 114(11), 1452–1468. https://doi.org/10.1130/0016-7606(2002)114<1452:SEOAMB>2.0.CO;2
- Yonkee, W. A., Dehler, C. D., Link, P. K., Balgord, E. A., Keeley, J. A., Hayes, D. S., et al. (2014). Tectono-stratigraphic framework of Neoproterozoic to Cambrian strata, west-central U.S Protracted rifting, glaciation, and evolution of the North American Cordilleran margin. Earth-Science Reviews, 136, 59–95. https://doi.org/10.1016/j.earscirev.2014.05.004
- Yonkee, W. A., & Weil, A. B. (2015). Tectonic evolution of the Sevier and Laramide belts within the North American Cordillera orogenic system. Earth-Science Reviews, 150, 531–593. https://doi.org/10.1016/j.earscirev.2015.08.001

RONEMUS ET AL. 33 of 34

References From the Supporting Information

10.1029/TR037i003p00320

- Allen, P., & Allen, J. (1990). Basin analysis: Principles and applications. Blackwell Scientific Publications.
- DeCelles, P. G., Gray, M. B., Ridgway, K. D., Cole, R. B., Pivnik, D. A., Pequera, N., & Srivastava, P. (1991). Controls on synorogenic alluvial-fan architecture, Beartooth Conglomerate (Palaeocene), Wyoming and Montana. Sedimentology, 38(4), 567–590. https://doi.org/10.1111/j.1365-3091.1991.tb01009.x
- Fleck, R. J., Sutter, J. F., & Elliot, D. H. (1977). Interpretation of discordant ⁴⁰Art/³⁹Ar age-spectra of mesozoic tholeiites from Antarctica. Geochimica et Cosmochimica Acta, 41(1), 15–32. https://doi.org/10.1016/0016-7037(77)90184-3
- Gehrels, G., & Pecha, M. (2014). Detrital zircon U-Pb geochronology and Hf isotope geochemistry of Paleozoic and Triassic passive margin strata of western North America. *Geosphere*, 10(1), 49–65. https://doi.org/10.1130/GES00889.1
- Gómez, E., Jordan, T. E., Allmendinger, R. W., & Cardozo, N. (2005). Development of the Colombian foreland-basin system as a consequence of diachronous exhumation of the northern Andes. GSA Bulletin, 117(9–10), 1272–1292. https://doi.org/10.1130/B25456.1
- Guenthner, W. R., Reiners, P. W., & Chowdhury, U. (2016). Isotope dilution analysis of Ca and Zr in apatite and zircon (U-Th)/He chronometry. Geochemistry, Geophysics, Geosystems, 17(5), 1623–1640. https://doi.org/10.1002/2016GC006311
- House, M. A., Farley, K. A., & Stockli, D. (2000). Helium chronometry of apatite and titanite using Nd-YAG laser heating. *Earth and Planetary Science Letters*, 183(3), 365–368. https://doi.org/10.1016/S0012-821X(00)00286-7
- Kuiper, K., Deino, A., Hilgen, F., Krijgsman, W., Renne, P., & Wijbrans, & Jr. (2008). Synchronizing rock clocks of Earth history. Science, 320(5875), 500–504. https://doi.org/10.1126/science.1154339
- Min, K., Mundil, R., Renne, P. R., & Ludwig, K. R. (2000). A test for systematic errors in ⁴⁰Ar/³⁹Ar geochronology through comparison with U/Pb analysis of a 1.1-Ga rhyolite. *Geochimica et Cosmochimica Acta*, 64(1), 73–98. https://doi.org/10.1016/S0016-7037(99)00204-5
- Pullen, A., Ibáñez-Mejia, M., Gehrels, G. E., Giesler, D., & Pecha, M. (2018). Optimization of a laser ablation-single collector-inductively coupled plasma-mass spectrometer (Thermo Element 2) for accurate, precise, and efficient zircon U-Th-Pb geochronology. *Geochemistry, Geophysics, Geosystems*, 19(10), 3689–3705. https://doi.org/10.1029/2018GC007889
- Renne, P. R., Swisher, C. C., Deino, A. L., Karner, D. B., Owens, T. L., & DePaolo, D. J. (1998). Intercalibration of standards, absolute ages and uncertainties in ⁴⁰Ar/³⁹Ar dating. *Chemical Geology*, 145(1), 117–152. https://doi.org/10.1016/S0009-2541(97)00159-9
- Schoene, B., Condon, D. J., Morgan, L., & McLean, N. (2013). Precision and accuracy in geochronology. *Elements*, 9(1), 19–24. https://doi.org/10.2113/gselements.9.1.19
- Sclater, J. G., & Christie, P. A. F. (1980). Continental stretching: An explanation of the post-mid-Cretaceous subsidence of the central North Sea basin. *Journal of Geophysical Research*, 85(B7), 3711–3739. https://doi.org/10.1029/JB085iB07p03711
- Stacey, J. S., & Kramers, J. D. (1975). Approximation of terrestrial lead isotope evolution by a two-stage model. Earth and Planetary Science Letters, 26(2), 207–221. https://doi.org/10.1016/0012-821X(75)90088-6
- Sundell, K. E., Gehrels, G. E., & Pecha, M. E. (2021). Rapid U-Pb geochronology by laser ablation multi-collector ICP-MS. *Geostandards and*
- Geoanalytical Research, 45(1), 37–57. https://doi.org/10.1111/ggr.12355
 Wetherill, G. W. (1956). Discordant uranium-lead ages, I. Eos, Transactions American Geophysical Union, 37(3), 320–326. https://doi.org/
- Zeitler, P. K., & Tremblay, M. M. (2020). Measuring noble gases for thermochronology. *Elements*, 16(5), 343–344. https://doi.org/10.2138/gselements.16.5.343

RONEMUS ET AL. 34 of 34